NASA
Technical Paper 1303

AVRADCO
Technical Report 78-53



# Experimental Investigation of Effects of Blade Tip Geometry on Loads and Performance for an Articulated Rotor System

William H. Weller

JANUARY 1979

NASA

U.S. ARMY AVRADCOM

NASA
Technical Paper 1303

AVRADCOM
Technical Report 78-53

# Experimental Investigation of Effects of Blade Tip Geometry on Loads and Performance for an Articulated Rotor System

William H. Weller
*Structures Laboratory, AVRADCOM Research and Technology Laboratories*
*Langley Research Center*
*Hampton, Virginia*

National Aeronautics
and Space Administration

**Scientific and Technical
Information Office**

1979

## SUMMARY

Wind-tunnel tests of an aeroelastically designed helicopter rotor model were carried out to determine the effects on dynamic response and aerodynamic performance of varying the design of the outboard 8 percent of the blade lengths. Four different blade tip geometries or shapes having different amounts of planform sweep, thickness and chordwise taper, and anhedral angle were studied. Each configuration was tested at several shaft angles of attack for advance ratios of 0.20, 0.30, 0.35, and 0.40. For each combination of shaft angle and advance ratio, rotor lift was varied over a wide range to include high lift conditions.

From these tests, it was found that aft sweep of the blade tips decreased oscillatory beamwise and chordwise bending moments on the blade, while tip anhedral increased the bending moments. Both blade tip sweep and anhedral resulted in significant reductions in the oscillatory torsional moments along the blade and in the control-system forces. In comparison to the rectangular tips, the blades with a combination of tip sweep and anhedral indicated a 40-percent reduction in oscillatory torsional moments at an advance ratio of 0.4. Blade tip anhedral yielded the best aerodynamic performance for hover and at advance ratios up to 0.30. At higher advance ratios the configurations with tip sweep only had the lowest power requirements and the performance for the anhedral tips was better than that for rectangular tips.

## INTRODUCTION

The majority of helicopter rotors now in service have in common the design of the outer portion of each blade as a straight, uncambered, rectangular segment of constant thickness. While attractive from the standpoint of manufacturing ease, such a design has not been proven as the optimum for performance, blade loads, or fuselage vibrations. Research has suggested that design changes away from this standard would be beneficial for helicopter operational characteristics. One example of this research is reported in reference 1, which presents the results from tests of an "aeroelastically adaptive rotor system." The philosophy of this approach is to devise a passive means of inducing dynamic twist of the blades to improve rotor performance and reduce vibratory loads at high advance ratios. This dynamic twist would diminish the degrading influence of built-in twist at high advance ratios and built-in twist could then be increased over conventional values for improved performance in hover and at low advance ratios. References 1 to 4 suggest that overall benefits would accrue from combining built-in twists higher than on conventional rotors with other blade design changes which produce both a $\sin \psi$ and $\cos 2\psi$ dynamic twist variation (positive nose-up) in forward flight. This dynamic twist would improve rotor performance and loads at the higher advance ratios, partially overcoming the detrimental effects of built-in twist.

This report presents results of wind-tunnel tests using a four-bladed articulated rotor model. This model was designed and built by Sikorsky Aircraft whose personnel also participated in the tests. The purpose of the tests was to determine the effects on rotor dynamic response and performance of varying the design of the outboard 8 percent of the blade lengths. The aeroelastically designed rotor model could accommodate different tips and four sets were tested involving variations in sweep, thickness and chordwise taper, and anhedral. Wind-tunnel tests were performed in the Langley transonic dynamics tunnel using an aeroelastic rotor experimental system (ARES), which is a universal model-rotor test stand designed mainly for studies of main rotor aeroelasticity. The rotor with each of the four tip sets was tested at several shaft angles of attack for advance ratios of 0.20, 0.30, 0.35, and 0.40. For each combination of shaft angle and advance ratio, rotor lift was varied over a wide range to high lift conditions. Rotor response and aerodynamic performance were obtained from the tests, and representative data are presented in this report.

Use of trade names or names of manufacturers in this report does not constitute an official endorsement of such products or manufacturers, either expressed or implied, by the National Aeronautics and Space Administration.

## SYMBOLS

Units used for the physical quantities defined in this paper are given in the International System of Units (SI).

$A_f$ equivalent fuselage flat-plate drag area, $m^2$

$a$ airfoil lift-curve slope, $rad^{-1}$

$b$ number of blades

$C_D$ rotor drag coefficient, $D/\pi R^2\rho(\Omega R)^2$

$C_L$ rotor lift coefficient, $L/\pi R^2\rho(\Omega R)^2$

$C_Q$ rotor torque coefficient, $Q/\pi R^3\rho(\Omega R)^2$

$c$ blade chord at $x = 0.5$, m

$D$ rotor drag force, N

$I$ blade mass moment of inertia about flapping hinge, $kg\text{-}m^2$

$L$ rotor lift force, N

$M_t$ rotor tip Mach number in hover

$P$ harmonic order of rotor rotational speed

$Q$ rotor torque, N-m

| | |
|---|---|
| $R$ | blade radius, m |
| $R_n$ | Reynolds number based on $c$ and $\Omega R$ |
| $r$ | radial blade station measured from center of rotation, m |
| $V$ | tunnel velocity, m/sec |
| $x$ | nondimensional blade station measured from center of rotation, $r/R$ |
| $\alpha_s$ | rotor shaft angle of attack (positive with fuselage nose-up), deg |
| $\gamma$ | rotor Lock number, $\rho acR^4/I$ |
| $\mu$ | advance ratio, $V/\Omega R$ |
| $\rho$ | density of test medium, $kg/m^3$ |
| $\sigma$ | rotor solidity, $bc/\pi R$ |
| $\phi_n$ | phase angle of nth harmonic component of response, deg |
| $\psi$ | blade azimuth position, deg |
| $\Omega$ | rotational speed, rad/sec |
| $\omega$ | rotating natural frequency of rotor blade, rad/sec |

## EXPERIMENTAL APPARATUS AND PROCEDURES

### Test Facility

The experimental program was conducted in the Langley transonic dynamics tunnel (TDT) shown schematically in figure 1. The TDT is a continuous-flow tunnel with a slotted test section which is capable of operation over a Mach number range from 0 to 1.20 at stagnation pressures from 0.01 to 1 atm. The tunnel test section is 4.9 m square with cropped corners and has a cross-section area of 23 $m^2$. The present investigation was conducted in Freon-12, primarily at a density of 3.09 $kg/m^3$. A limited number of measurements were also made at densities of 1.55 and 4.53 $kg/m^3$.

During testing, use was made of the TDT computerized data acquisition system. The data system includes a digital computer, transducer signal conditioners, amplifiers, and calibration signal sources sufficient to handle 60 channels of data. From the amplifiers, data are routed to a direct-record FM tape recorder which can accept up to 13 channels of data. A second FM tape recorder, not formally part of the data system, may be used to record an additional 13 channels of data. The recorders are operated at tape speeds of 0.09525 m/sec or greater. Data from the signal amplifiers are also routed to a 60-channel analog-to-digital system and then to the system computer for processing. Although final data reduction was performed off-line; the data

acquisition system was used on-line to process data and display information, such as rotor performance characteristics, which are needed during the testing.

## Aeroelastic Rotor Experimental System

The aeroelastic rotor experimental system (ARES) shown in figures 2 to 4 serves as a powered rotor test stand for wind-tunnel testing related to helicopter dynamics. Figure 4 presents a detailed view of the model illustrating the more important features. The frame of the ARES is formed by pairs of longerons and braces on each side connecting the forward and aft bulkheads. The frame is enclosed by a fiberglass shell to simulate a fuselage. The longerons are pinned to a yoke which forms part of the steel post mount to provide a pivot for varying the model pitch attitude.

The ARES rotor shaft is driven by a variable frequency sychronous motor, rated at 35 kW output at a rotational speed of 1256 rad/sec. The motor is connected to the rotor shaft through a two-stage speed reduction system using V-belts. The total speed reduction is approximately 10:1 resulting in a maximum rotor operating speed of 125.6 rad/sec. This speed limit is suitable for testing Mach scaled rotor models in Freon-12 or Froude-scaled models in air. Rotor speed is controlled by varying the electric line frequency to the synchronous motor.

The ARES is remotely controlled from the wind-tunnel control room. The pitch attitude of the model can be changed, using a hydraulic actuator and an electric servo system, over a range from $20^{\circ}$ nose down to $8^{\circ}$ nose up. The model features a complete main rotor control system. The swashplate (shown in fig. 4) is mounted on the rotor shaft. It is raised, lowered, or tilted by three assemblies - each combining a hydraulic actuator, electric servo, and linear potentiometer - to achieve collective pitch, lateral-, and longitudinal-cyclic swash-plate motions for rotor control. For tests involving high-frequency control inputs, the hydraulic actuators are used for generating transient or sinusoidal inputs about the steady-state control positions. This capability is useful for determining rotor frequency response and subcritical stability characteristics. For the tests reported herein this capability was used to verify that the rotor models mounted on the ARES were free of ground resonance instability.

The ARES is instrumented to provide continuous displays of all model control settings and selected rotor loads. The model pitch attitude is measured by a servo accelerometer and the rotor control positions are determined by potentiometers connected to the swashplate. Rotor-shaft speed is determined by a magnetic sensor. The rotating blade data are transferred to the fixed system through a 60-ring, horizontal disk, slip-ring assembly using two brushes per ring. The rotor forces and moments are measured by using a six-component strain-gage balance mounted below the pylon and drive system. The balance is fixed in the shaft system and pitches with the fuselage. Fuselage aerodynamic forces and moments are not sensed by the balance due to the nature of the ARES design.

## Model Rotor System

The model was a four-bladed articulated rotor with coincident lead-lag and flapping hinges at 5.56 percent radius and with zero pitch-flap coupling. The rotor had a 2.743-m diameter, Lock number of 9.7 (based on $\rho = 3.09$ kg/m$^3$), and solidity of 0.084. The blades were aeroelastically designed but did not represent any full-scale production rotor. The blades had a chord of 9.05 cm and an SC 1095 airfoil (table I) from the root cutout to 51 percent radius and from 84 percent radius to the outboard tip attachment point at 91 percent radius. Between 51 and 84 percent radius a drooped nose was added to achieve a cambered SC 1095 R8 airfoil with a 9.30-cm chord. The blade radial twist distribution is shown in figure 5.

The blades were originally designed for testing in air at full-scale Mach numbers. However, the model was converted to a Freon-12 test article by adding ballast to the blades and operated at a reduced rotor rotational speed (69.12 rad/sec) to maintain hover tip Mach number (0.628) and blade Lock number. The normalized natural frequencies of the model, as configured for Freon testing, were higher than those for the original (air) configuration. The objective of the tests was to determine trends of rotor operational characteristics with changes to the blade tips, and the model is suitable for that purpose. Scale factors relating a conceptual full-scale rotor to the models tested are listed in table II based on matching advance ratio and the ratios of blade natural frequency to rotor speed and assuming a length scale factor of 6.0.

Blade construction consisted of a basically oval titanium spar, Nomex[1] core in the trailing portion and foam filler in the nose to maintain contour. Fiberglass cloth was bonded around the Nomex, spar, and filler to form a closed blade skin. At 91 percent radius a blade joint enabled tip configuration changes to be made. The four tip geometries or shapes shown schematically in figure 6 were tested and reflected differing degrees of planform sweep, anhedral, and thickness taper. Photographs of the baseline and anhedral tips installed are presented in figures 7 and 8, respectively. The tapered and anhedral tips included linear thickness taper from 96 and 92 percent radius, respectively, to the tip where the thickness had been reduced by 40 percent from that of the basic SC 1095 airfoil on the inboard portion of the blade. In addition, the anhedral tip had 10° of built-in anhedral, beginning at 92 percent radius. The blade inboard of 92 percent radius and the rectangular and baseline tips were all balanced about the quarter-chord of the basic blade. The anhedral tip was balanced about 28 percent chord. Chordwise balance for the tapered tip was not known. The baseline and anhedral tips had increasingly aft aerodynamic center displacements relative to the rectangular tip. The aerodynamic center for the tapered and baseline tips were approximately the same. The spanwise distributions of structural properties for the blades and the rotating blade natural frequencies were furnished by Sikorsky Aircraft and are presented in tables III and IV, respectively.

---

[1] Nomex: Trade name of E. I. duPont de Nemours & Co., Inc.

One rotor blade was instrumented with four-arm strain-gage bridges to measure the moments about three orthogonal axes. The beamwise (or flatwise) axis was in the chordwise direction, the torsional axis lay along the quarter-chord line in the spanwise direction, and the chordwise axis was perpendicular to the other two. Beamwise and chordwise bending moments at 22, 40, 60, and 80 percent radius and torsion at 23, 41, and 81 percent radius were measured. Shaft torque and pitch-link axial load were also measured. Rotor blade flapping and lagging relative to the hub were measured by angular potentiometers mounted on the hub and geared to the blade root hardware.

## Experimental Procedure and Data Reduction

Rotor aerodynamic performance and dynamic response were measured for all blade configurations over wide ranges of shaft angle of attack, rotor lift, and advance ratio. Each run was initiated by setting the collective pitch to a low value, bringing the rotor speed up to 69.12 rad/sec, and pitching the model to the first shaft angle of attack. The free-stream speed was established to yield the first advance ratio. Collective pitch was increased, generally by $2^{\circ}$ increments, until excessive rotor loads were encountered. Then, the collective pitch was returned to the original setting, the shaft angle was increased by $3^{\circ}$, and the procedure was repeated. After data were recorded at all desired shaft angles, the tunnel speed was increased to produce the next desired advance ratio, and the process was repeated for each remaining advance ratio. At each test point, rotor first harmonic flapping relative to the shaft was eliminated so that the rotor was maintained at a trimmed-to-shaft condition. The maximum and minimum values of lift coefficient achieved during tests of the rectangular tip configuration are identified in figure 9 for each combination of shaft angle and advance ratio.

Rotor performance and dynamic response were recorded at each combination of rotor trim, shaft angle, and tunnel speed. The tunnel operating conditions, balance data, and model control settings were recorded on punched cards. The rotor dynamic response data and the once-per-revolution rotor pulse signal were recorded on analog tape.

Rotor aerodynamic performance measurements were processed by making corrections for deadweight tares and balance interactions. The aerodynamic contributions of the hub are included in the data presented herein. The measurements were transferred from the balance centroid to the hub. The thrust, rotor power, and propulsive force, normalized by rotor solidity, were then computed. The normalized lift and drag coefficients were determined by rotating the transferred measurements into the wind-axis system.

Rotor dynamic response was determined from the data recorded on magnetic tape. From each channel, approximately 2 sec were digitized at a rate of 1000 samples per second. The mean values were found and subtracted from each sample prior to the dynamic-response data processing. The oscillatory response of each of the three moments (chordwise, beamwise, and torsional) was calculated as one-half of the peak-to-peak dynamic response. In addition, a Fourier analysis was performed and the magnitude (1/2 peak-to-peak) of selected Fourier components of the moments at integral multiples of the rotor rotational speed

are presented. Note that the sum of the response harmonics as presented may be greater than the oscillatory response because of the possibility of phase differences between the harmonics in a Fourier series.

## PRESENTATION OF RESULTS

The rotor with the rectangular tips was tested over the operating envelope of figure 9. Tests of the baseline, tapered, and anhedral tip configurations were conducted over basically the same range of experimental parameters. Representative measured results from those tests are presented graphically and discussed in subsequent paragraphs. The organization of the figures and discussion is as follows:



## DISCUSSION OF RESULTS

### Measured Characteristics Repeatability

Measured dynamic-response repeatability is illustrated in figure 10. The oscillatory and first two harmonic moments obtained from three runs are compared for beamwise bending at 60 percent radius, chordwise bending at 22 percent radius, and torsion at 41 percent radius. The torsional data show the most scatter, although the variation is primarily due to a shift in the data for one run. The data of figure 10 show good agreement in both magnitude and trend. Analysis of other repeat cases indicates that these data are representative of the worst cases and that the quality of all data are suitable for the purposes of this report.

Measured performance repeatability is illustrated in figure 11. For two hover tests the measured performance showed a shift of less than 0.00015 on $C_Q/\sigma$. For wind-on tests (fig. 11(b)) three sets of data are shown and fall within a band of $C_Q/\sigma = \pm 0.0001$.

### Effect of Reynolds Number on Hover Performance

In reference 5, experimental data are presented which demonstrate the effect of Reynolds number on aerodynamic performance measured on a model rotor. The data were obtained in a Freon-12 test medium and the Reynolds number variation was achieved by changing the tunnel atmospheric density. The trend is best illustrated by figure 10 of reference 5, which indicates that rotor $C_Q/\sigma$ decreases with increasing Reynolds number for fixed $C_L/\sigma$. It is significant that the increment in $C_Q/\sigma$ between full-scale and aeroelastic-model

($\sigma$ = 0.0464) data is approximately the same as that for the larger chord model ($\sigma$ = 0.1100) between sets of its data at the same respective values of Reynolds number. This situation suggests that the difference in performance between the full-scale and aeroelastic model with the same solidities might be mostly attributable to Reynolds number effects. Even though the effects of rotor solidity and blade elasticity are more significant overall, the effect of Reynolds number is still an important consideration during model design and testing.

A similar test was performed during the experimental program reported herein; the articulated rotor model with tapered tips was operated in hover at three atmospheric densities. The middle density value (3.09 kg/m$^3$) yielded a Lock number of 9.7. The resulting data are plotted in figure 12. The Reynolds numbers in the figure are based on blade chord at $x = 0.50$ and tip velocity. From figure 12 the differences between curves are close to the repeatability margins and, thus, the effect of Reynolds number change is not as significant as indicated in figure 10 of reference 5; furthermore, the trend is not consistent. However, blade coning and its associated effect is greater for the articulated rotor than for the teetering rotor model used in reference 5. Using the hover performance analysis of reference 6, it was determined that the effect of coning was to increase $C_Q/\sigma$ with coning angle for constant $C_L/\sigma$. Using the data for the median atmospheric density as a reference and at $C_L/\sigma = 0.089$, the analysis indicated that an increment on $C_Q/\sigma$ of approximately 0.00024 should be added to the low density data and subtracted from the high density data to eliminate the effect of coning. The data of figure 12, if corrected for coning, would show a trend of decreasing $C_Q/\sigma$ with increasing Reynolds number. The data presented in subsequent sections are not corrected for either coning or Reynolds number effects.

## Rectangular Tip Rotor Characteristics

Spanwise distributions of blade oscillatory bending moments and the first three harmonic components for the rectangular tip configuration are plotted in figure 13. The designation P denotes harmonic orders of the rotor rotational speed. The data pertain to lift coefficients of $C_L/\sigma = 0.0515$ and $C_L/\sigma = 0.0962$. The oscillatory and harmonic moments are presented for beamwise, chordwise, and torsional moments along the blade. For all load components and at both values of $C_L/\sigma$, the first harmonic is the most significant in magnitude and principally determines the shape of the oscillatory moment distributions. The magnitudes and shapes of the various distributions in figure 13, as well as the relative importance of the harmonic magnitudes, do not significantly change with $C_L/\sigma$ except for the chordwise moment. Over the inboard half of the blade, the first harmonic and oscillatory chordwise moments for $C_L/\sigma = 0.0962$ are at least double the corresponding values for $C_L/\sigma = 0.0515$ (fig. 13(b)). Over the outboard half of the blade the variation of chordwise moments with $C_L/\sigma$ is not as great.

Figures 14 and 15 illustrate the measured aerodynamic performance characteristics of the rotor with rectangular tips for advance ratios of 0.2, 0.3, 0.35, and 0.4. The data are plotted as helicopter performance coefficients normalized by rotor solidity. Variations of torque (fig. 14) and drag (fig. 15)

coefficients with lift coefficient are shown. The performance data are plotted for several shaft angles of attack at each advance ratio. The values of shaft angle were selected to encompass the operating attitudes of a typical full-scale helicopter in level flight. The data in figure 15 can be interpolated to approximate shaft attitudes for various gross weights, maneuver conditions, and fuselage drag areas. From the lift and interpolated shaft angle, the data in figure 14 can then be employed to determine power requirements.

## Effect of Tip Configuration on Rotor Dynamic Response

Spanwise distributions of blade dynamic response.- Comparisons of spanwise distributions of the oscillatory and first two harmonic moments measured on the four rotors are presented in figures 16, 17, and 18 for beamwise bending, chordwise bending, and torsion, respectively. In figure 16(a) the first harmonic of the beamwise moment over the outboard half of the blade is highest for the anhedral tip configuration. The first harmonic beamwise moments are slightly lower on the rotors with tip sweep only (baseline and tapered) than for the rectangular blade tip model. The second harmonic of the beamwise moments (fig. 16(b)) shows no consistent trend with tip design, and the oscillatory-distribution trends (fig. 16(c)) primarily reflect those for the first harmonic component. The chordwise moments presented in figure 17 do not indicate any clear and significant trends with tip sweep. The anhedral tipped blade did have higher first harmonic and oscillatory chordwise moments than those for the rectangular tip configuration.

The effects of blade tip sweep and anhedral are much more significant on the torsional moments and pitch-link forces as shown in figure 18. For the purpose of comparing pitch-link force and torsional moment trends, an equivalent moment at 5.6 percent radius has been derived from the pitch-link force and the offset between the feathering axis and the pitch horn (0.0356 m). The equivalent moment is plotted in figure 18, when data are available, along with the measured torsional moments. Relative to the rectangular tip configuration, both blade tip sweep and anhedral cause a reduction in oscillatory and harmonic torsional moments. Comparing the rectangular and anhedral tip data at 23 percent radius, the oscillatory moment is reduced by 40 percent and the harmonics by over 50 percent due to the combined effects of tip sweep and anhedral. The mean torsional moment trends are illustrated in figure 18(d). For comparison, mean torsional moment distributions measured in hover for the same value of $C_L/\sigma$ are presented in figure 19. Tip sweep and anhedral both cause nose-down increments in the mean value of the moment. The relationships between the data correspond to the order of the tips with regard to increasingly aft location of the aerodynamic center. These results are to be expected because upward lift on the tip in combination with the aft sweep of the aerodynamic center and the drag acting on the part of the blade with anhedral would both lead to nose-down moment increments about the elastic axis of the inboard portion of the blade.

Control loads.- Variations of the oscillatory and mean values of torsional moment at 23 percent radius and the pitch-link axial force with $C_L/\sigma$ are shown in figures 20 and 21, respectively. The tip sweep and anhedral result in lower values of the oscillatory torsional moment (fig. 20(a)) throughout the range of lift coefficients achieved. For the anhedral tips the oscillatory

moment decreases with lift coefficient for values of $C_L/\sigma$ below 0.08 and increases thereafter. The oscillatory pitch-link forces (fig. 21(a)) indicate a similar trend, although the initial decrease with lift is not as prominent. The mean value of the torsional moment (fig. 20(b)) becomes more negative (nose-down) with $C_L/\sigma$ as sweep and anhedral are added to the tips, primarily due to the displacement of the tip aerodynamic center away from an extension of the elastic axis of the inboard portion of the blade. The mean pitch-link forces (fig. 21(b)) also reflect an increase in the nose-down (tension) sense with increased lift with the anhedral having the greater change. The increment in mean torsional moment between the data for the anhedral and tapered tips at the lower values of $C_L/\sigma$ (fig. 20(b)) was not evident in the pitch-link trends of figure 21(b). With this exception the torsional data at 23 percent radius and the pitch-link forces reflect similar trends for both oscillatory and mean values of load.

Because of the lack of pitch-link data for some test conditions, the torsional moment at 23 percent radius is used to illustrate control-force trends with advance ratio as in figure 22. For advance ratios above 0.2, blade tip sweep and anhedral both reduce the oscillatory amplitudes of the torsional moments and, therefore, the oscillatory control-system forces. At an advance ratio of 0.4 the data suggest that the combination of anhedral and sweep would reduce the oscillatory control-system forces by 40 percent in comparison to the response for a rectangular tip blade.

The mean values of torsional moments (fig. 22(b)) indicate that the mean value of the pitch-link force would increase slightly with tip sweep, probably because of the increased amount of tip aerodynamic center offset from the inboard blade elastic axis. The mean value of the pitch-link force was also expected to increase with anhedral, although this increase is not found in figure 22(b).

A difference between the mean values of torsion at 23 percent radius and the equivalent moment formed from the pitch-link force for the anhedral tip is evident in figures 18(d) and 19. Data for the tapered tip configuration did not indicate such a difference. Therefore, care is required in attempting to deduce pitch-link force trends from blade torsional moments for the anhedral tip configuration.

Outboard blade loads.- As evident from the preceding discussion, the design of the blade tip influences the forces incurred on the rotor, particularly the torsional moments. The effects of tip design can best be understood by examining measured response trends at the outboard stations, which eliminates the influences of blade elastic deflection at stations inboard. Variations of torsional response at 81 percent radius with $C_L/\sigma$ are illustrated in figure 23. The first harmonic component of the torsional moment (fig. 23(a)) is significantly reduced by blade tip sweep. However, the most significant trend arises from the use of anhedral, which causes a decreasing torsion moment with increasing lift trend for values of $C_L/\sigma$ below 0.08. Similar trends are observed for the second harmonic component of torsion as shown in figure 23(b), although the anhedral tip blade incurred larger 2P moments than the tapered tip at the lower values of $C_L/\sigma$. The larger second harmonic canceled in part the benefit of the lower 1P moment on the anhedral tip blade. Thus, the oscillatory

trends (fig. 23(d)) do not indicate as significant an improvement by using tip anhedral as is suggested from examination of the first harmonic component only. Further, the oscillatory torsional moment trends, which generally agree with those of figure 20(a), indicate that at $C_L/\sigma$ values greater than 0.10 the anhedral tip blade may encounter larger moments than those on the blades with tip sweep only. The contributions from the higher harmonics, such as 6P (fig. 23(c)), were more significant for the anhedral blades. The mean torsional moment trends in figure 23(e) resemble those of figure 20(b) with regard to relative tip effects.

The effects of blade tip sweep and anhedral on the torsional moments can be partially explained by considering the transfer of the bending moments acting on the tip to the inboard portion of the blade. Figure 24 shows schematically how the combinations of aft sweep with beamwise moment (lift) and anhedral with chordwise moment (drag) lead to torsional moment components inboard of the elastic axis break. The torsional moments on the tip would likewise be partly resolved into beamwise and chordwise bending directions inboard of the tip. Due to the relative magnitudes of the three moment components, the effect of tip torsional moment on inboard bending moments would be small. The sense of the coupling between tip bending moments and the torsional component is negative (nose-down), torsion resulting from positive beamwise (up) and chordwise (aft) moments or a 180° phase relationship between the bending moments and the corresponding torsional moment components.

The lack of measurements outboard of 81 percent radius precludes accurate determination of the magnitudes of the torsional moment components arising from tip sweep and anhedral, but the outboard blade bending moment data can be used to show trends. Figure 25 illustrates trends of the first two harmonics of torsion with sweep and anhedral. For convenience, the reference points on the rotor azimuth for $\phi_1$ and $\phi_2$ differ so that $\phi_1$ may be used in a sine expression and $\phi_2$ as the argument of the cosine function. For the test conditions of figure 25, the phase angle for the beamwise bending moments in the area of the blade tip is approximately 146°. Aft sweep of the blade tip should result in a torsional moment component with a phase angle 180° greater than that of the beamwise moments, or 326°. Therefore, the primary trend of the torsional moment with increasing tip sweep or tip beamwise moment is illustrated by the vector at 326° phase in figure 25(a). The vector at 310° illustrates trends with increasing anhedral angle. This vector is determined from the chordwise bending moments measured on the outboard portion of the blade. The trend vectors for increasing blade tip sweep and based on the beamwise moments closely parallel the measured torsional data for both harmonics. The trend with increasing anhedral angle correlates with measured torsional moments for the first harmonic. The lack of agreement for the second harmonic of the torsional moment may be attributable to the chordwise-moment phase angle changing over the outboard 20 percent of the blade.

As discussed in reference 1, improvements in rotor forward flight performance can be achieved through the introduction of passive means of controlling dynamic blade twist. The optimum dynamic twist with regard to the first two harmonic components are $\sin \psi$ and $\cos 2\psi$ variations (nose-up is positive). The variation with tip configuration of both amplitude and phase of the first two harmonics of the torsional moment at 81 percent radius is significant

as shown in figure 25. The optimum situation is where both $\phi_1$ and $\phi_2$ are zero. As shown in figure 25, blade tip sweep and anhedral cause changes in the amplitude and phase of the first two torsional moment harmonics which should result in improved aerodynamic performance relative to that for the rectangular tip configuration. This effect is illustrated in subsequent discussion.

As shown previously, the first harmonic component is the major contributor to the oscillatory bending moments on the blade and principally determines the trends of oscillatory moment with tip shape. Therefore, to study the primary effects of tip design on bending moments only the first harmonic component need be considered. As shown in figures 16(a) and 17(a), blade tip sweep results in lower bending moments, while tip anhedral causes increased bending moments in comparison to data for the rectangular tips. Figure 26 presents azimuthal variations of the first harmonics of beamwise and chordwise bending moments measured on the outboard portion of the blade. From figure 26, it is evident that the increase in 1P bending moments with tip anhedral occurs as the blade approaches the forward or aft axes of the rotor disk (e.g., where part of the free stream radially strikes the anhedral tip over the forward part of the rotor disk causing a downward beamwise moment). The reduction in 1P bending moments with tip sweep also stems from the blade passing over the forward or aft rotor disk axes.

### Effect of Tip Configuration on Rotor Performance

The effects of tip shape on rotor performance are demonstrated in figures 27 and 28. In hover and at the lower advance ratios (0.20 and 0.30), the anhedral tip blade requires less power than the other blade configurations. At the highest advance ratio (0.35), however, tip sweep only appears to be most beneficial. The anhedral blade did require less power than the rectangular blade at the high advance ratio, but more power than the other swept blades, even though the anhedral tip had the largest sweep. The anhedral induces a steady nose-down torsional moment (fig. 18(d)) resulting in more negative twist. The increased negative twist in addition to that built-in is beneficial for performance in hover and at lower advance ratios, but detrimental at higher advance ratios. Besides the steady wind-up of the blades, the design philosophy of the anhedral tip was based on causing a downward displacement of the tip vortex relative to the inboard part of the blade. Thus, the anhedral should increase the vertical separation between a blade and the tip vortex shed from the preceding blade passage. The benefit derived from the anhedral tip in displacing the tip vortex should diminish with increasing advance ratio.

## CONCLUDING REMARKS

Wind-tunnel tests were performed on a four-bladed articulated rotor model to determine the effects on rotor dynamic response and aerodynamic performance of modifying the blade tip design. The aeroelastic rotor model was constructed such that the outboard 8 percent of the blade could be altered. Four sets of tip planforms were tested: (1) rectangular; (2) swept; (3) double swept with thickness taper; and (4) swept with thickness taper, chordwise taper, and anhedral. Each configuration was tested at several shaft angles of attack for each advance ratio of 0.20, 0.30, 0.35, and 0.40. For each combination

of shaft angle and advance ratio, rotor lift was varied over a wide range to include high lift conditions.

The results from the tests indicate that aft sweep of the blade tips is generally beneficial in reducing the first harmonic component, as well as the oscillatory magnitude, of both beamwise and chordwise bending moments. Blade anhedral, on the other hand, produced slightly higher oscillatory bending moments along the blade. Blade torsional moments and control system forces were significantly reduced by adding sweep or anhedral. For an advance ratio of 0.4, the swept anhedral tip reduced the oscillatory torsional moment at the inboard measurement station by 40 percent in comparison to the data for the rectangular tips. Aerodynamic performance in hover and at low advance ratios (up to 0.3) was best for the configuration with anhedral tip. At the higher advance ratios, the tips with sweep alone provided the best performance, although the power requirements for the anhedral tip configuration were still less than that for the rectangular tips.

Langley Research Center
National Aeronautics and Space Administration
Hampton, VA 23665
October 26, 1978

## REFERENCES


1. Doman, Glidden S.; Tarzanin, Frank J.; and Shaw, John, Jr.: Investigation of Aeroelastically Adaptive Rotor Systems. Proceedings of Symposium on Rotor Technology, American Helicopter Soc., 1976.

2. Landgrebe, Anton J.; Moffitt, Robert C.; and Clark, David R.: Aerodynamic Technology for Advanced Rotorcraft. Proceedings of Symposium on Rotor Technology, American Helicopter Soc., 1976.

3. Lemnios, A. Z.; Smith, A. F.; and Nettles, W. E.: The Controllable Twist Rotor Performance and Blade Dynamics. Preprint No. 614, American Helicopter Soc., May 1972.

4. Wood, E. R.; and Buffalano, A. C.: Parametric Investigation of the Aerodynamic and Aeroelastic Characteristics of Articulated and Rigid (Hingeless) Helicopter Rotor Systems. TRECOM Tech. Rep. 64-15, U.S. Army, Apr. 1964. (Available from DDC as AD 607 656.)

5. Yeager, William T., Jr.; and Mantay, Wayne R.: Correlation of Full-Scale Helicopter Rotor Performance in Air With Model-Scale Freon Data. NASA TN D-8323, 1976.

6. Landgrebe, Anton J.; Moffitt, Robert C.; and Clark, David R.: Aerodynamic Technology for Advanced Rotorcraft - Part I. J. American Helicopter Soc., vol. 22, no. 2, Apr. 1977, pp. 21-27.

TABLE I.- SC 1095 AIRFOIL COORDINATES

| Chordwise station, cm | Upper surface, cm | Lower surface, cm |
|---|---|---|
| 0 | 0 | 0 |
| .0434 | .0885 | -.0720 |
| .0868 | .1345 | -.1102 |
| .1302 | .1710 | -.1380 |
| .1736 | .2022 | -.1588 |
| .2170 | .2291 | -.1771 |
| .2604 | .2517 | -.1927 |
| .3472 | .2890 | -.2196 |
| .4340 | .3185 | -.2413 |
| .8679 | .4053 | -.2934 |
| 1.3019 | .4478 | -.3177 |
| 1.7358 | .4713 | -.3298 |
| 2.1698 | .4799 | -.3341 |
| 2.6037 | .4791 | -.3333 |
| 3.4716 | .4583 | -.3194 |
| 4.3395 | .4201 | -.2925 |
| 5.2074 | .3645 | -.2534 |
| 6.0753 | .2925 | -.2022 |
| 6.9432 | .2048 | -.1406 |
| 7.8111 | .1068 | -.0729 |
| 8.6790 | .0226 | -.0061 |
| 8.9628 | .0365 | .0078 |

TABLE II.- MODEL SCALE FACTORS

| Parameter | Formula (a) | Scale factor (b) |
|---|---|---|
| Mach number | $V/\bar{c}$ | 1.0 |
| Structural frequency ratio | $\omega/\Omega$ | 1.0 |
| Advance ratio | $V/\Omega R$ | 1.0 |
| Lock number | $\rho a c R^4/I$ | 1.0 |
| Froude number | $\bar{c}^2/\ell$ | .85 |
| Reynolds number | $\rho\bar{c}\ell/\bar{\mu}$ | 3.67 |
| Length | $\ell$ | 6.0 |
| Structural stiffness | $\ell^4\rho\bar{c}^2$ | 2610.9 |
| Angular velocity | $\Omega$ | .376 |
| Linear velocity | $\bar{c}$ | 2.255 |
| Force | $\ell^2\rho\bar{c}^2$ | 72.52 |
| Moment | $\ell^3\rho\bar{c}^2$ | 435.1 |

[a] $\bar{c}$ is the ratio of speeds of sound in air and Freon-12; $\bar{\mu}$ is the ratio of coefficients of viscosity in air and Freon-12.

[b] Ratio of full-scale to model values based on length scale factor of 6.0 and Freon-12 test medium.

TABLE III.- STRUCTURAL PROPERTIES OF ROTOR MODEL

| Inboard station of segment r, m | Mass, kg/m | Structural stiffness, N-m$^2$ | | | Chordwise radius of gyration, m |
|---|---|---|---|---|---|
| | | Beamwise | Chordwise | Torsional | |
| 0 | ----- | ∞ | ∞ | ∞ | ------ |
| .076 | 7.592 | 22 384.6 | 22 385 | 2869.8 | 0.0183 |
| .174 | 1.634 | 174.2 | 4 611 | 168.7 | .0176 |
| .225 | .866 | 107.4 | 3 367 | 122.5 | .0155 |
| .253 | .364 | 57.1 | 1 813 | 66.0 | .0240 |
| .698 | .386 | 57.1 | 1 813 | 66.0 | .0237 |
| .945 | 1.840 | 57.1 | 1 813 | 66.0 | .0115 |
| 1.151 | 1.273 | 57.1 | 1 813 | 66.0 | .0128 |
| 1.218 | .539 | 89.5 | 2 847 | 103.6 | .0192 |
| 1.246 | .691 | 57.1 | 1 813 | 60.0 | .0192 |
| 1.288 | .364 | 33.4 | 1 074 | 38.7 | .0192 |
| 1.363 | .439 | 1.8 | 40 | 7.1 | .0193 |

TABLE IV.- MODEL BLADE ROTATING

NATURAL FREQUENCIES

| $\omega/\Omega$ | Mode identity |
|---|---|
| 0.30 | Chordwise |
| 1.04 | Beamwise |
| 3.67 | Beamwise |
| 6.24 | Beamwise |
| 8.91 | Chordwise |
| 11.00 | Torsion |

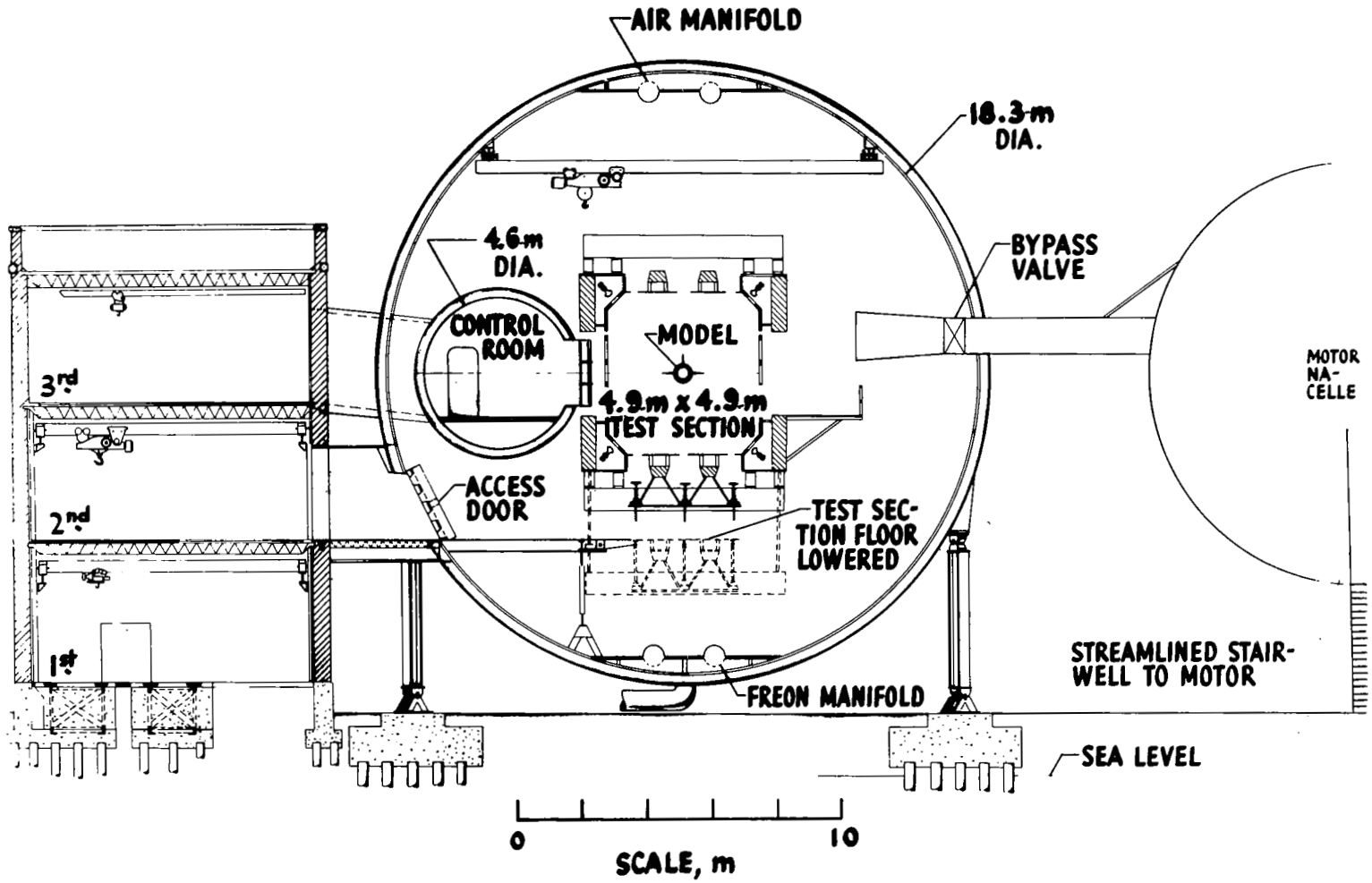


(a) Cross section.

Figure 1.- Major features of the NASA Langley transonic dynamics tunnel.

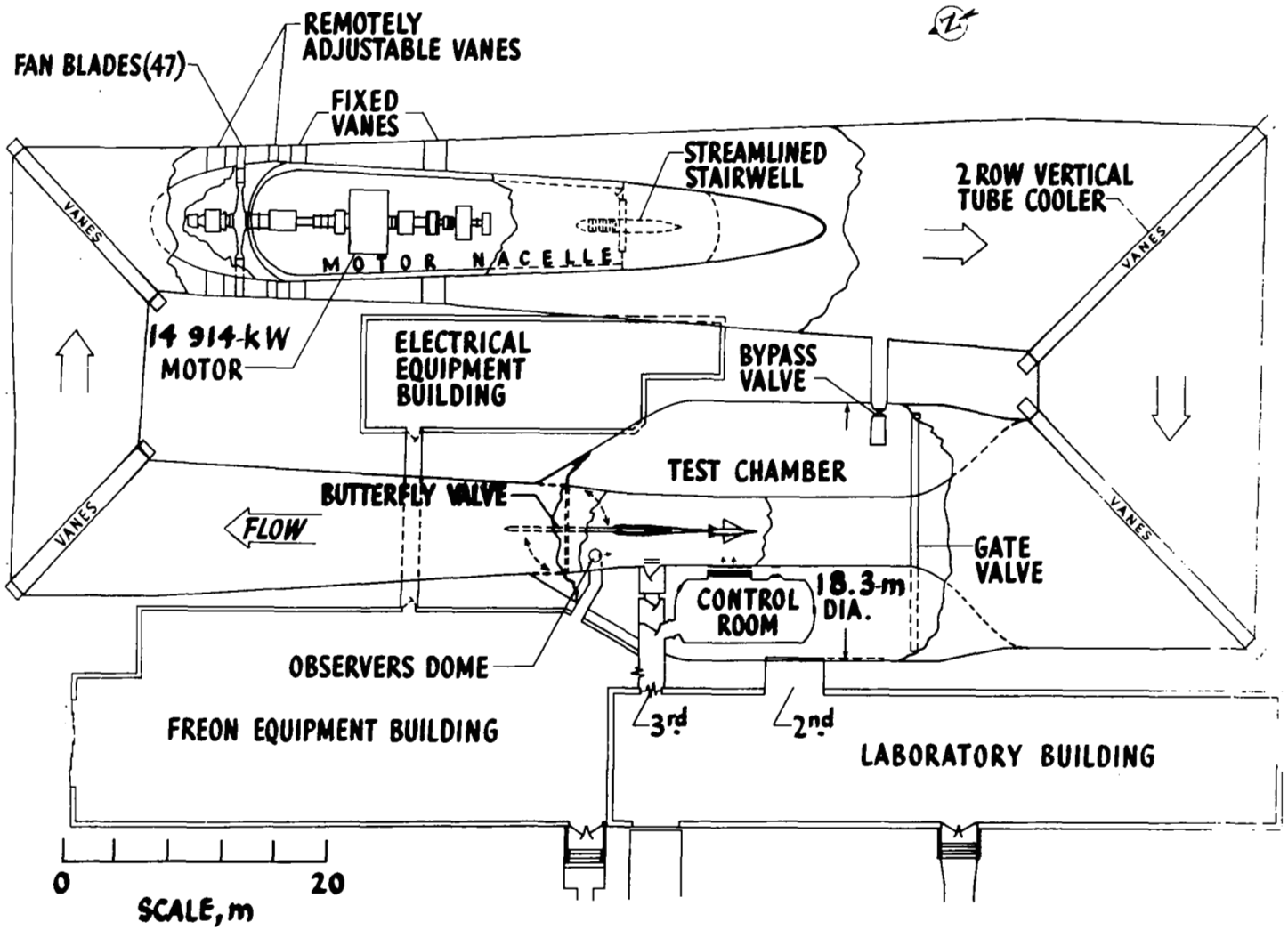


(b) Plan view.

Figure 1.- Concluded.

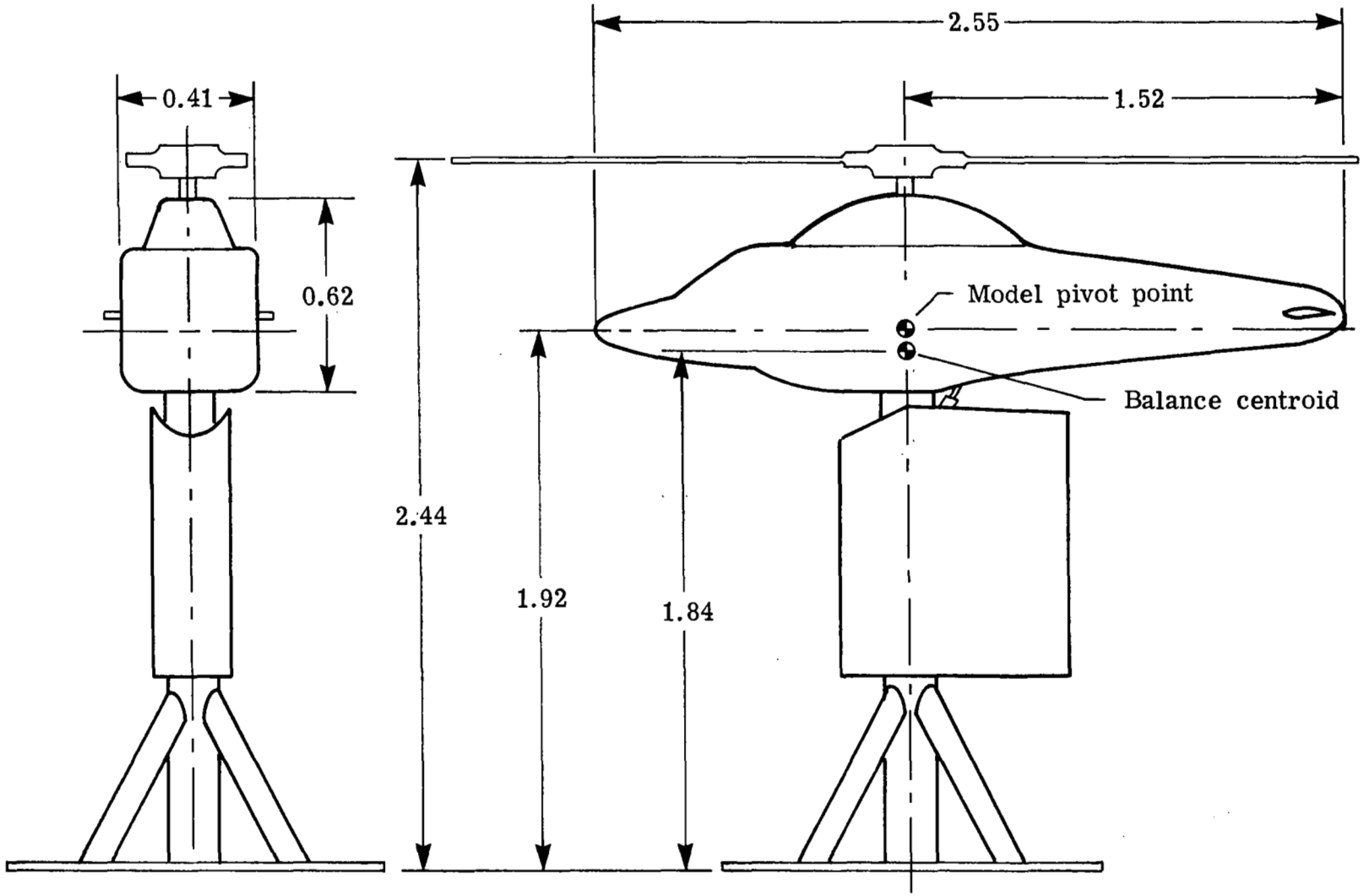


Figure 2.- Schematic diagram of aeroelastic rotor experimental system.
All dimensions are given in meters.

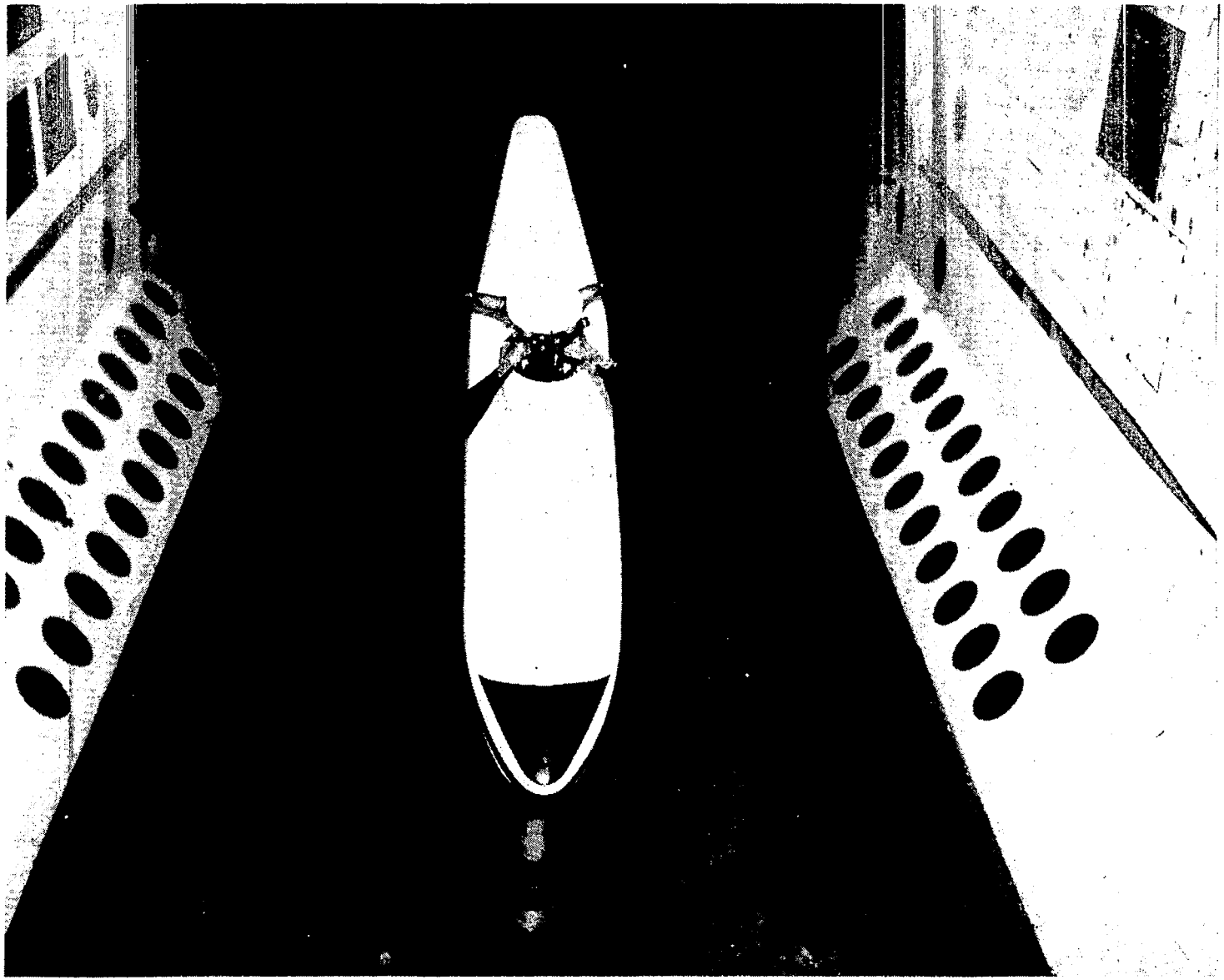

L-77-7526

Figure 3.- Rotor model mounted on aeroelastic rotor experimental system.

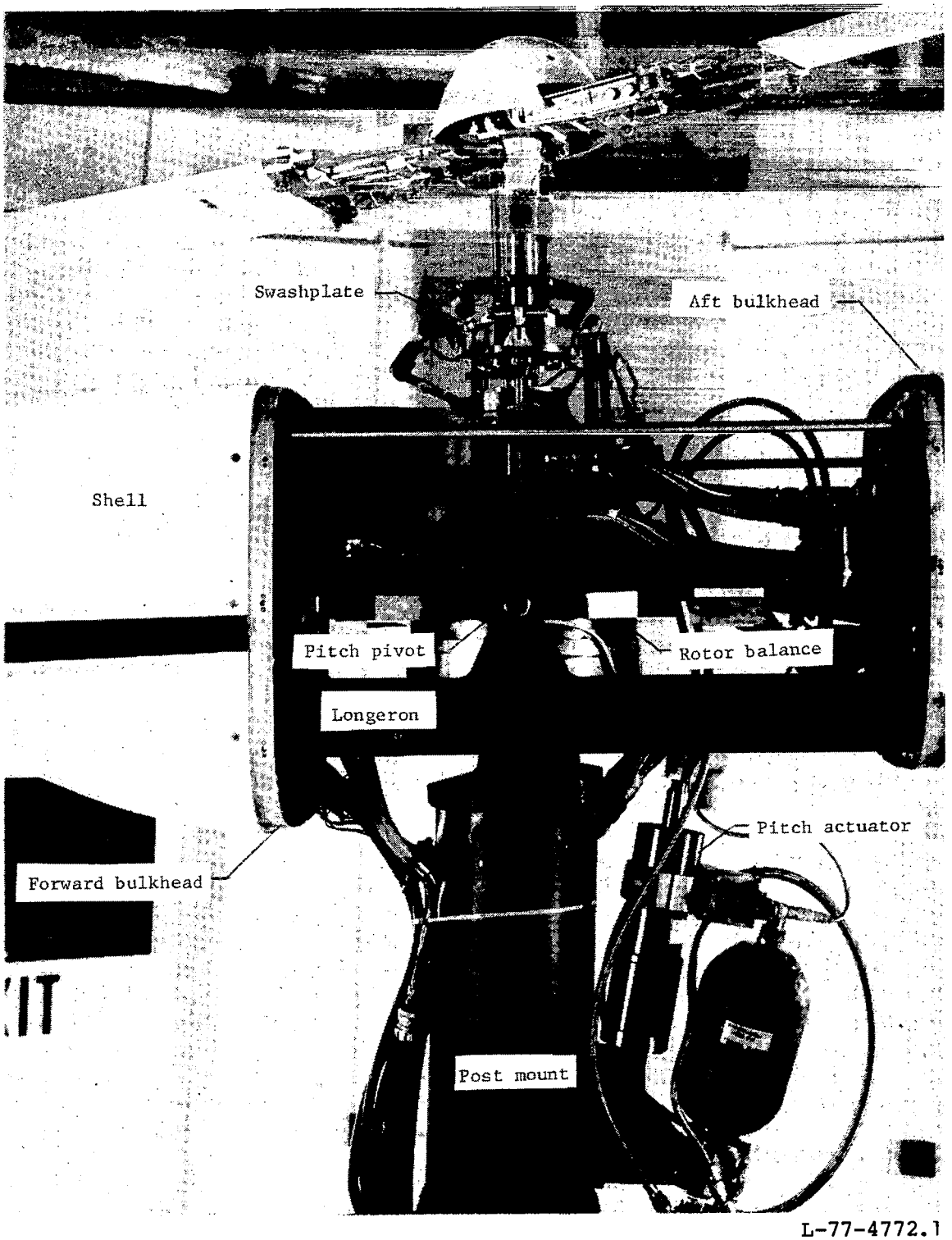


Figure 4.- Detailed view of aeroelastic rotor experimental system.

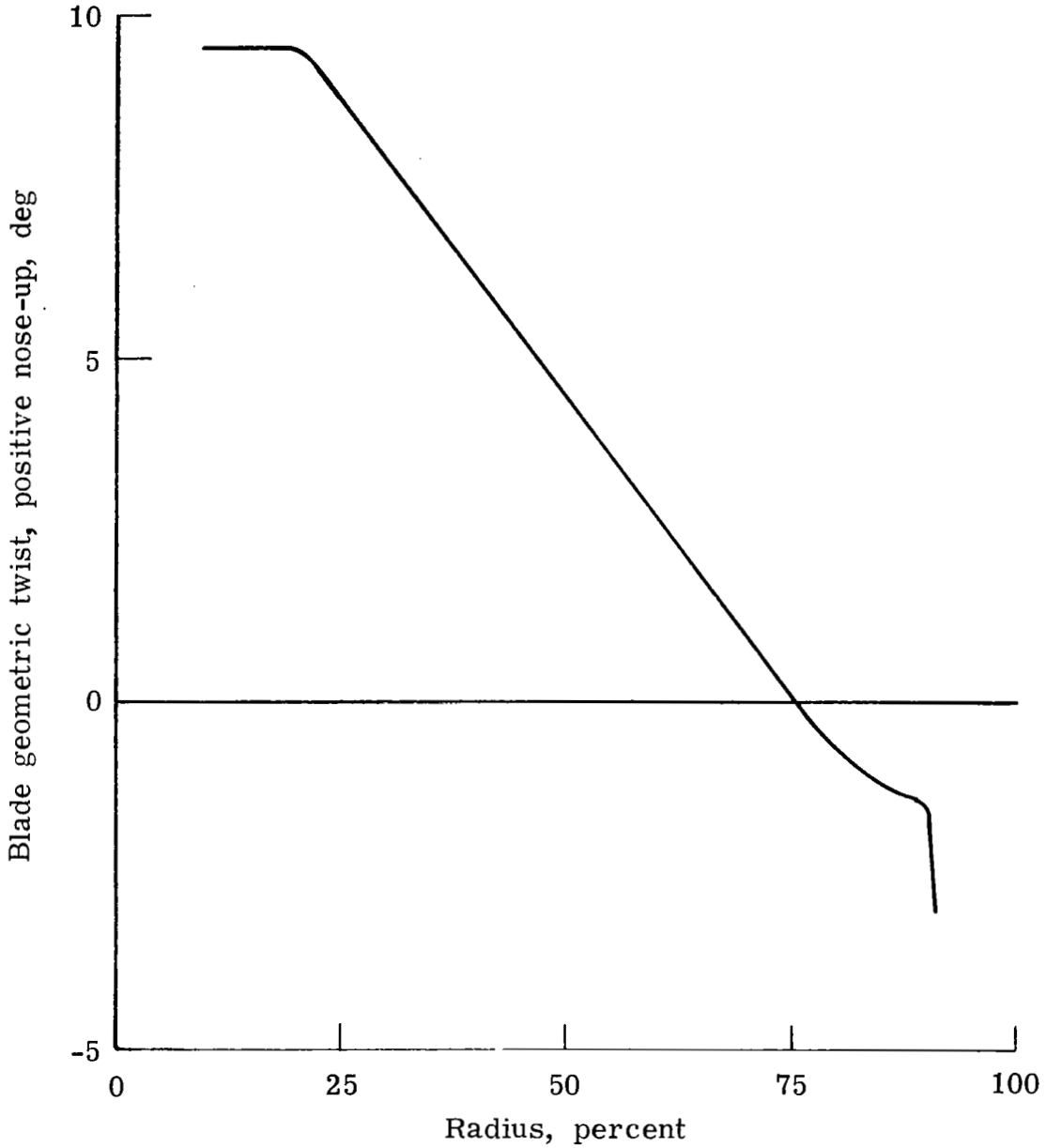


(a) Inboard of tip attachment point (x = 0.91).

Figure 5.- Model blade spanwise twist distribution.

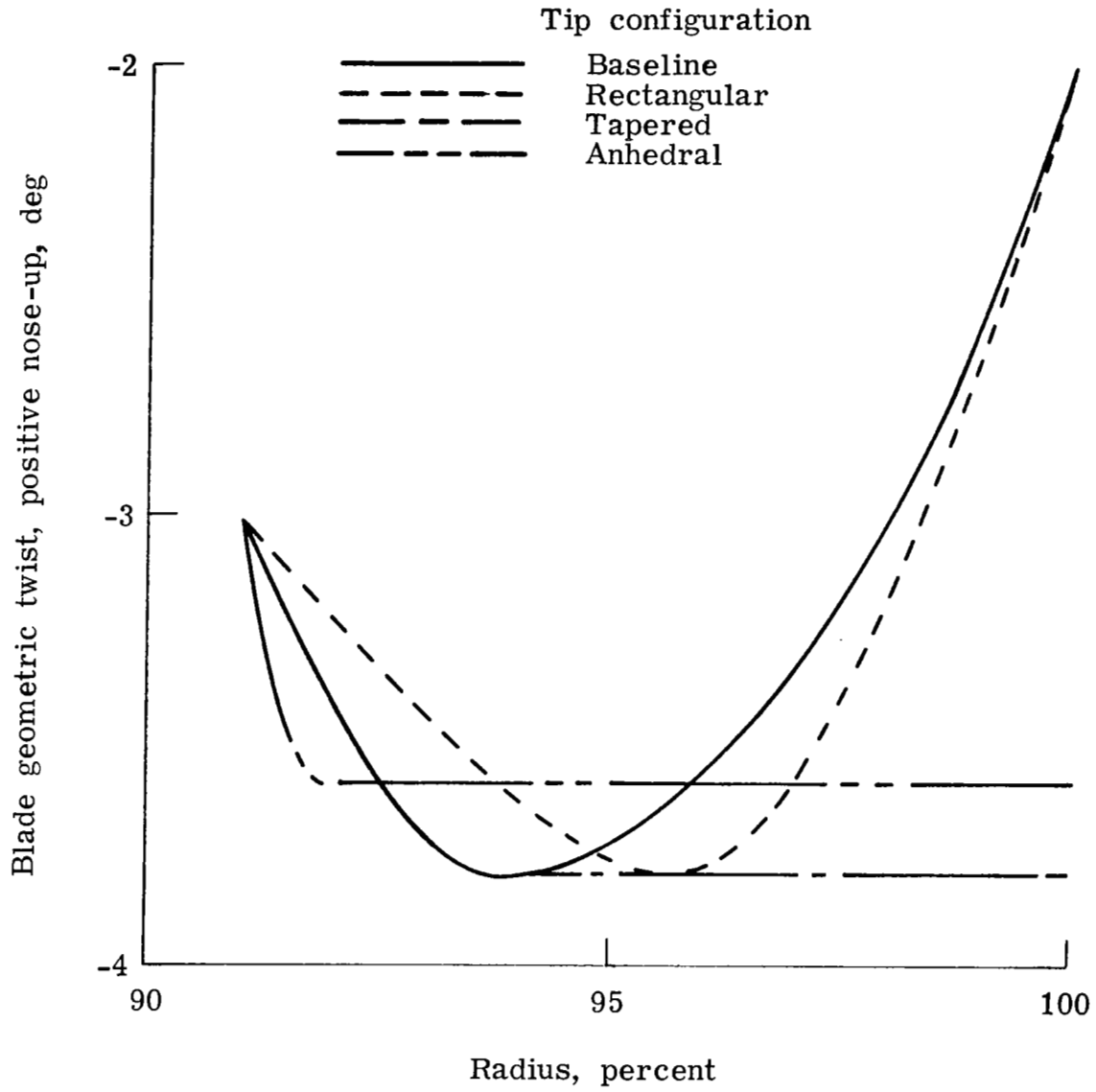


(b) Outboard of tip attachment point (x = 0.91).

Figure 5.- Concluded.

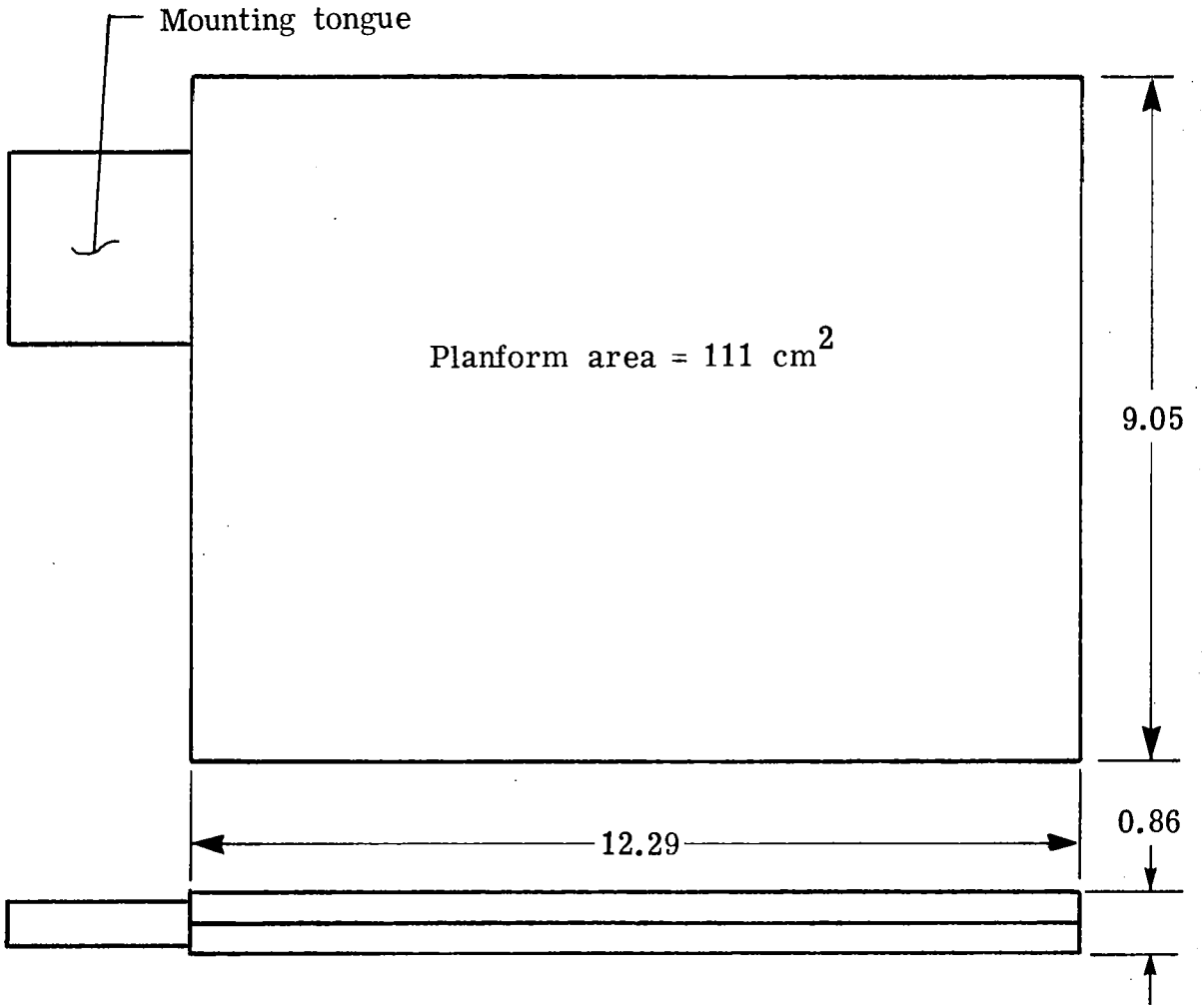


(a) Rectangular tip.

Figure 6.- Schematic diagrams of four blade tip configurations. All dimensions are given in centimeters.

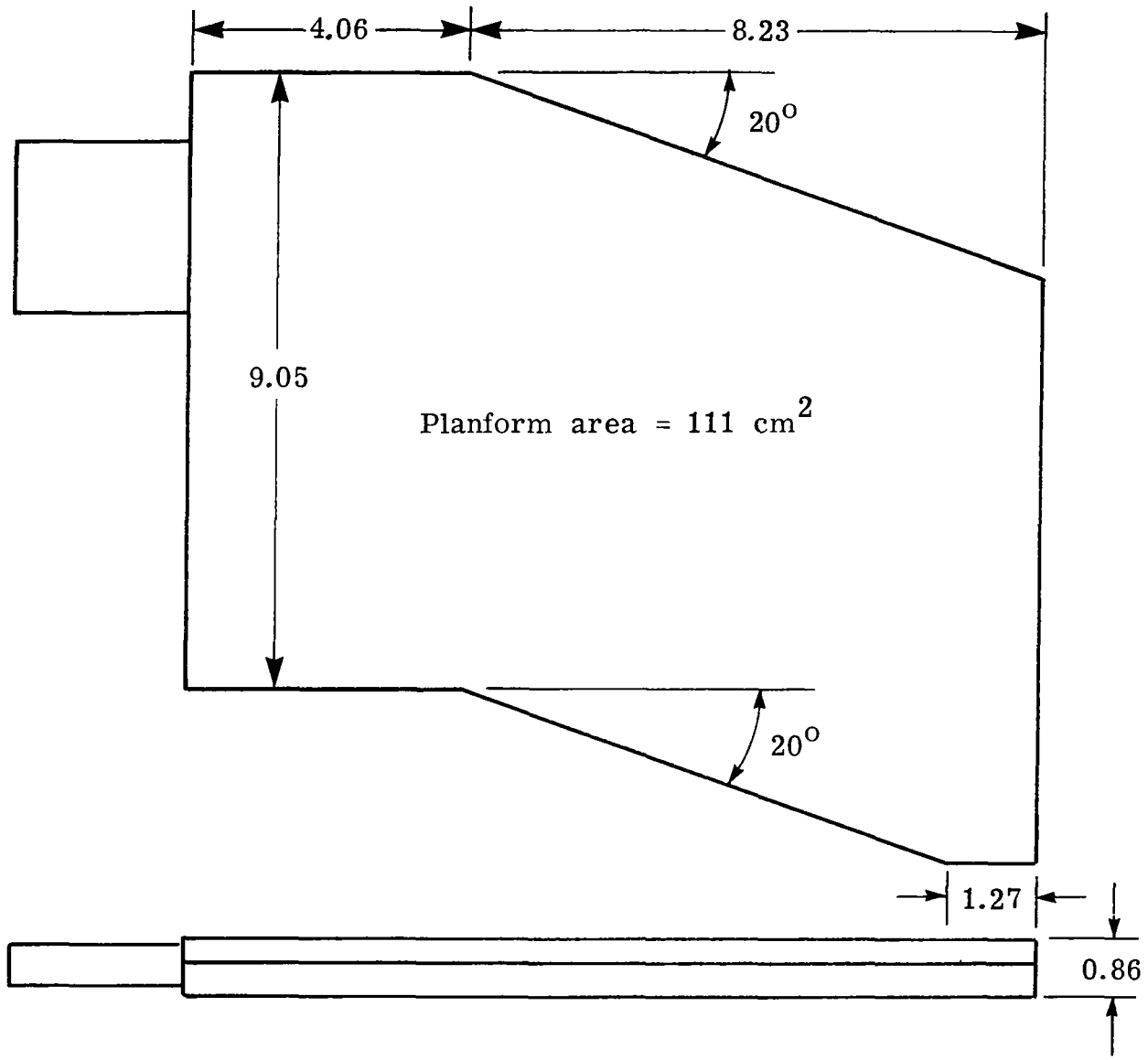


(b) Baseline tip.

Figure 6.- Continued.

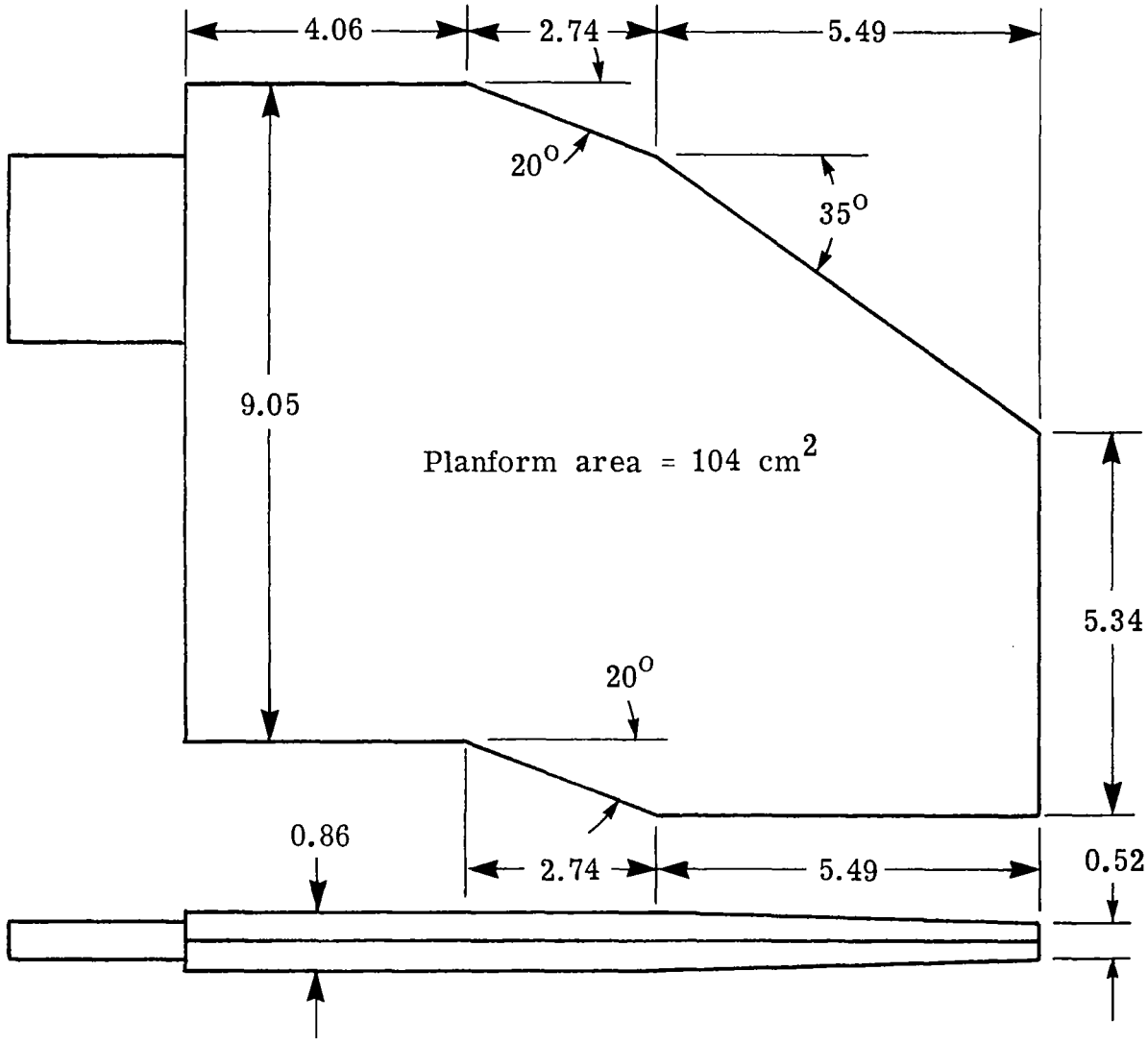


(c) Tapered tip.

Figure 6.- Continued.

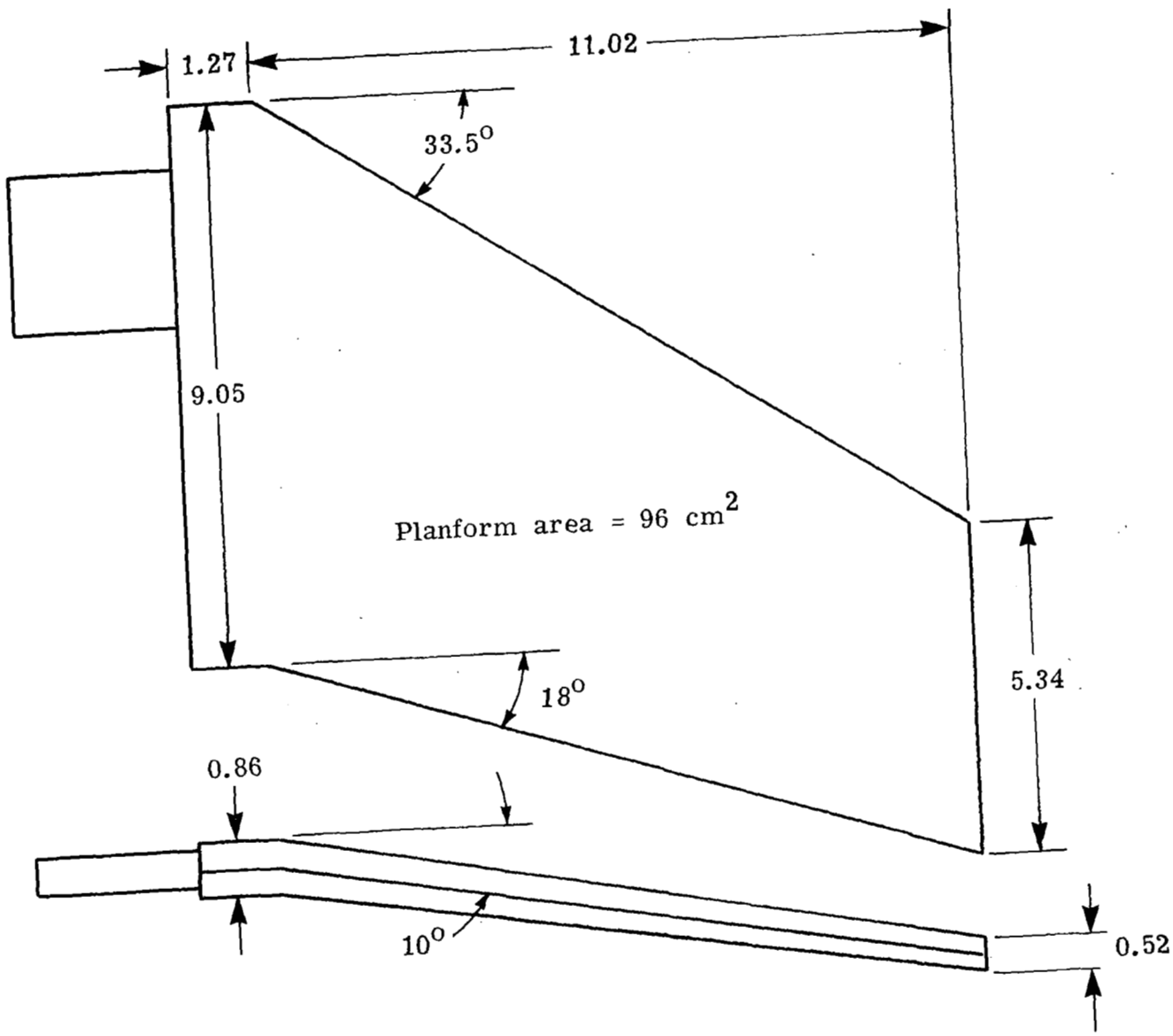


(d) Anhedral tip.

Figure 6.- Concluded.

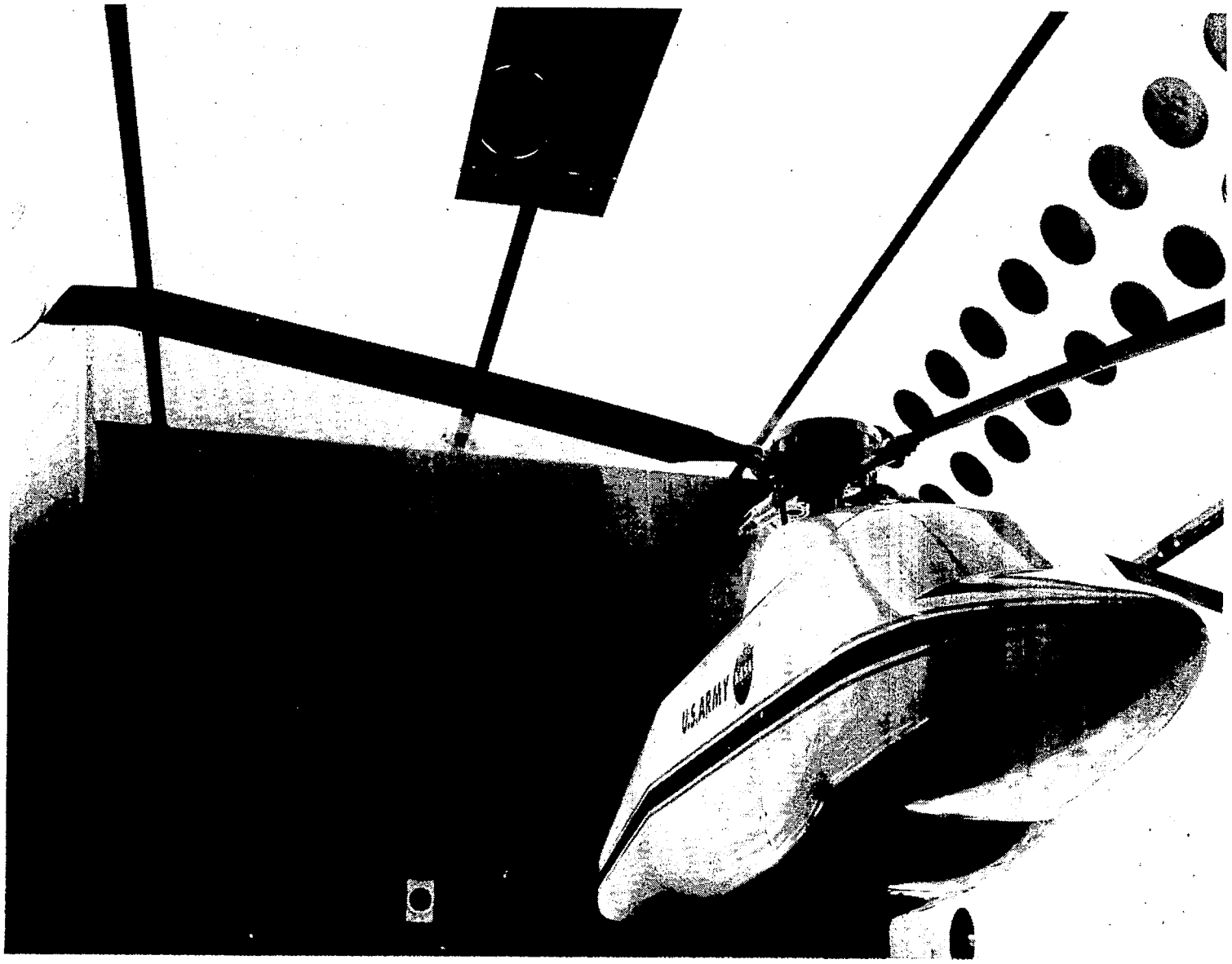


L-77-6985

Figure 7.- Model rotor with baseline tips installed.

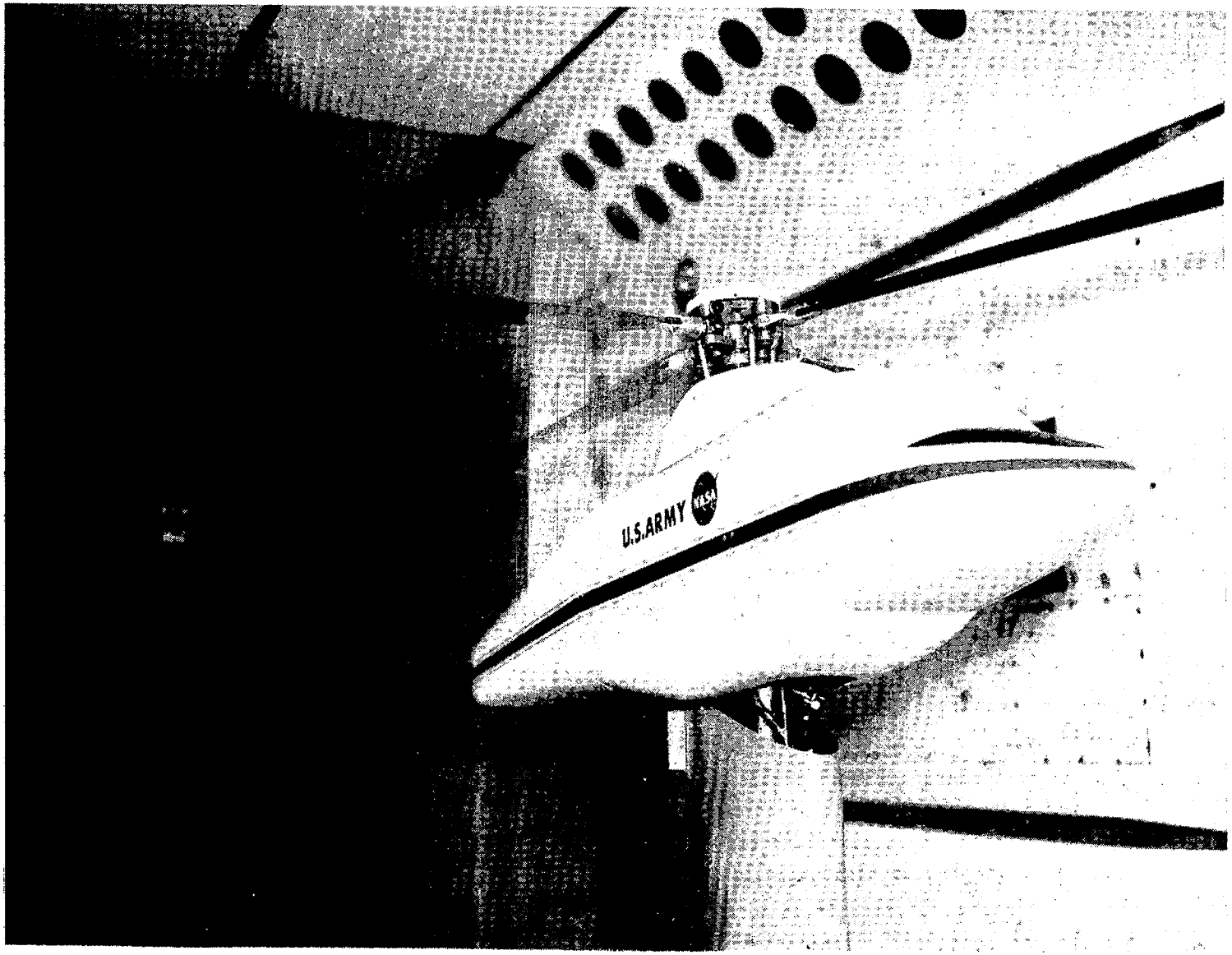


L-77-7530

Figure 8.- Model rotor with anhedral tips installed.

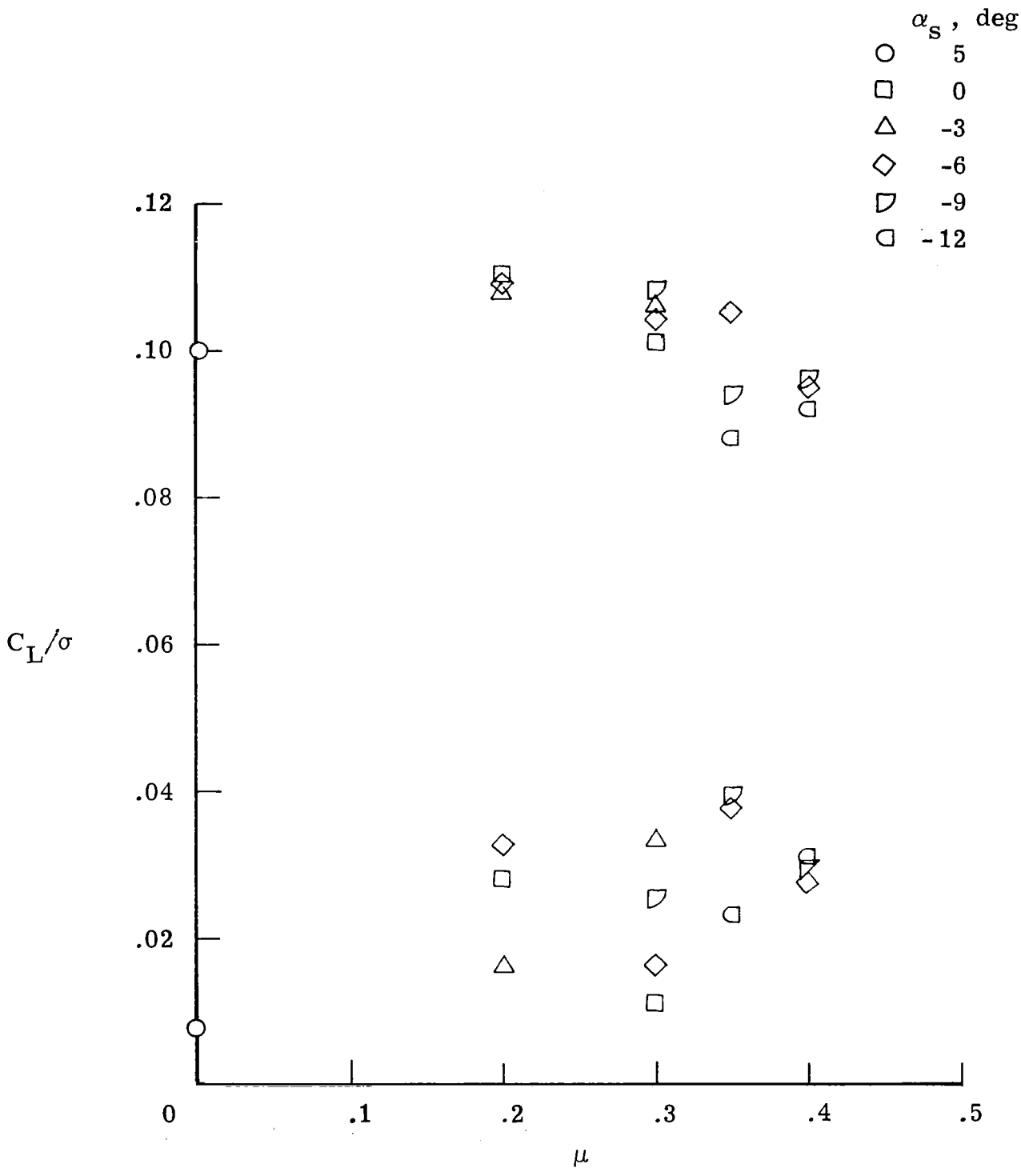


Figure 9.- Maximum and minimum values of $C_L/\sigma$ achieved during tests of rectangular tip configuration.

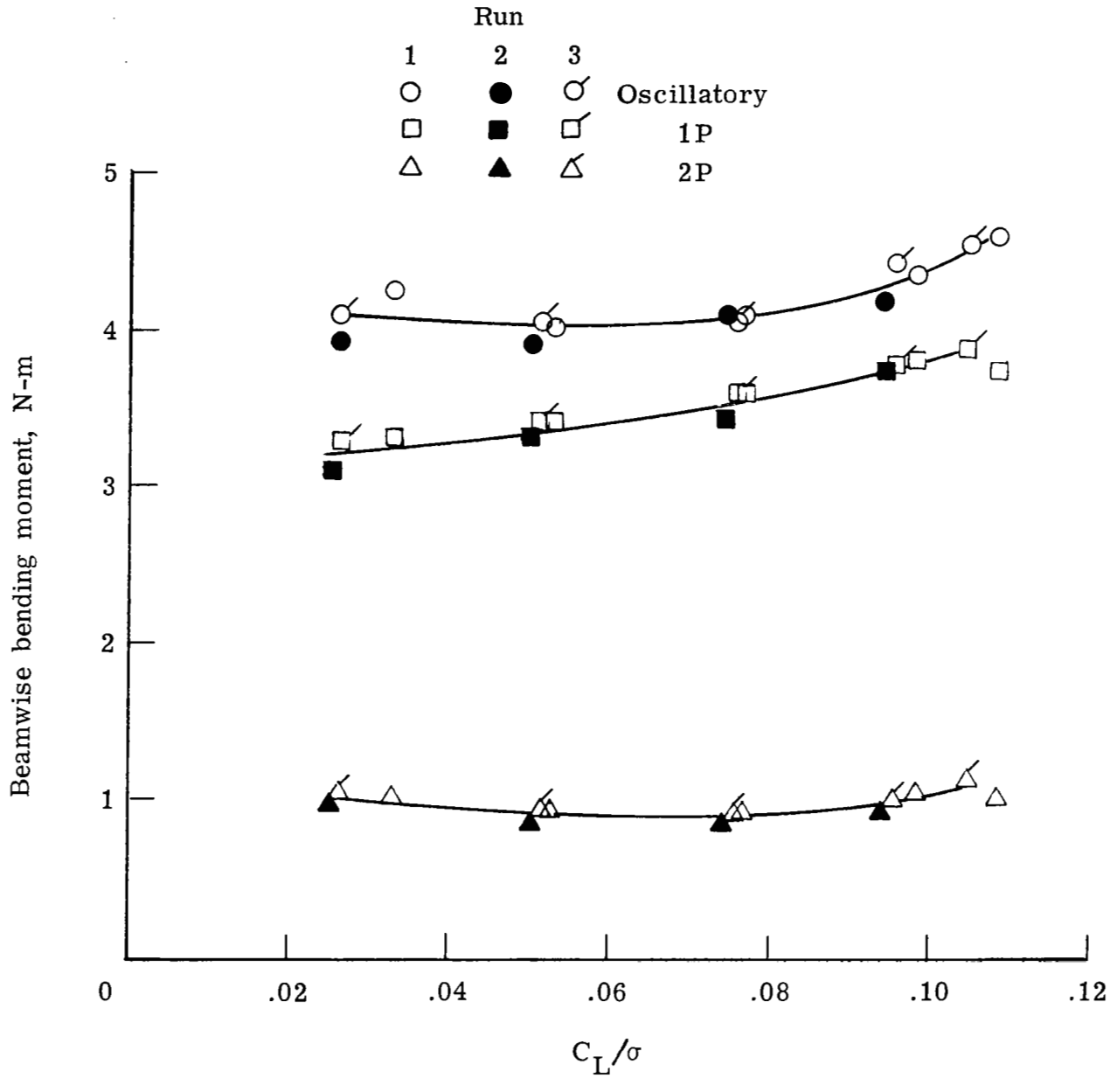


(a) Beamwise bending at x/R = 0.60.

Figure 10.- Measured dynamic-response repeatability for the rectangular blade tip configuration. $\mu = 0.3$; $\alpha_s = -9^\circ$.

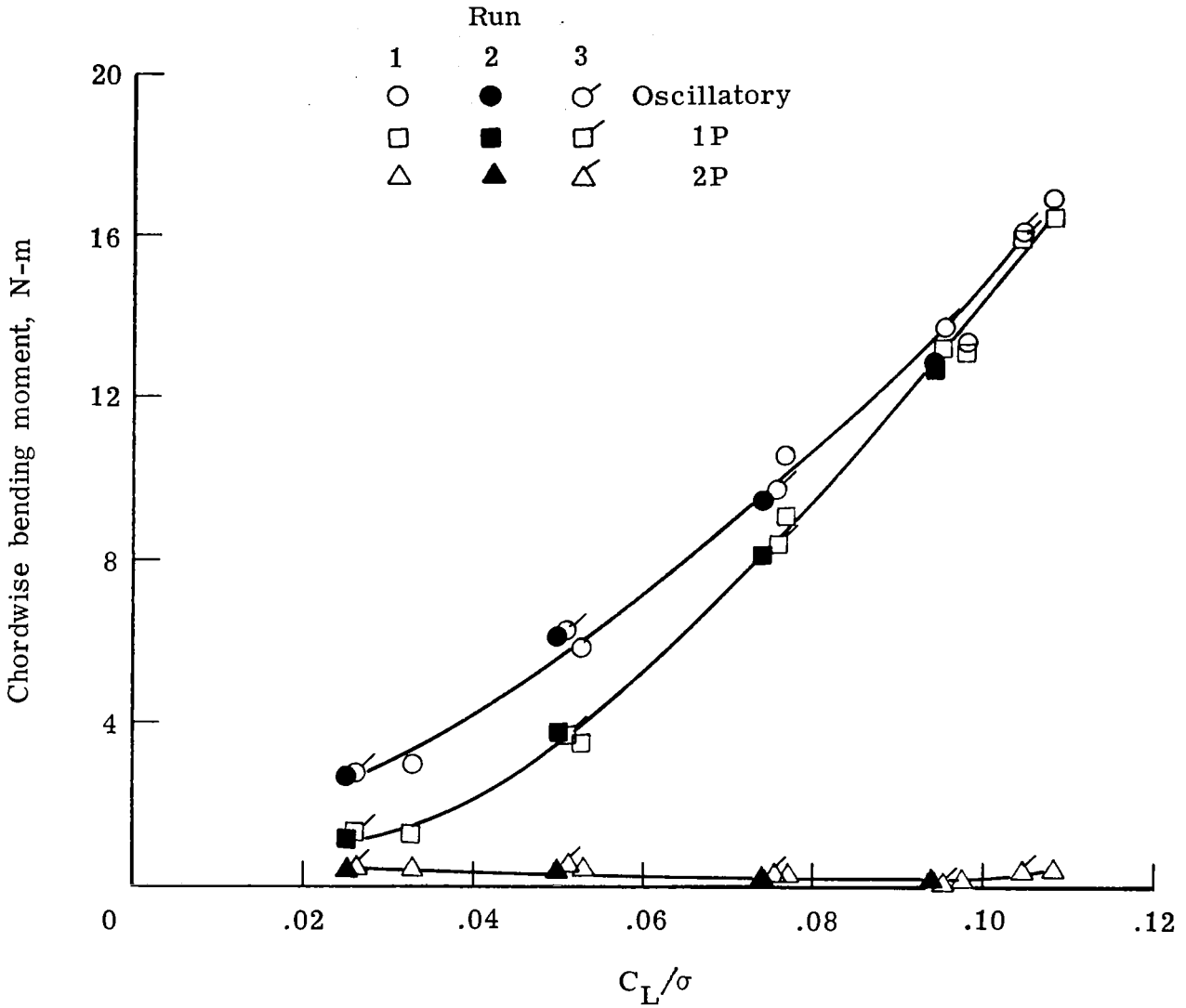


(b) Chordwise bending at x/R = 0.22.

Figure 10.- Continued.

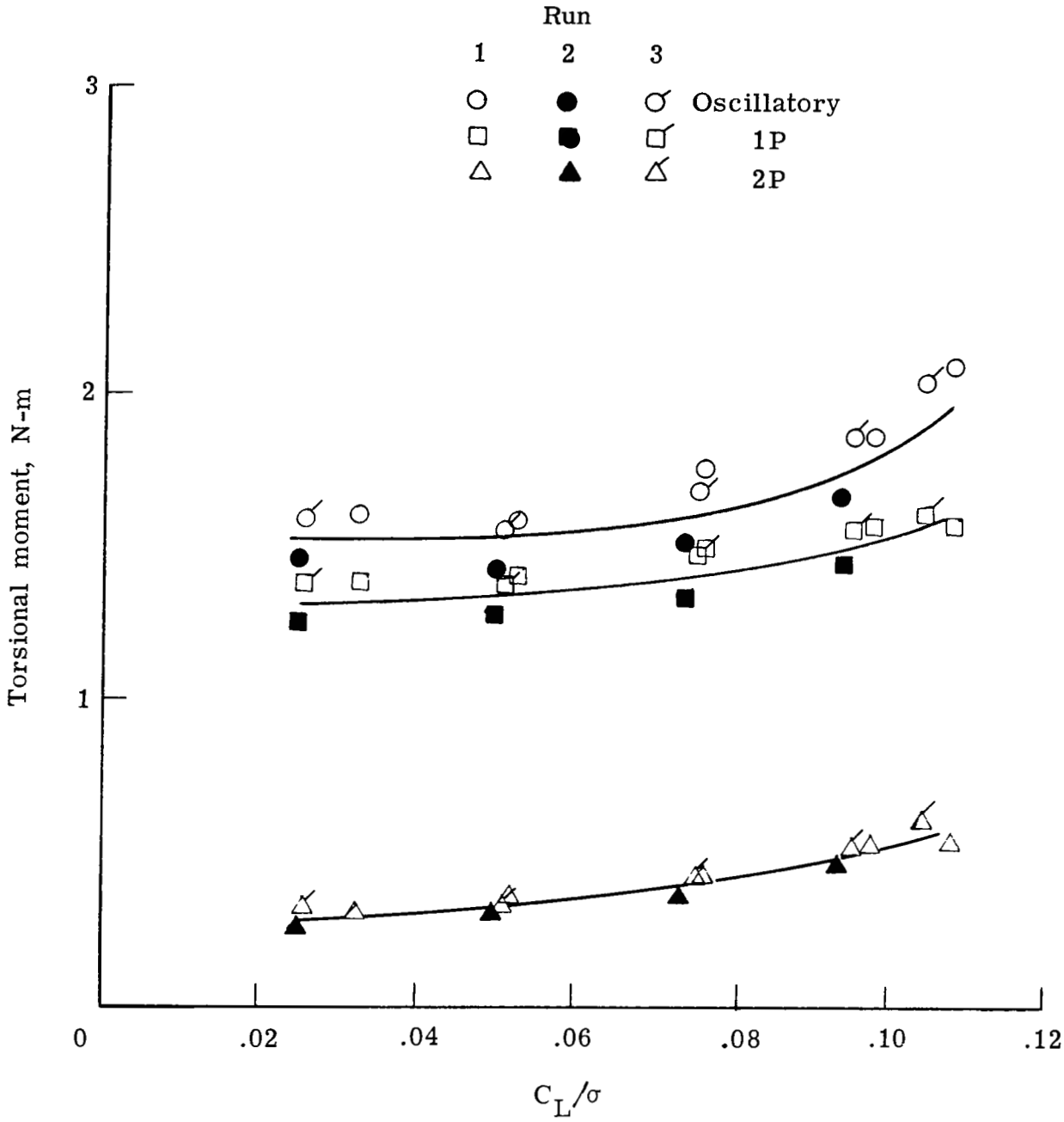


(c) Torsion at x/R = 0.41.

Figure 10.- Concluded.

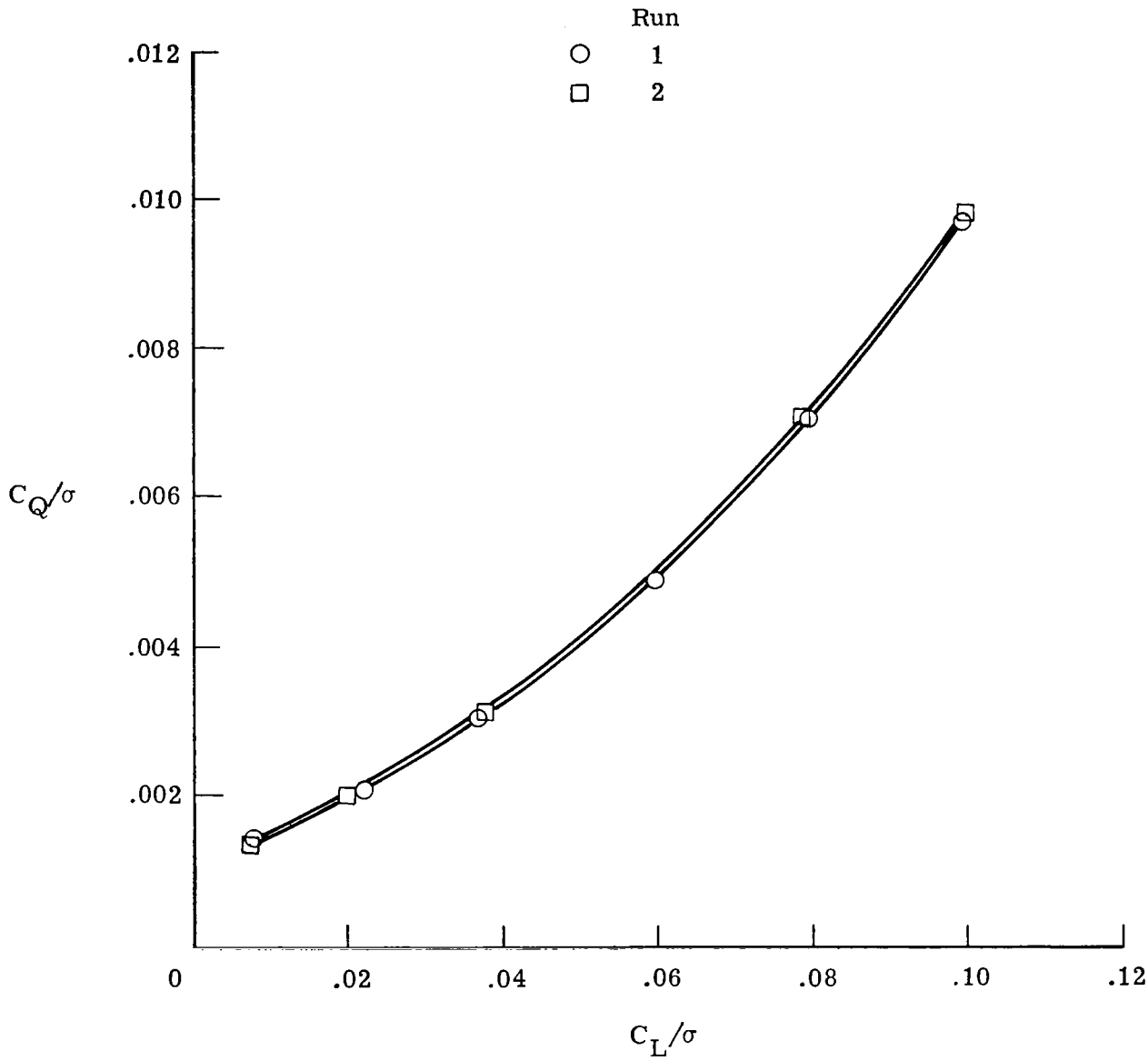


(a) $\mu = 0.0$ (in ground effect); $\alpha_s = 0.5^o$.

Figure 11.- Measured performance repeatability for the rectangular blade tip configuration.

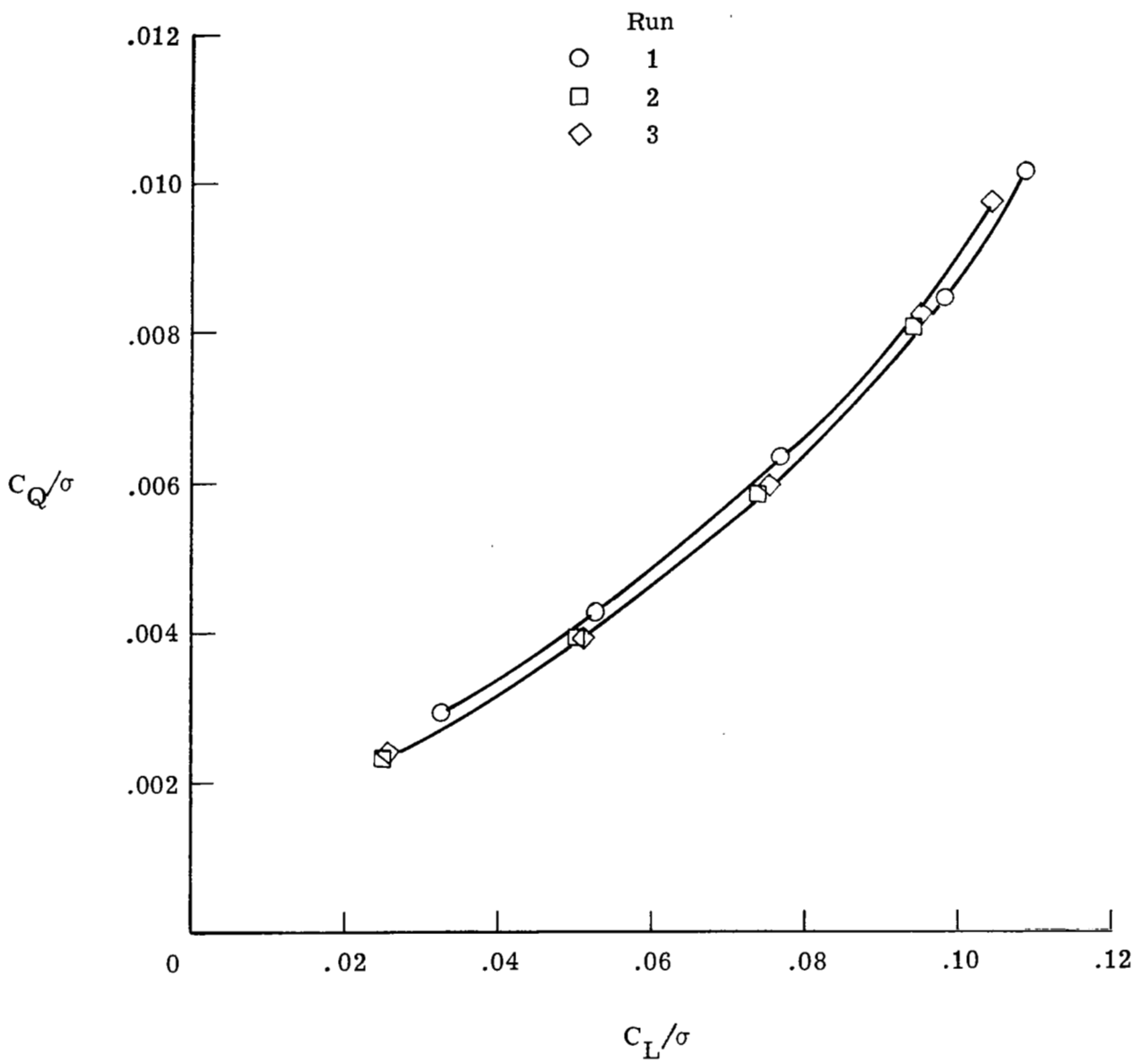


(b) $\mu = 0.3$; $\alpha_s = -9^\circ$.

Figure 11.- Concluded.

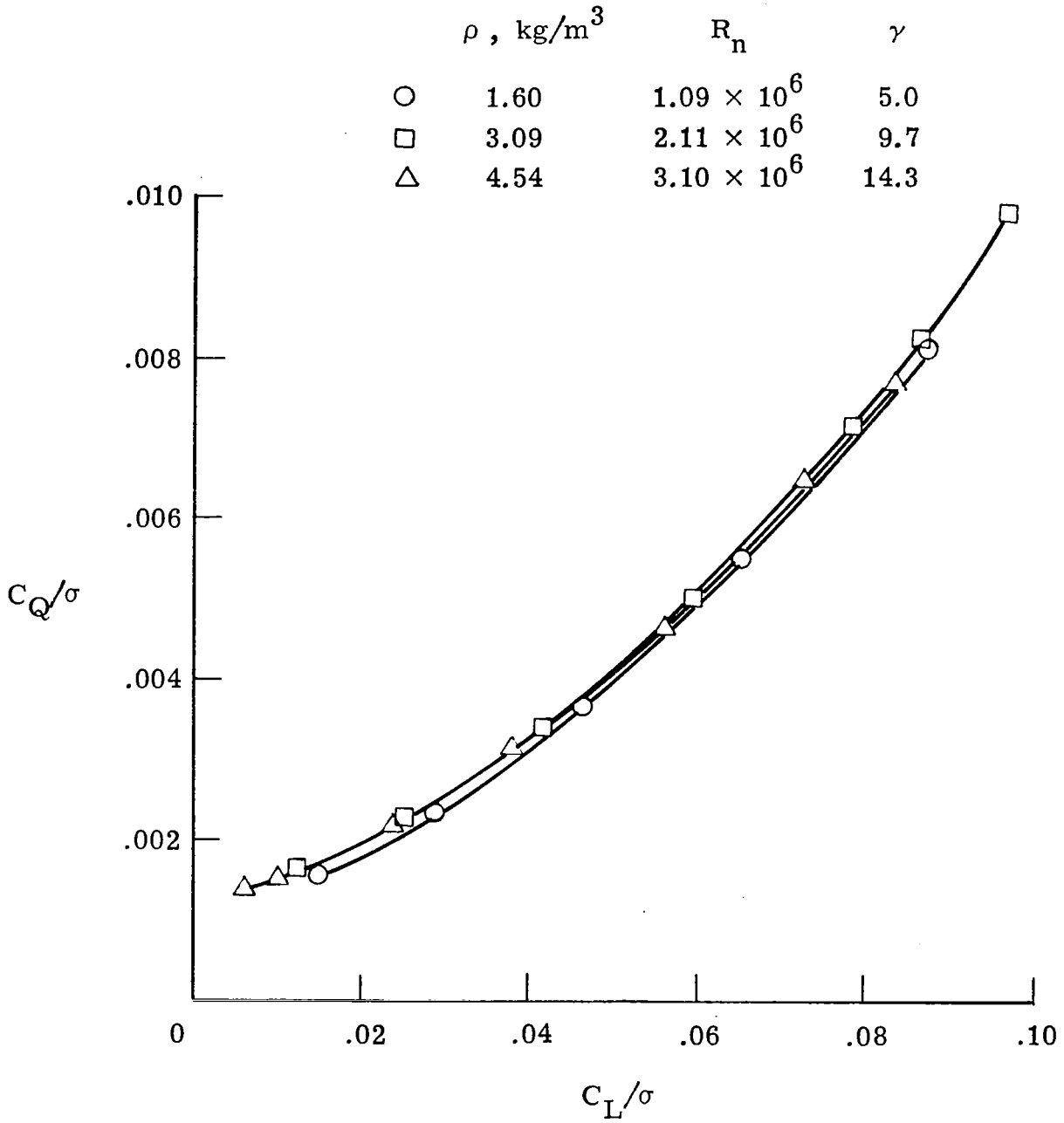


Figure 12.- Variation of rotor power with Reynolds number for the tapered tip configuration in ground-effect hover. $\alpha_s = 5^o$.

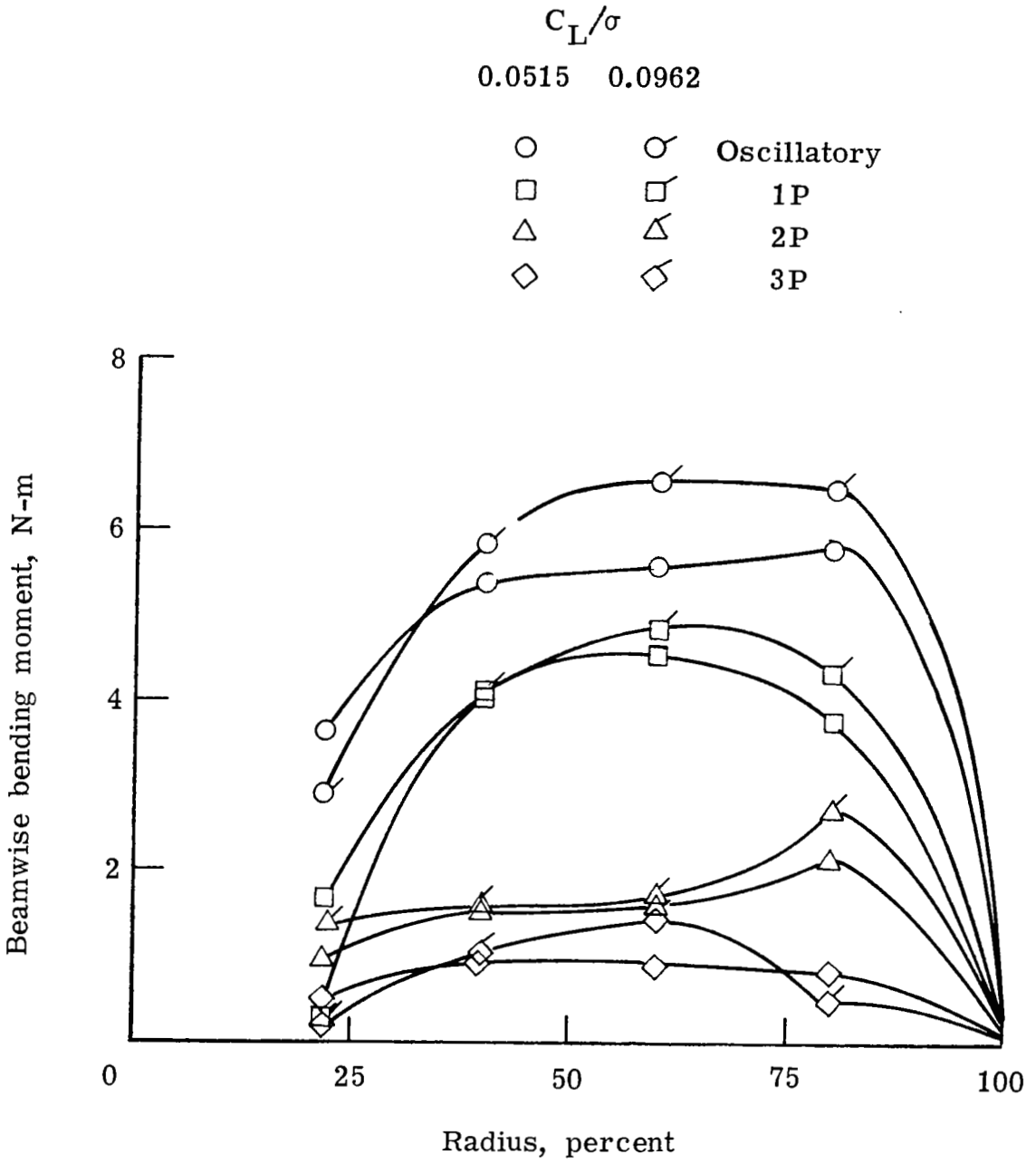


(a) Beamwise bending.

Figure 13.- Spanwise moment distributions measured on the rectangular tip configuration at two lift conditions. $\mu = 0.4$; $\alpha_s = -9^o$.

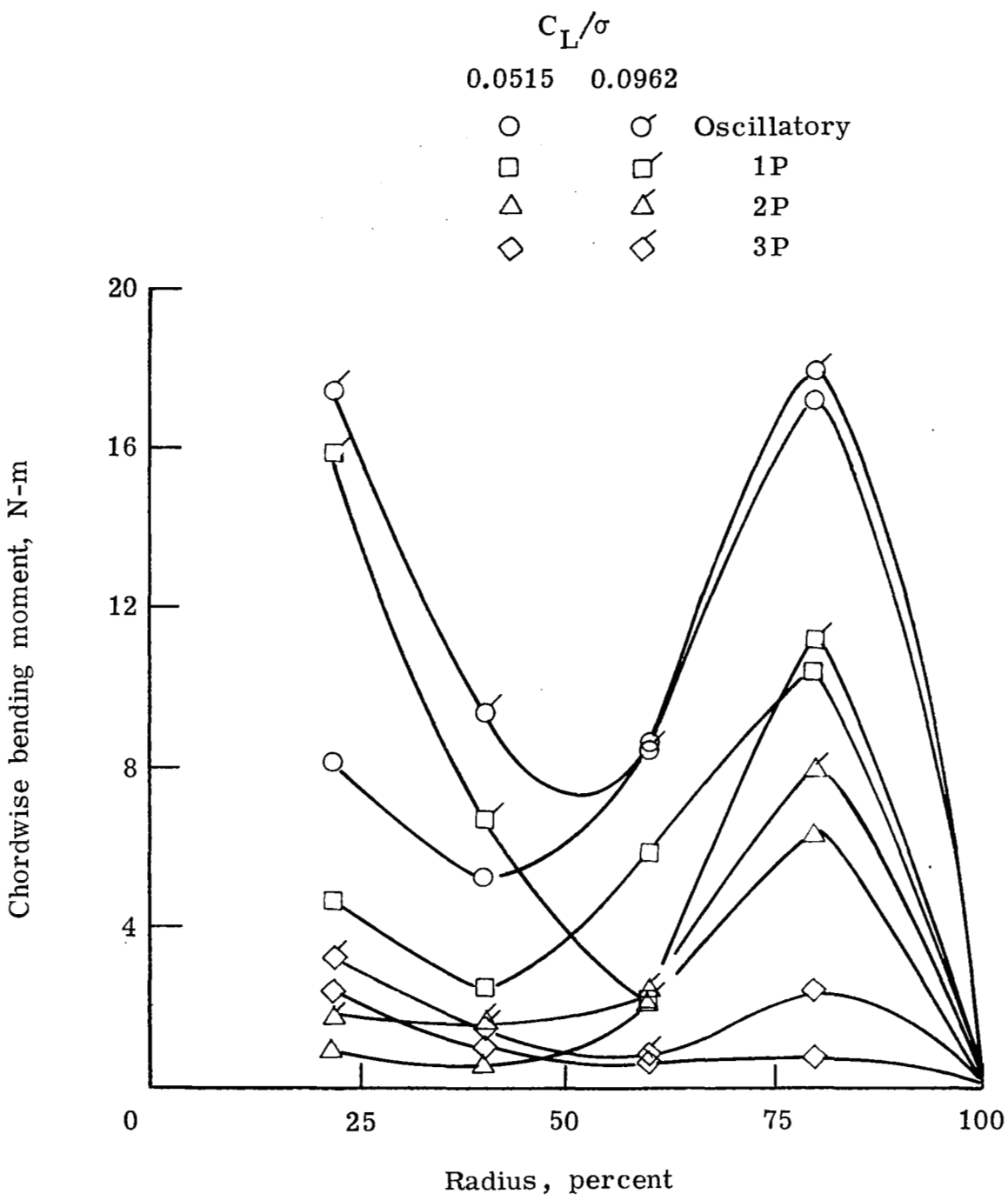


(b) Chordwise bending.

Figure 13.- Continued.

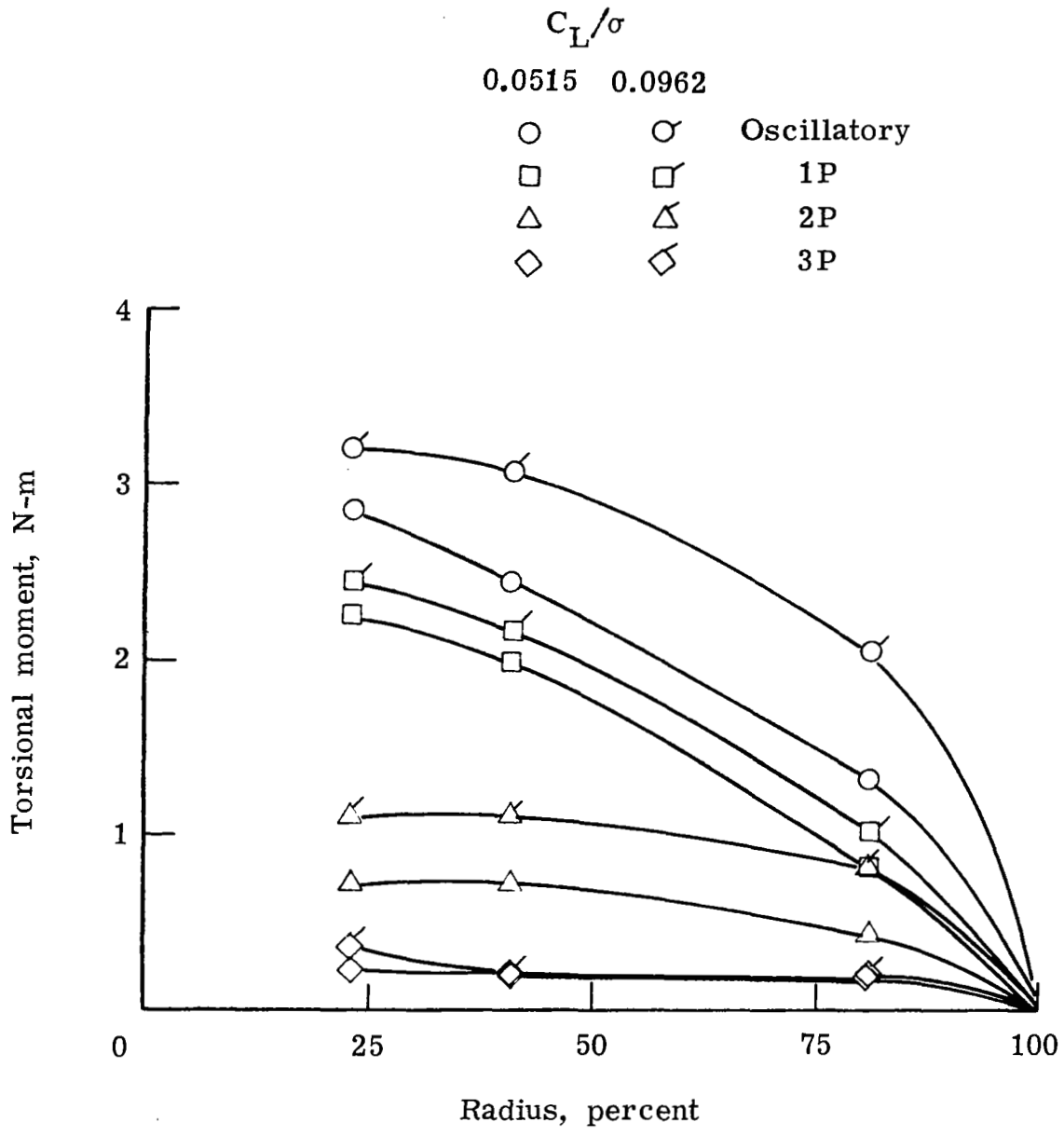


(c) Torsional moment.

Figure 13.- Concluded.

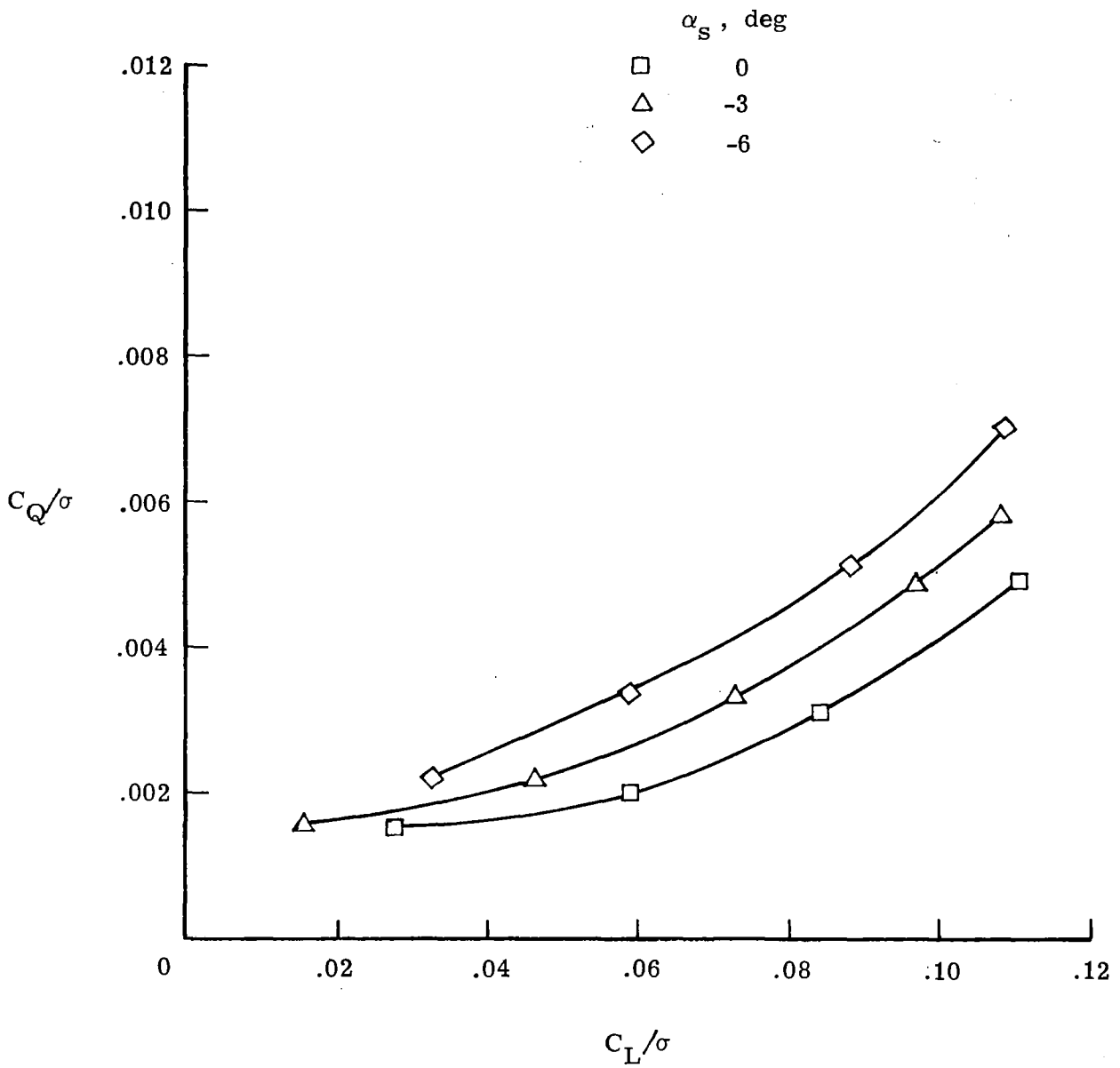


(a) $\mu = 0.2$.

Figure 14.- Variation of rotor torque and lift for the rectangular tip configuration.

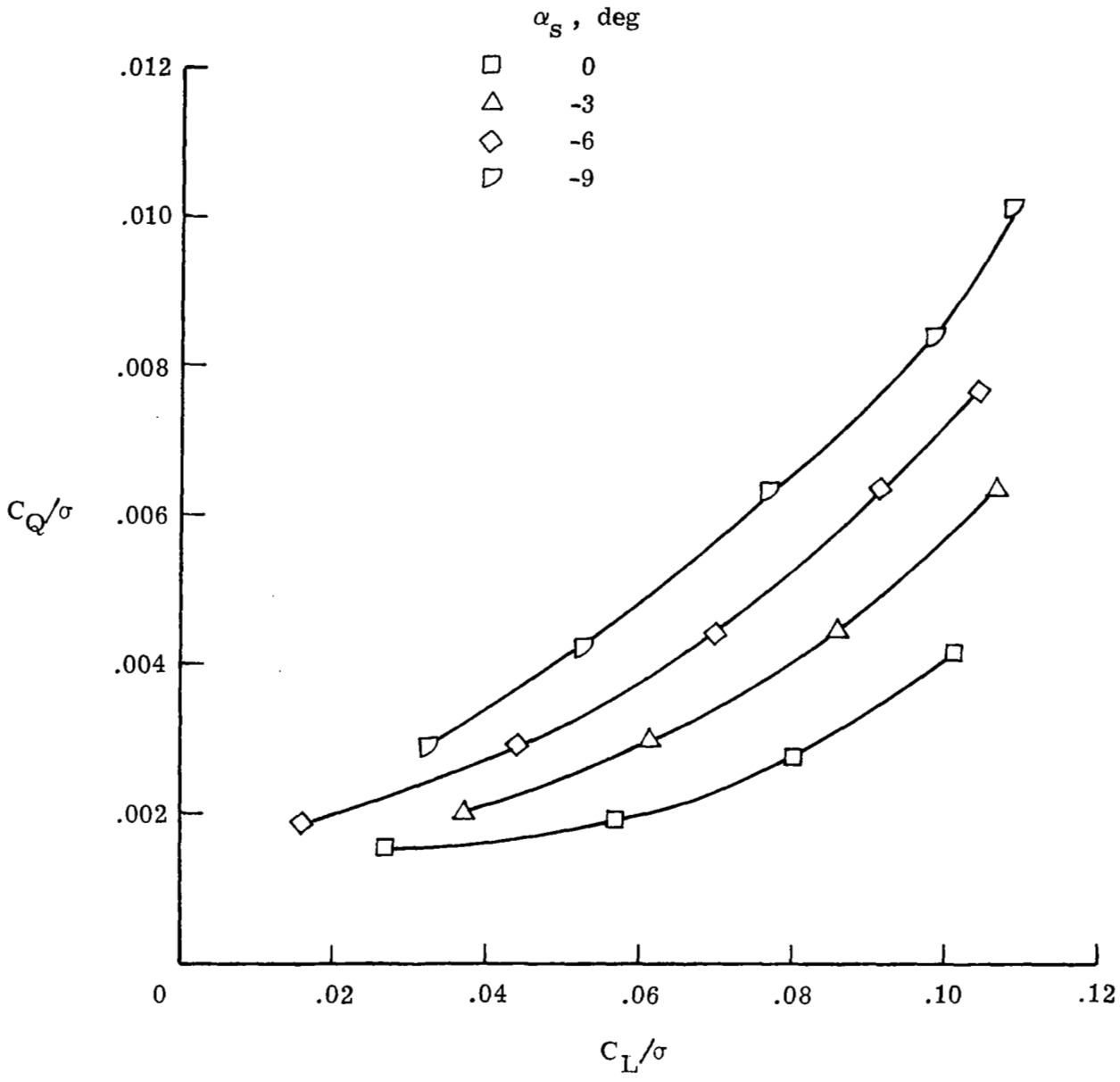


(b) $\mu = 0.3$.

Figure 14.- Continued.

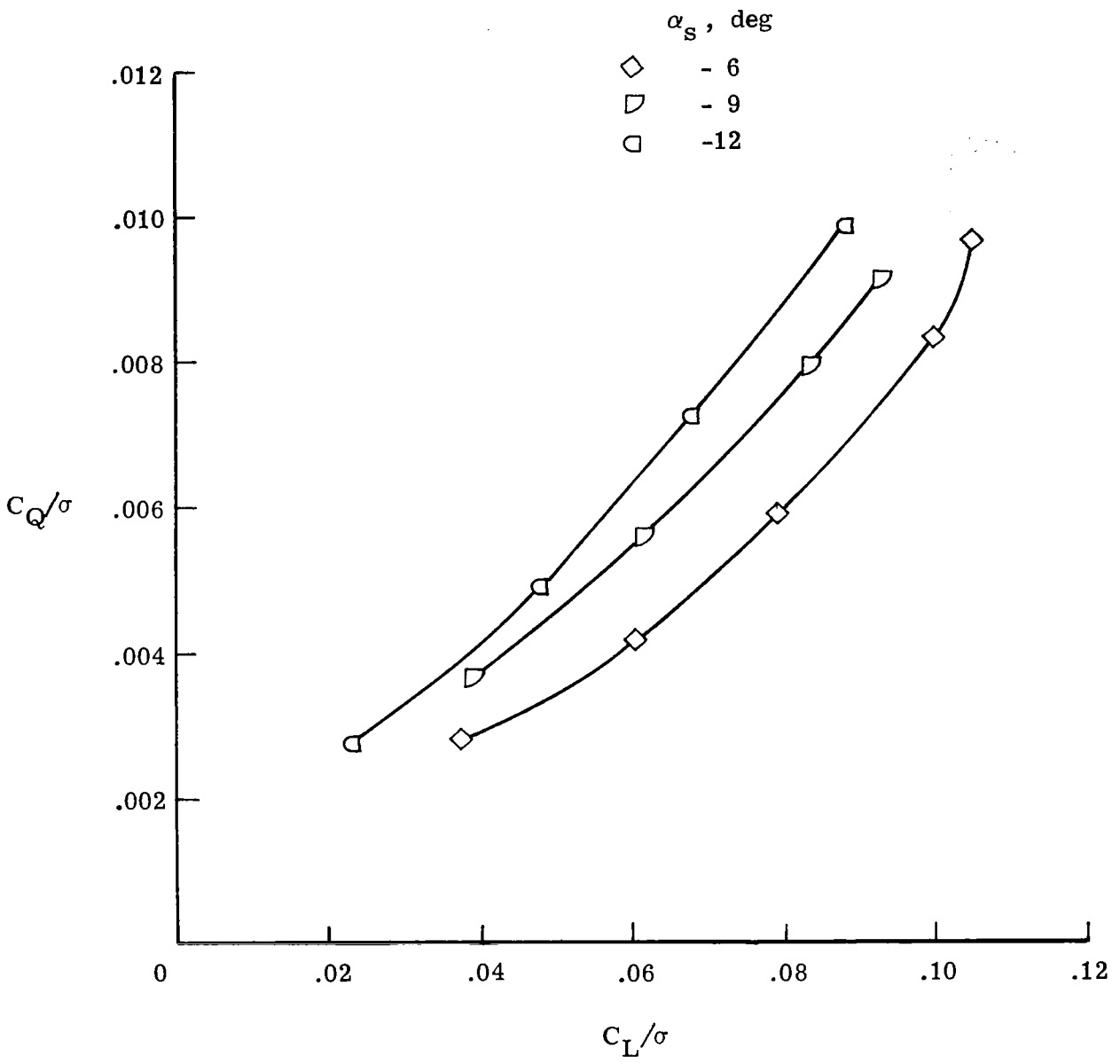


(c) $\mu = 0.35$.

Figure 14.- Continued.

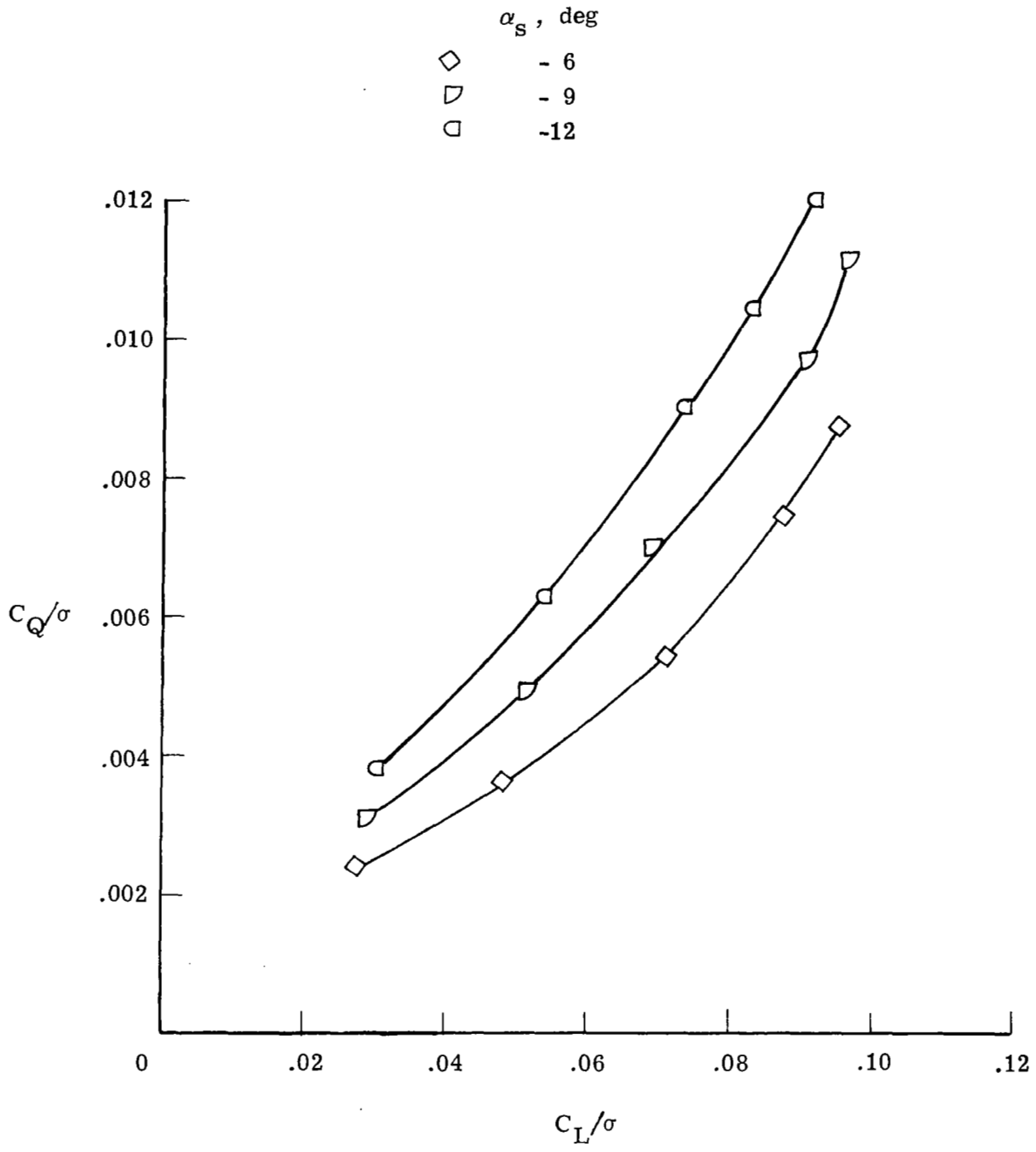


(d) $\mu = 0.4$.

Figure 14.- Concluded.

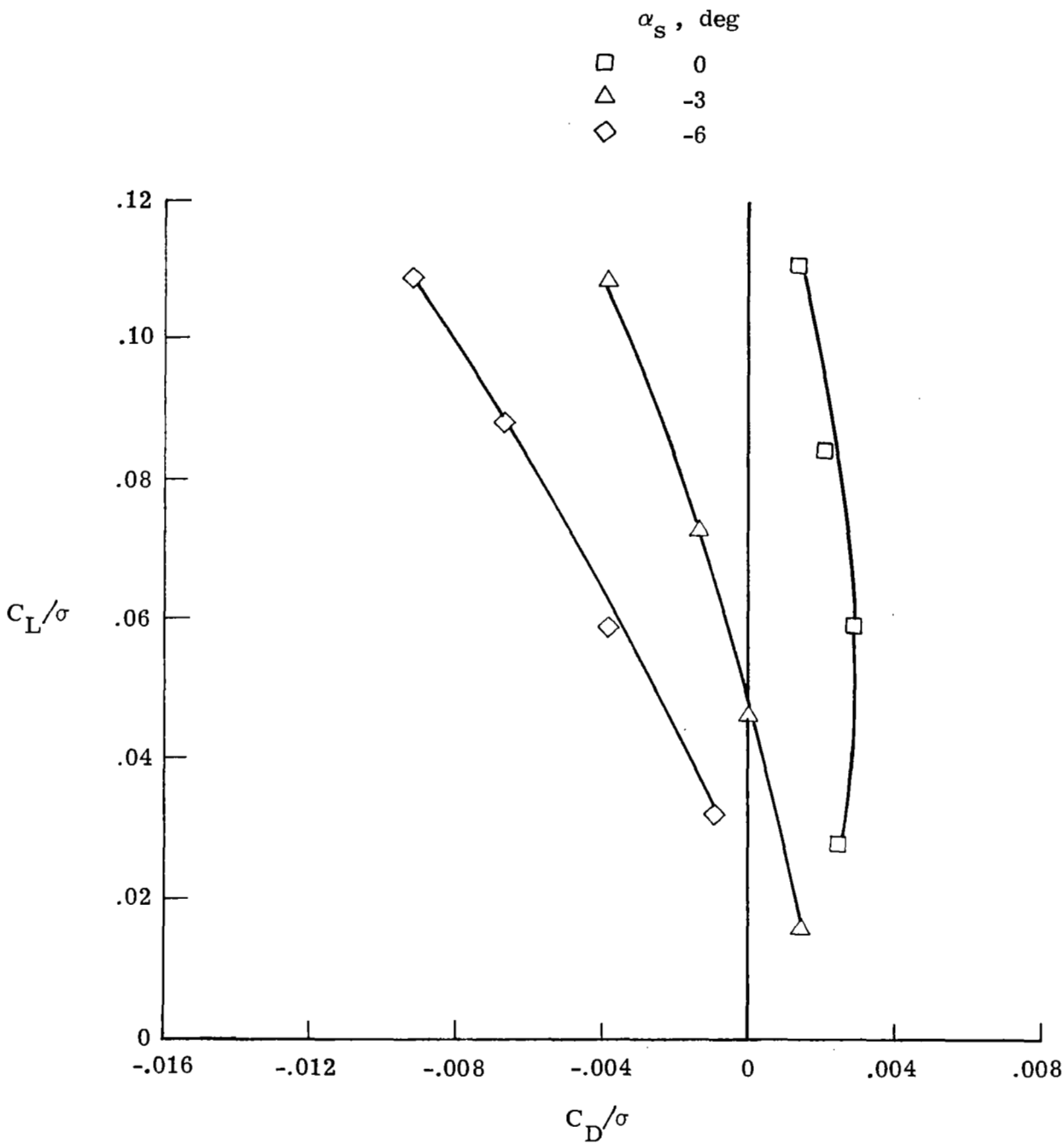


(a) $\mu = 0.2$.

Figure 15.- Variation of rotor lift and drag for the rectangular tip configuration.

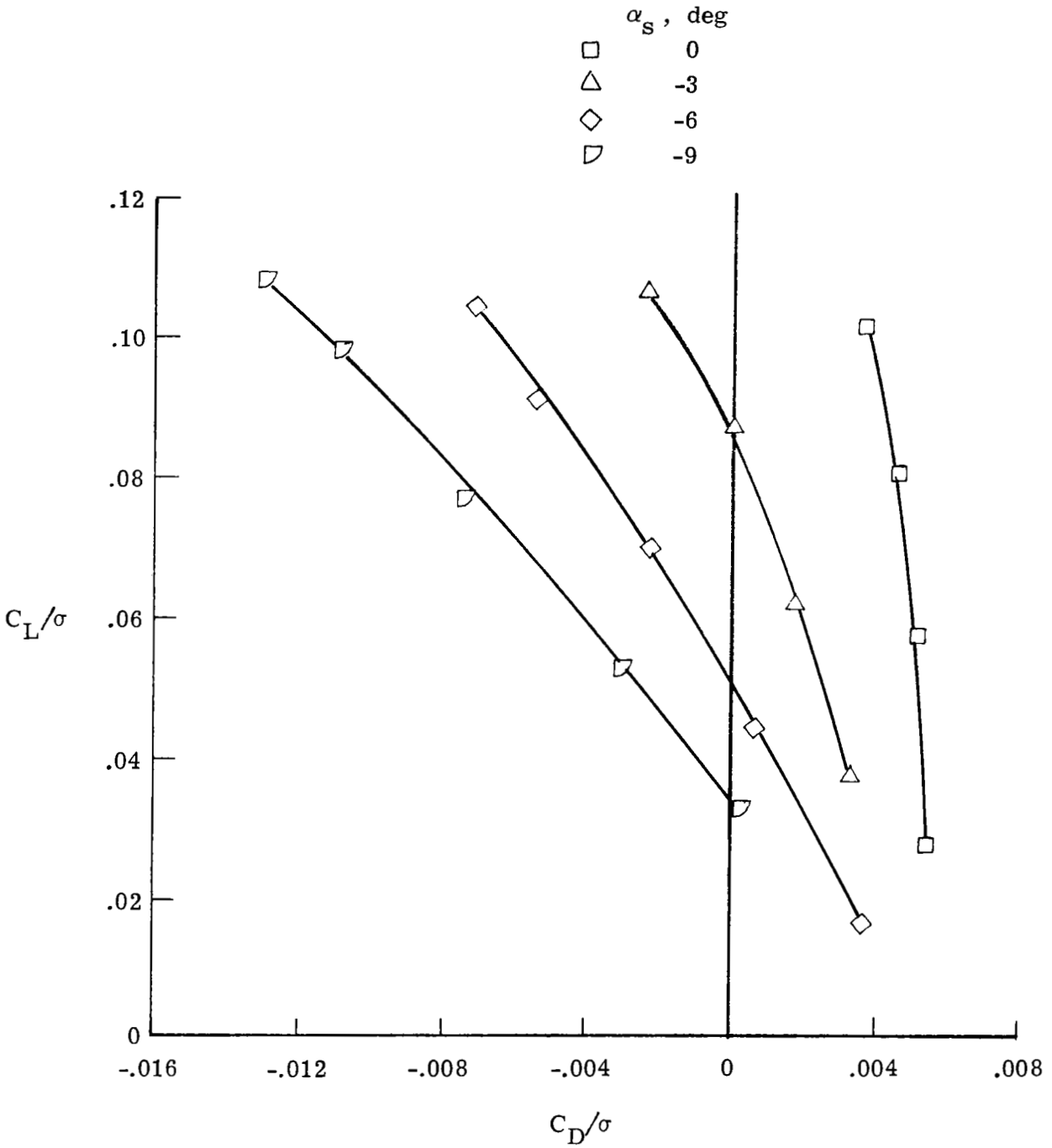


(b) $\mu = 0.3$.

Figure 15.- Continued.

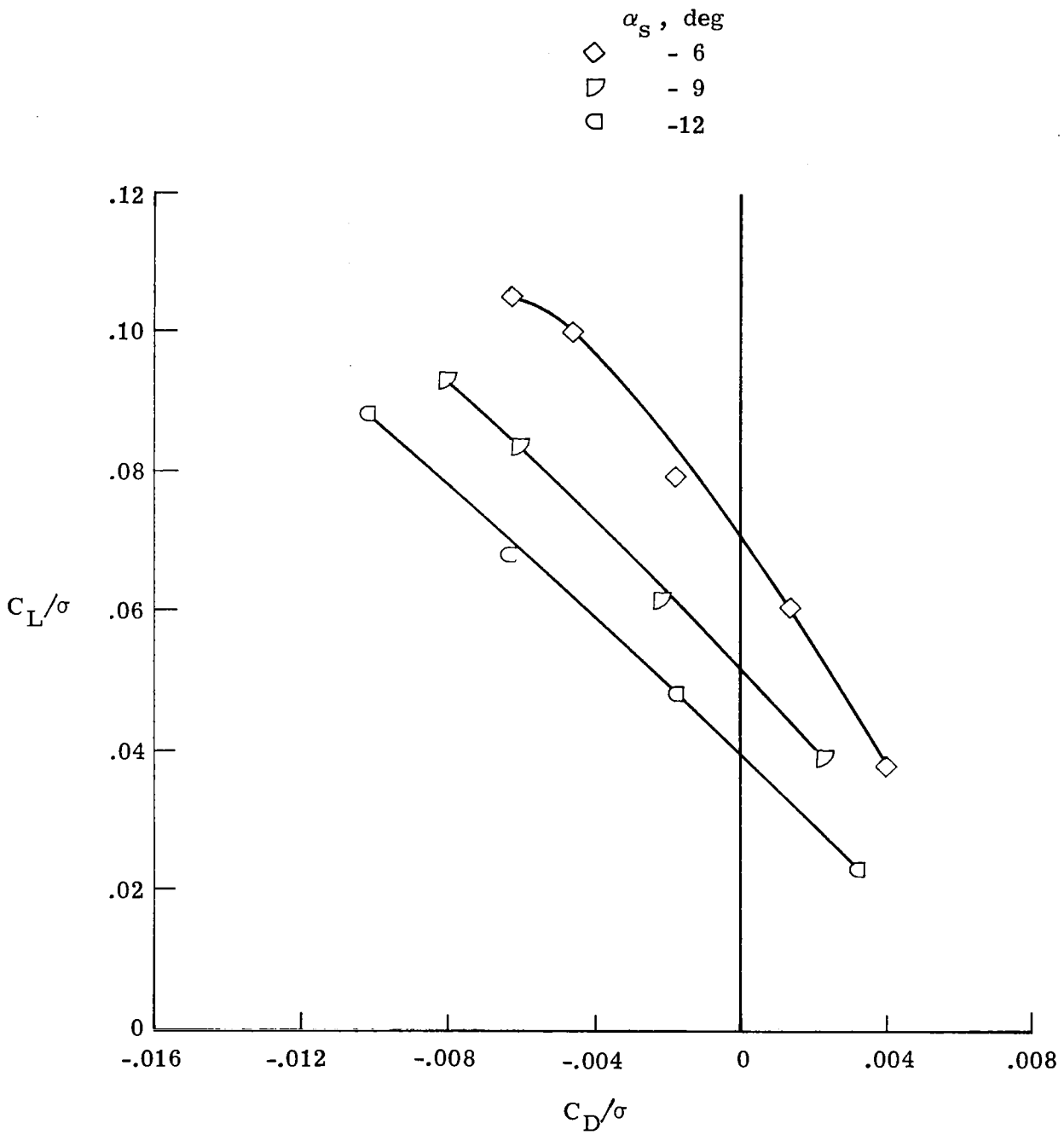


(c) $\mu = 0.35$.

Figure 15.- Continued.

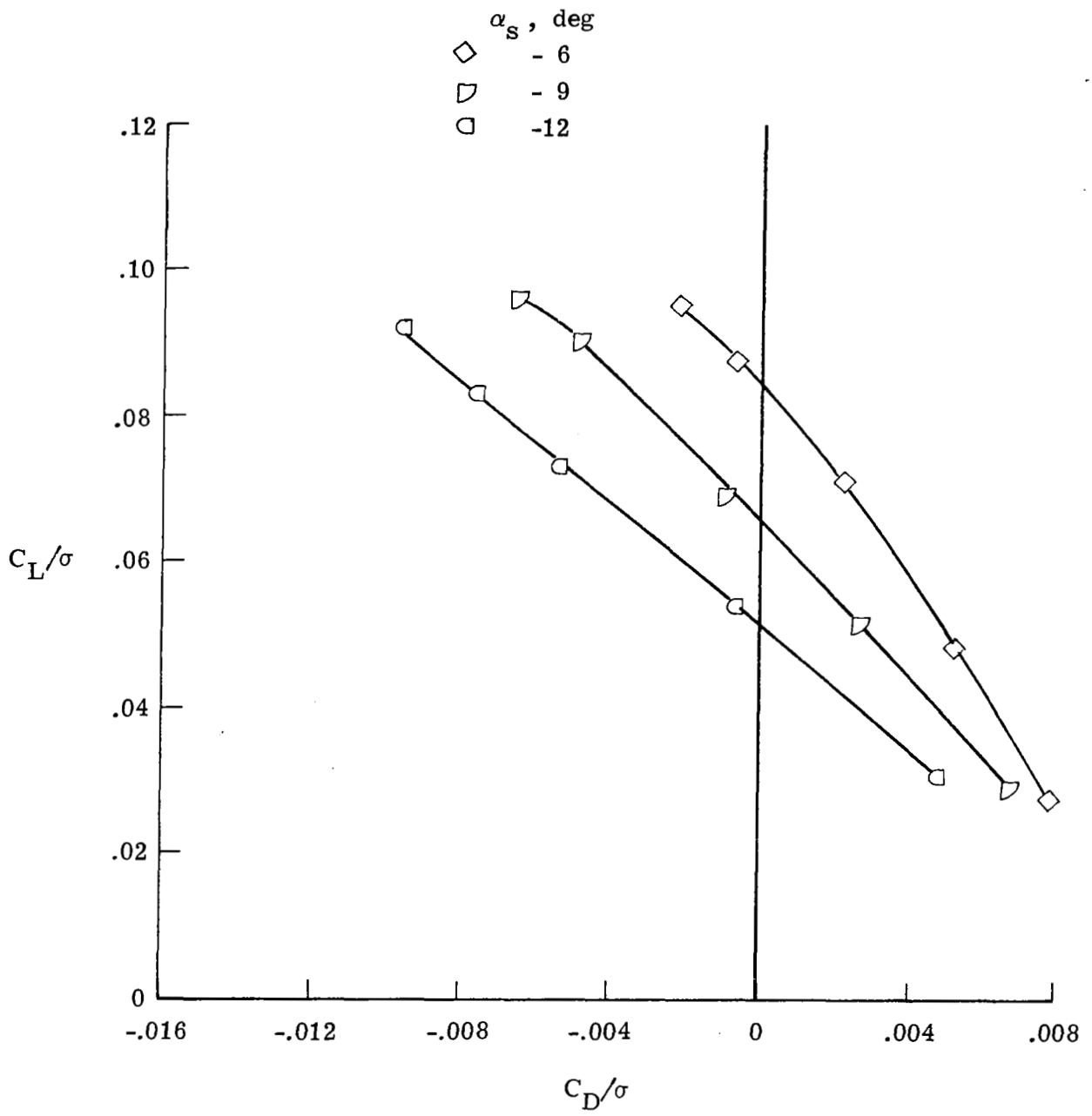


(d) $\mu = 0.4$.

Figure 15.- Concluded.

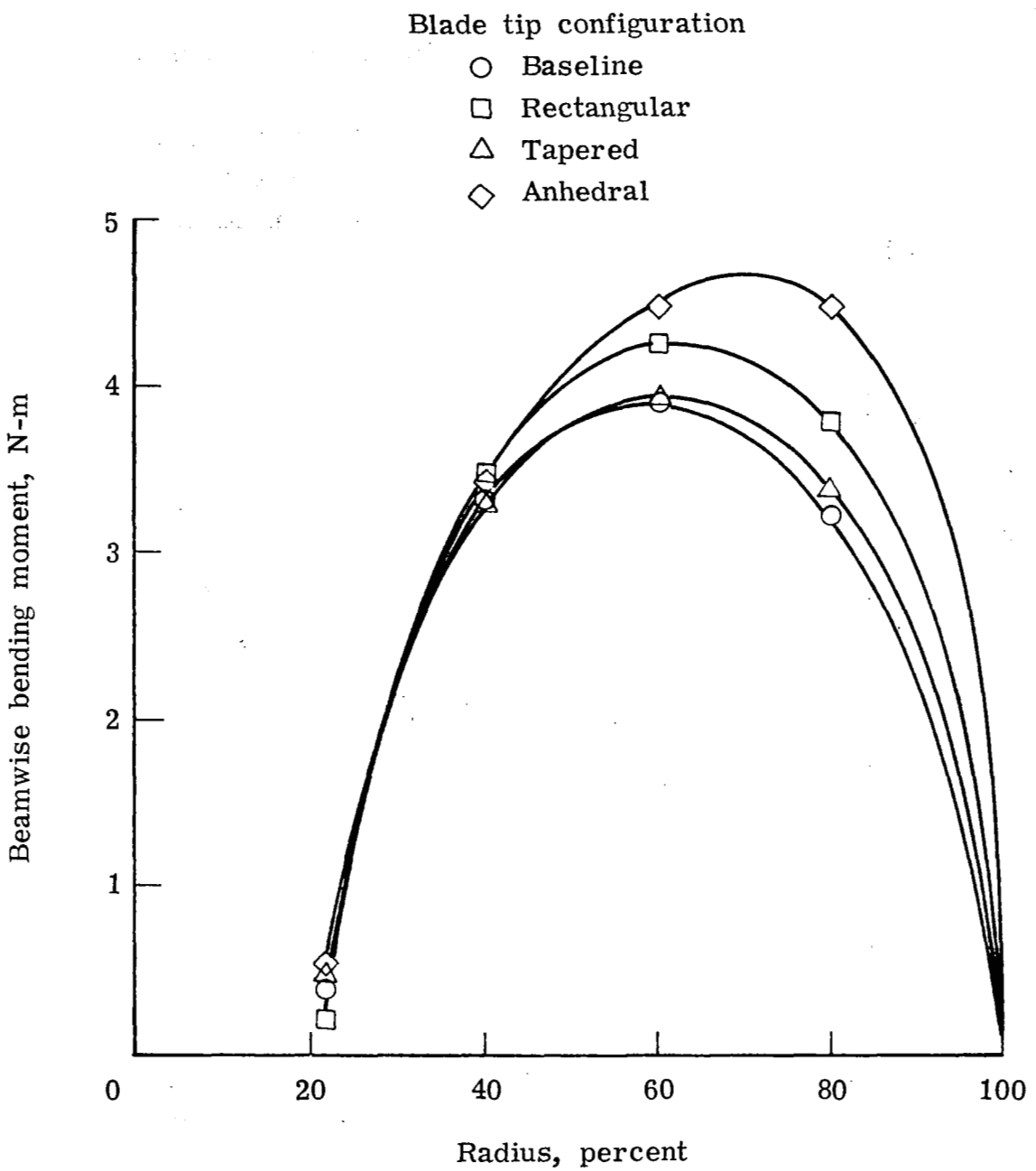


(a) First harmonic moment.

Figure 16.- Beamwise bending-moment distributions for four tip configurations. $\mu = 0.35$; $C_L/\sigma = 0.09$; $C_D/\sigma = -0.008$.

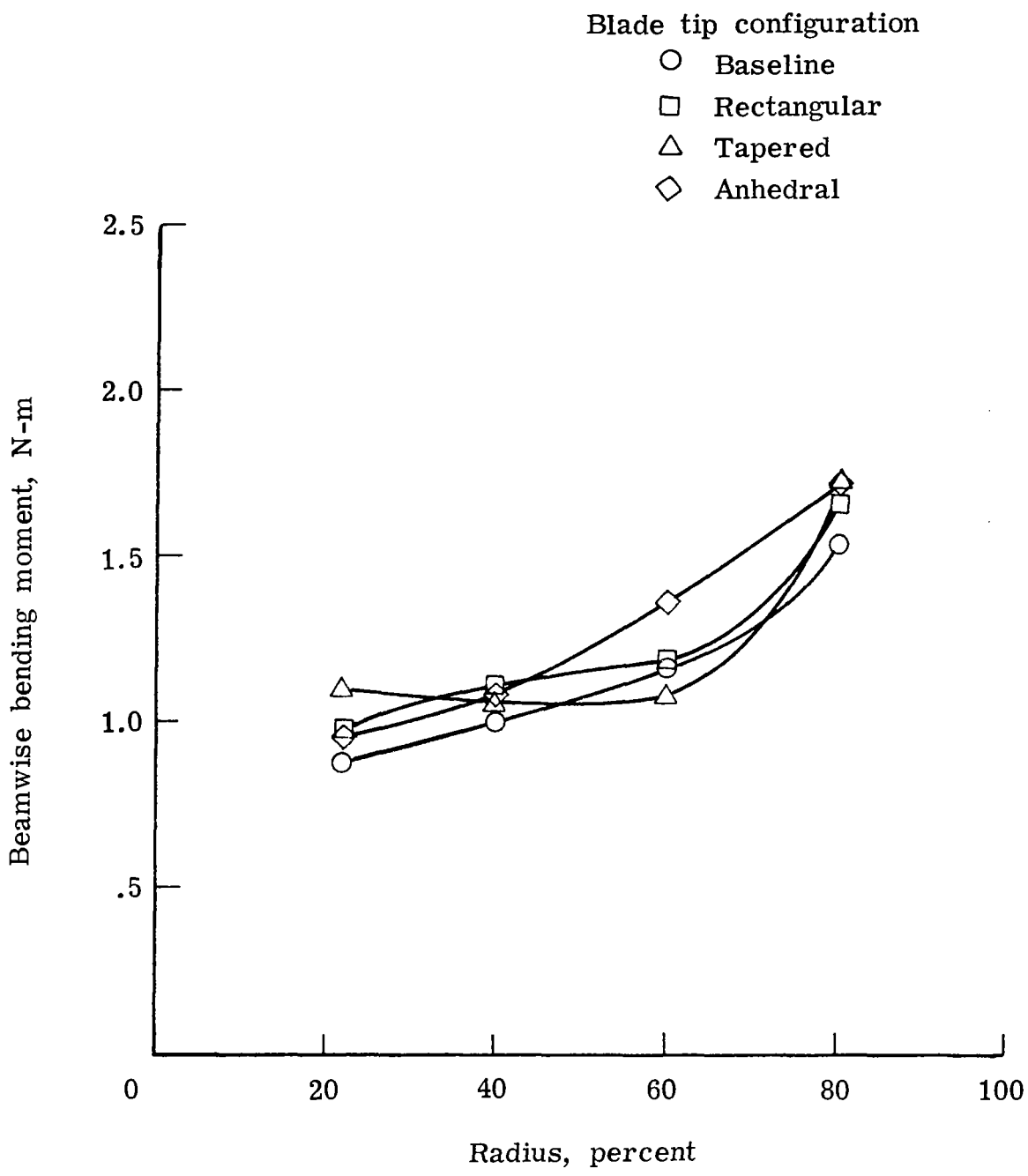


(b) Second harmonic moment.

Figure 16.- Continued.

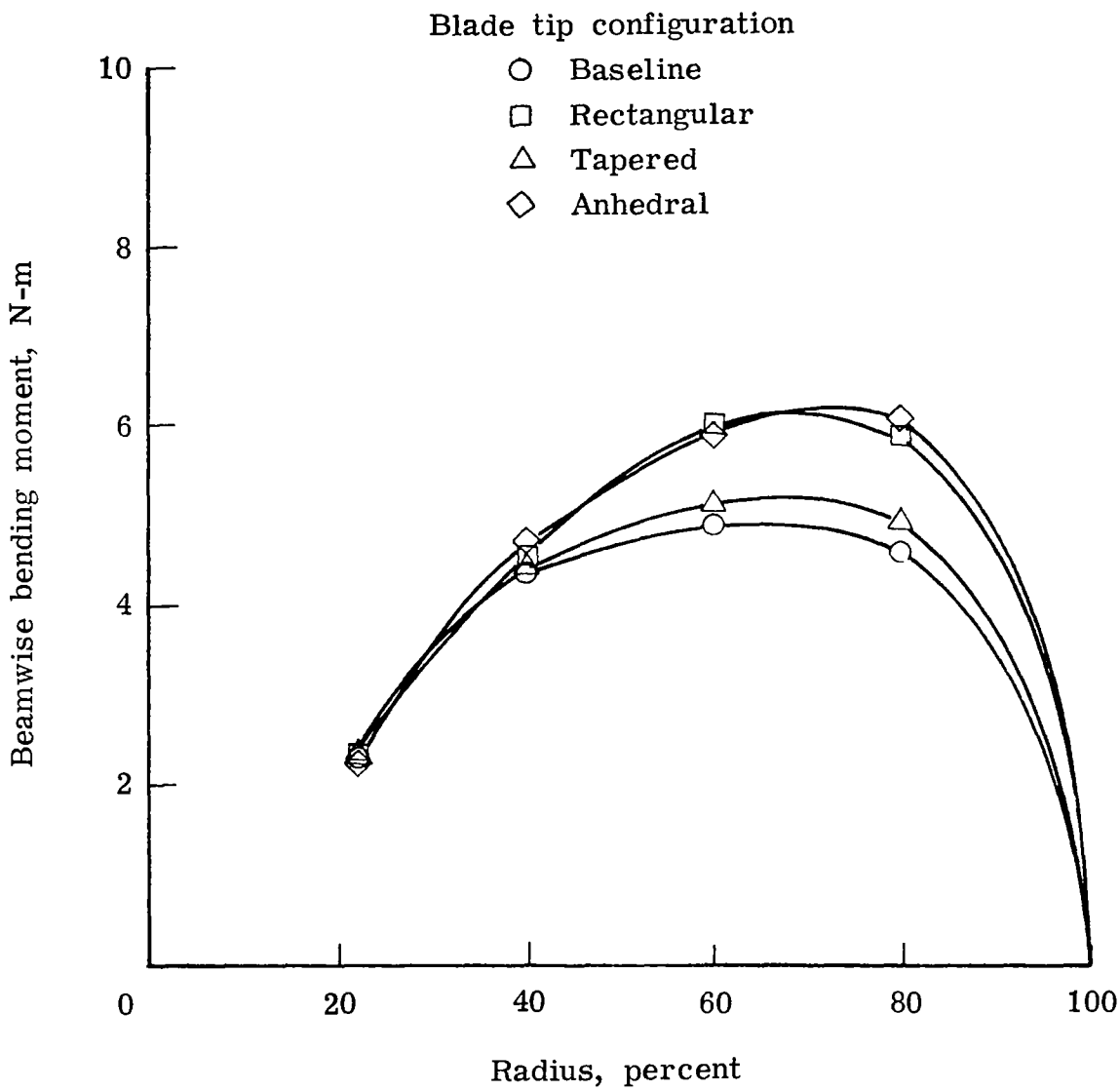


(c) Oscillatory moment.

Figure 16.- Concluded.

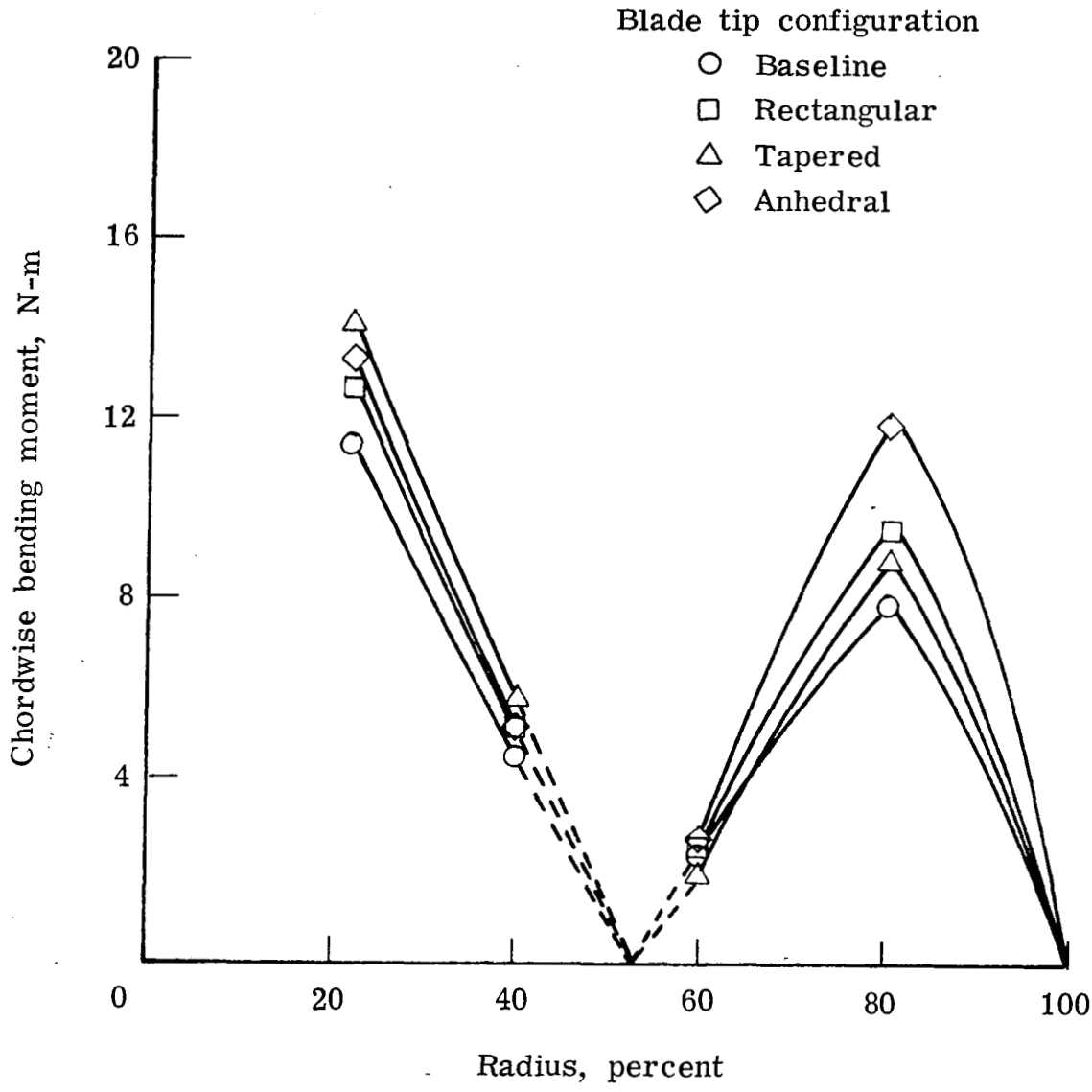


(a) First harmonic moment.

Figure 17.- Chordwise bending-moment distributions for four tip configurations. $\mu = 0.35$; $C_L/\sigma = 0.09$; $C_D/\sigma = -0.008$.

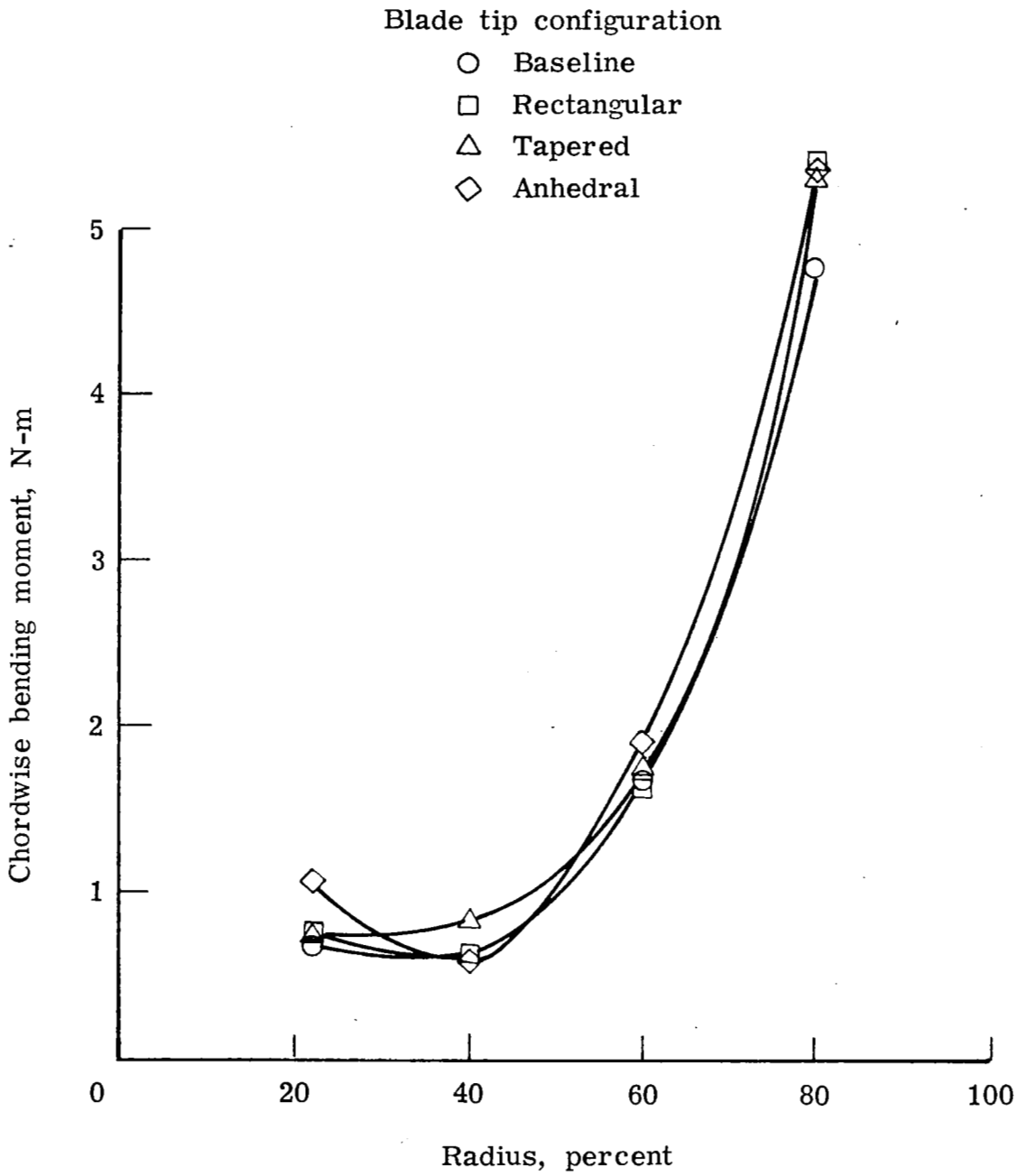


(b) Second harmonic moment.

Figure 17.- Continued.

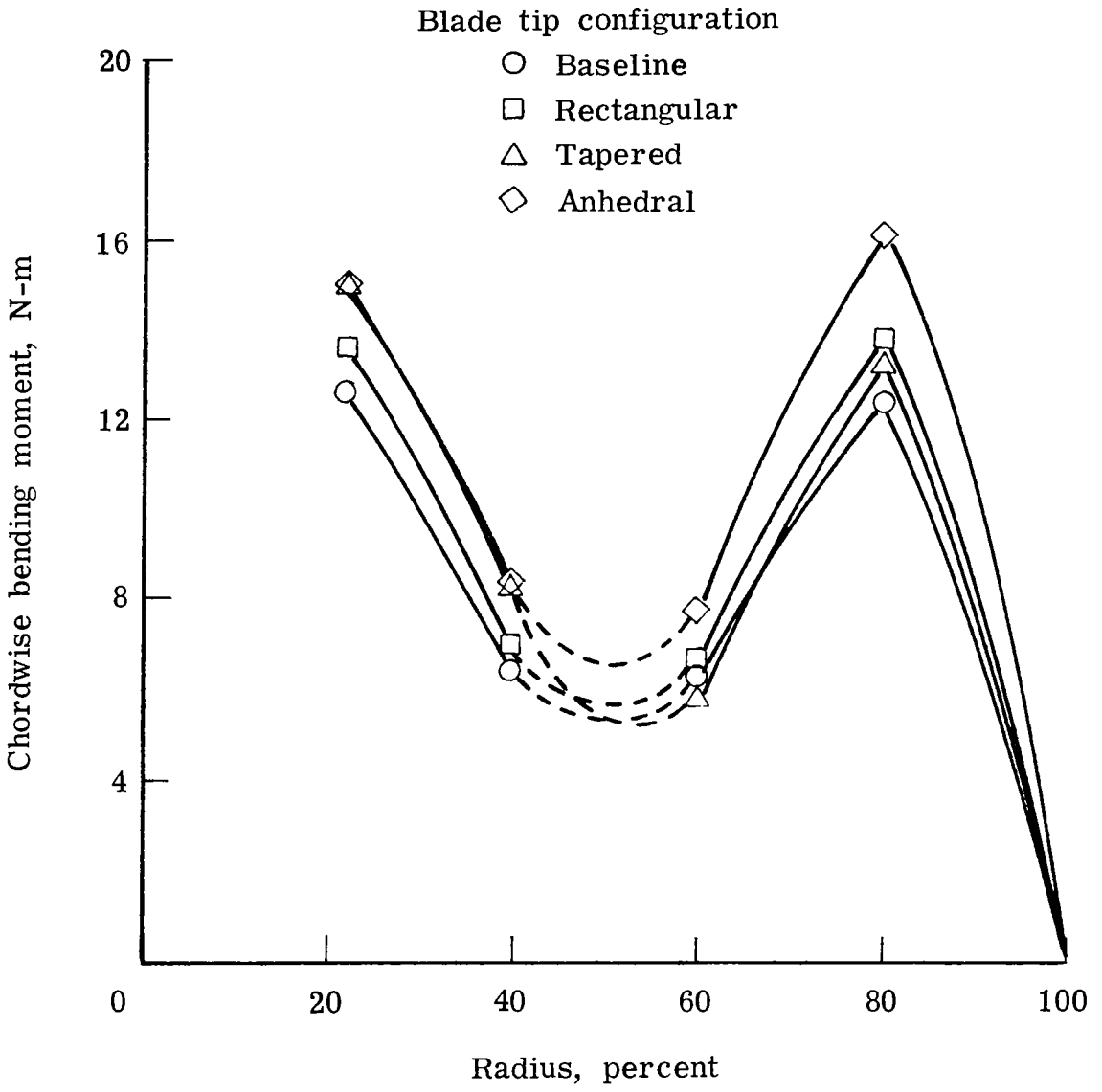


(c) Oscillatory moment.

Figure 17.- Concluded.

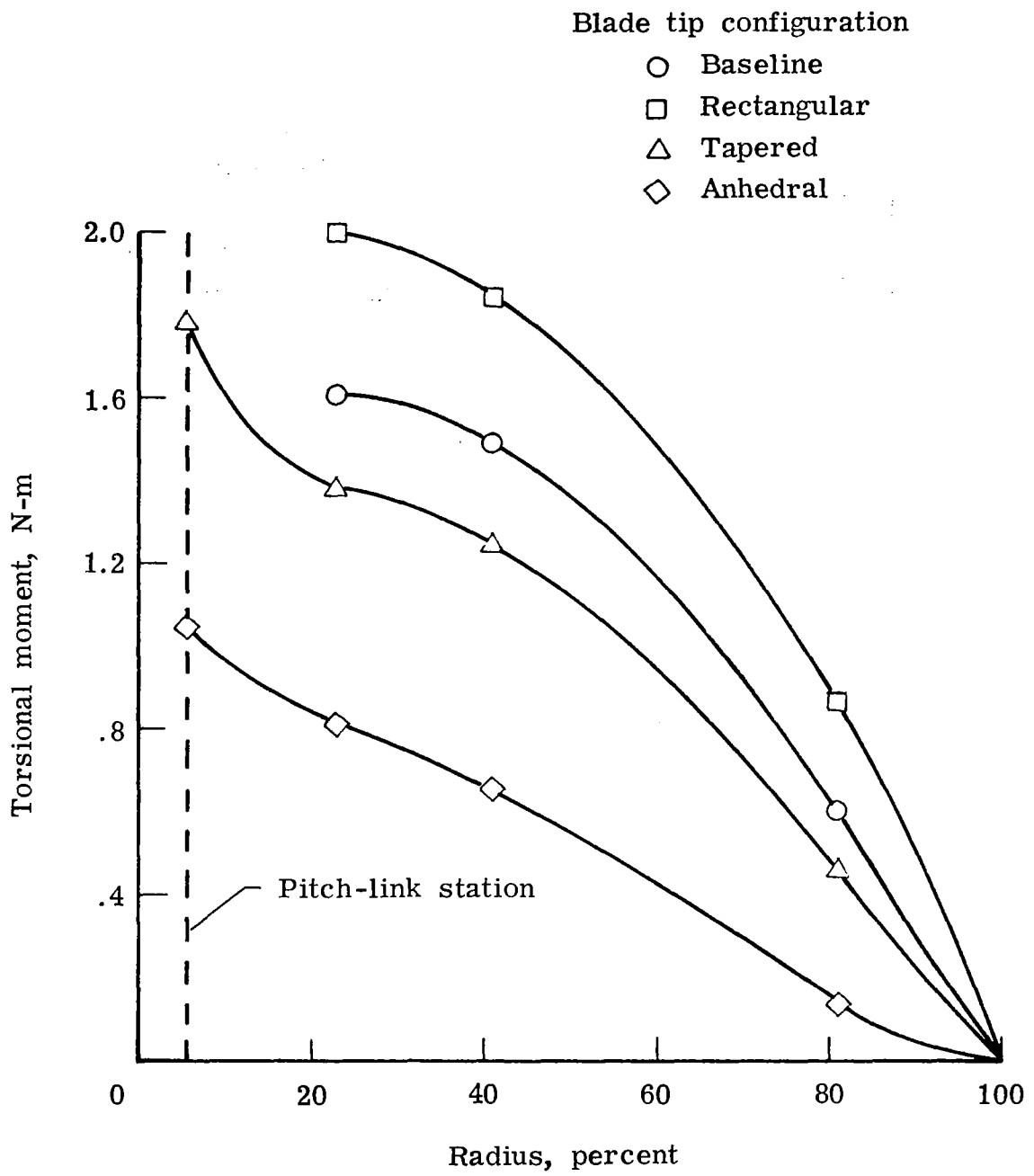


(a) First harmonic moment.

Figure 18.- Torsional moment distributions for four tip configurations. $\mu = 0.35$; $C_L/\sigma = 0.09$; $C_D/\sigma = -0.008$.

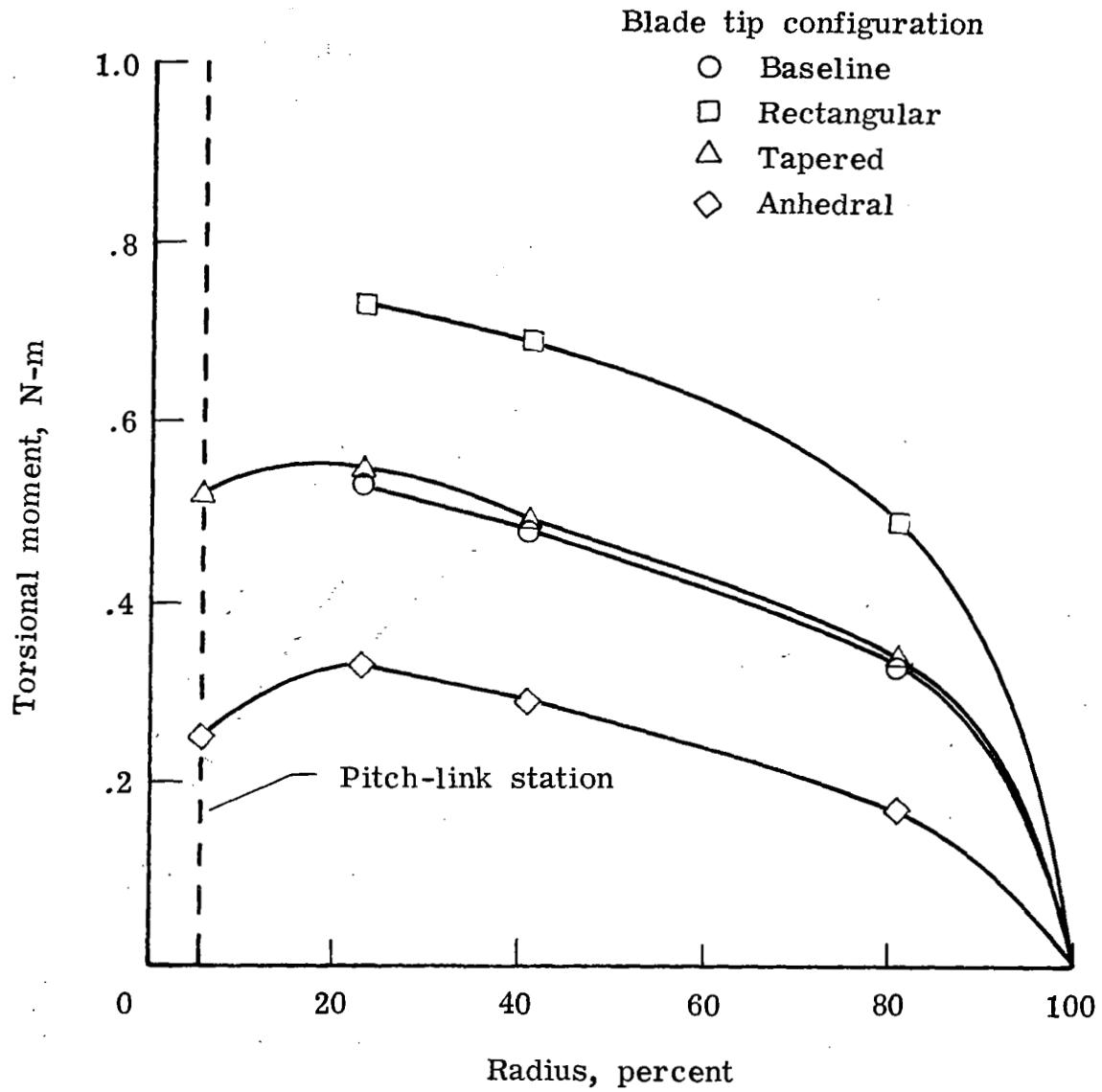


(b) Second harmonic moment.

Figure 18.- Continued.

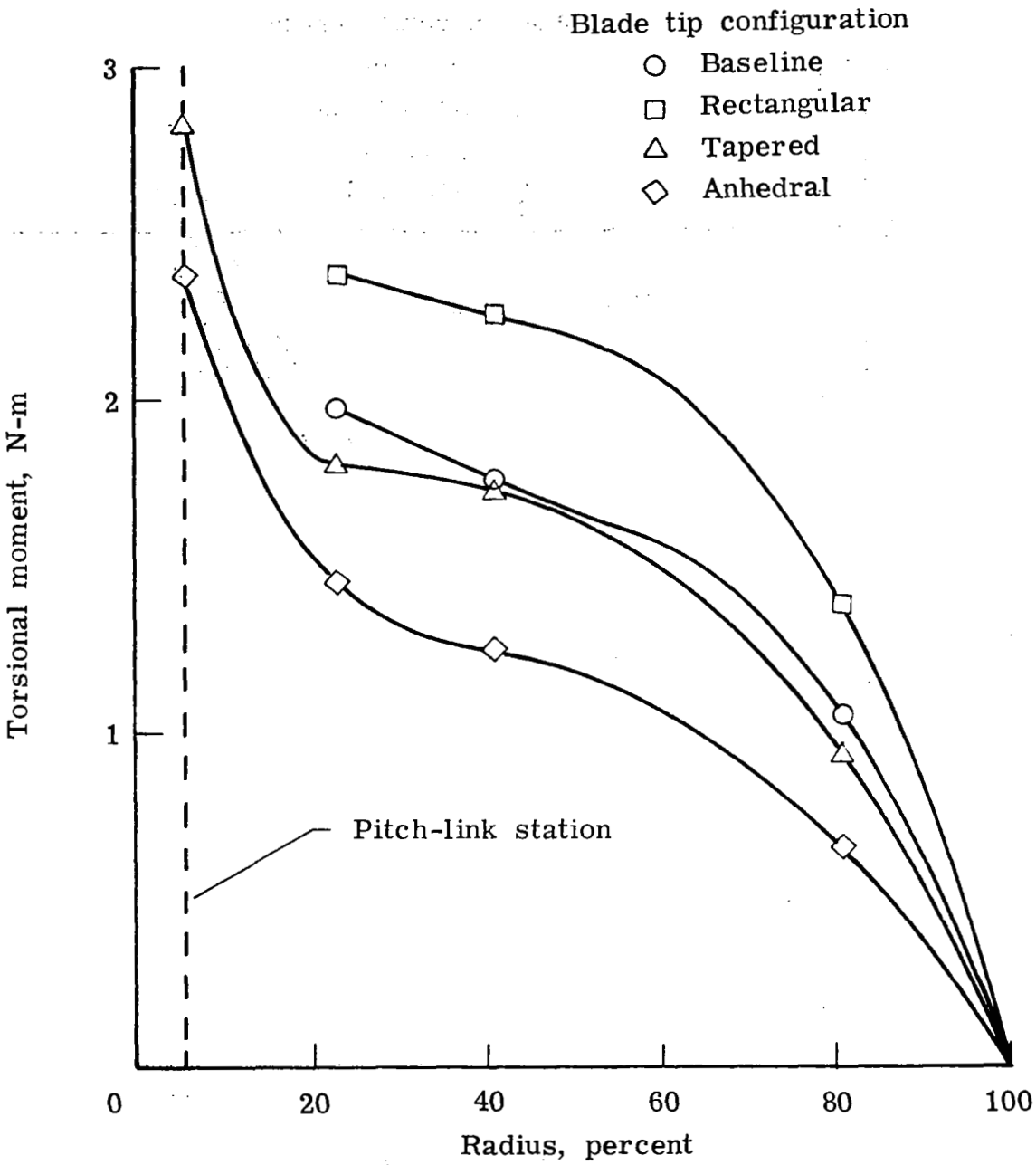


(c) Oscillatory moment.

Figure 18.- Continued.

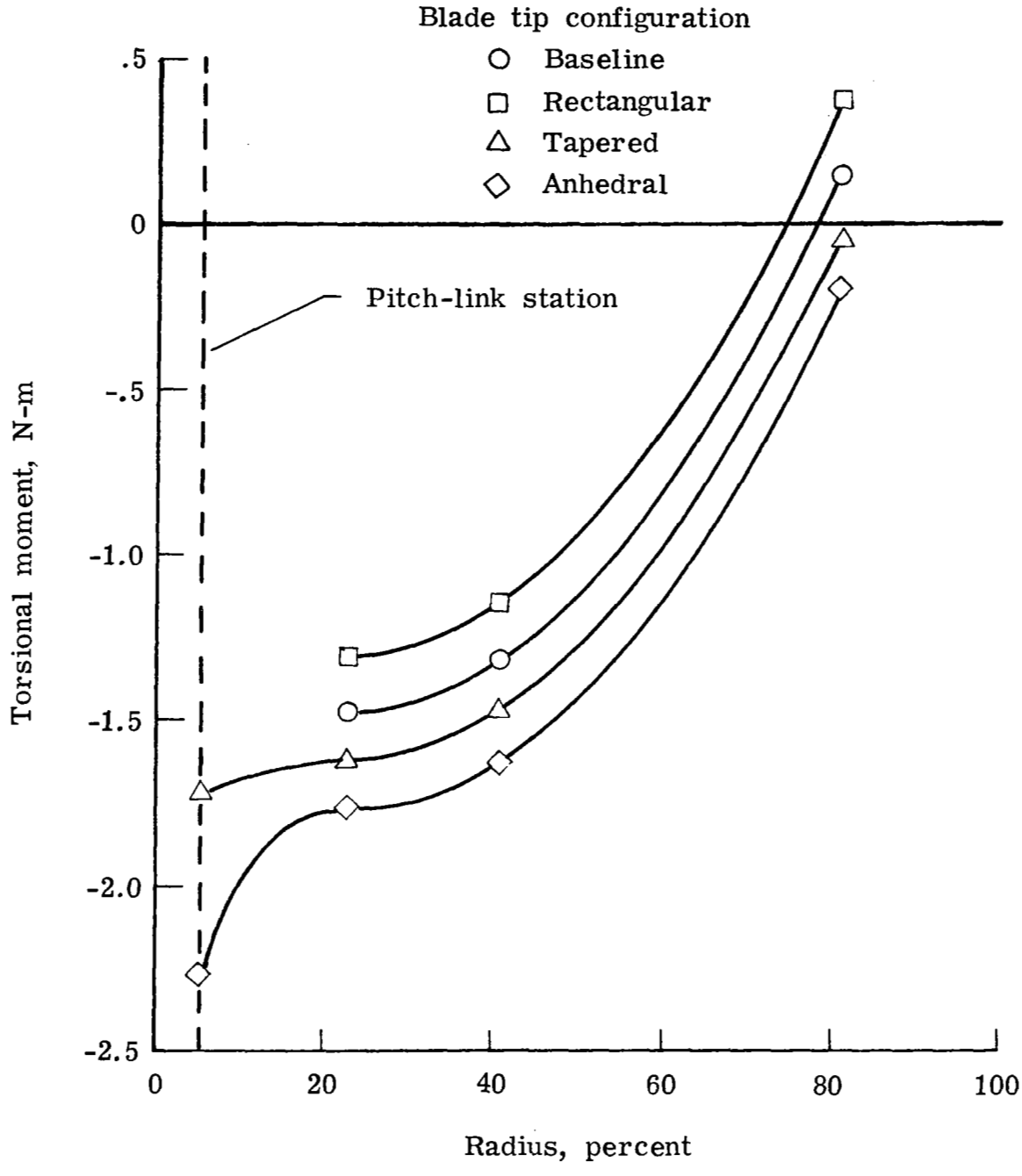


(d) Mean value of moment (positive nose-up).

Figure 18.- Concluded.

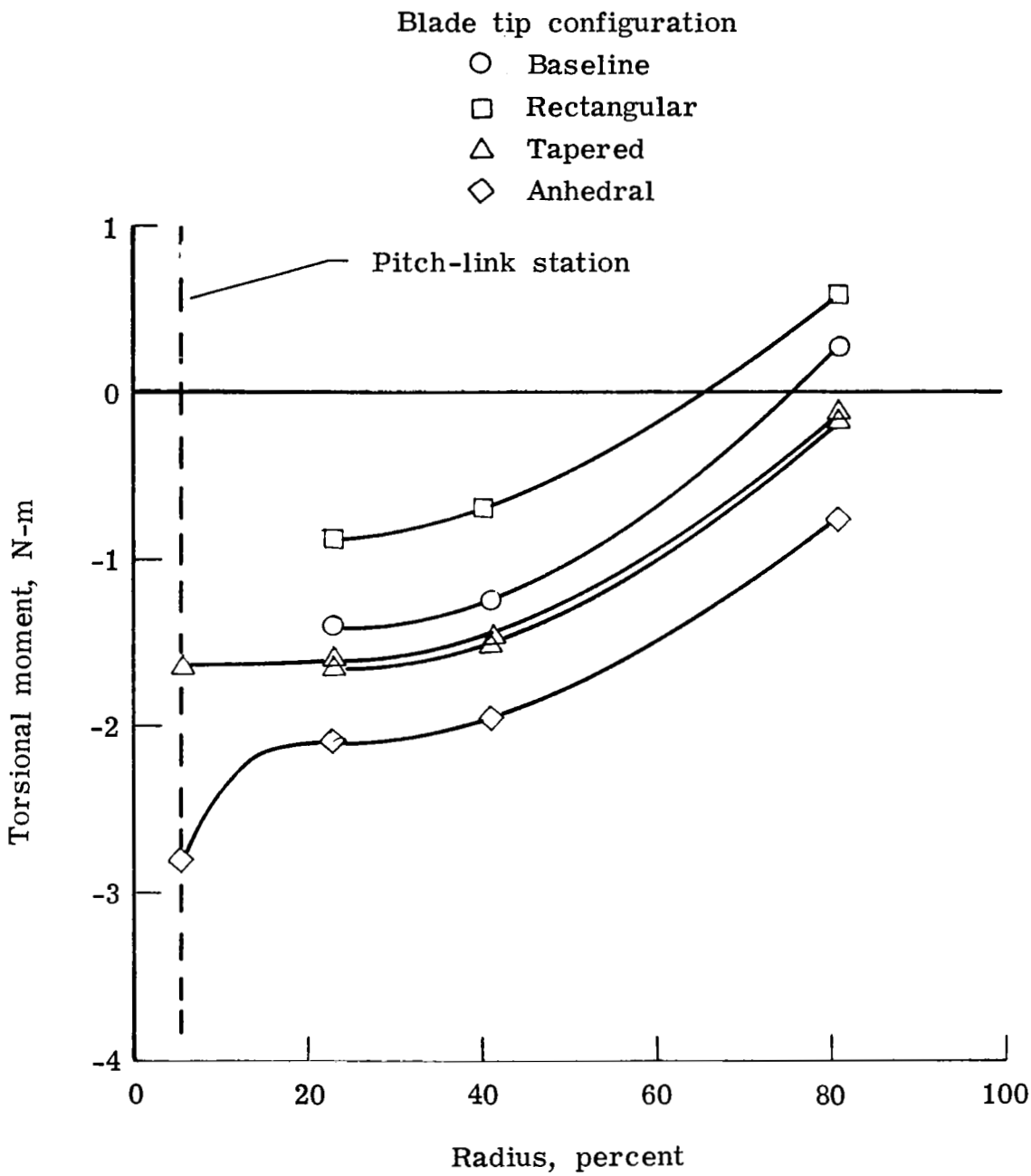


Figure 19.- Mean torsional moments measured in ground-effect hover for four blade tip configurations. Positive nose-up. $C_L/\sigma = 0.09$; $\alpha_s = 5^\circ$.

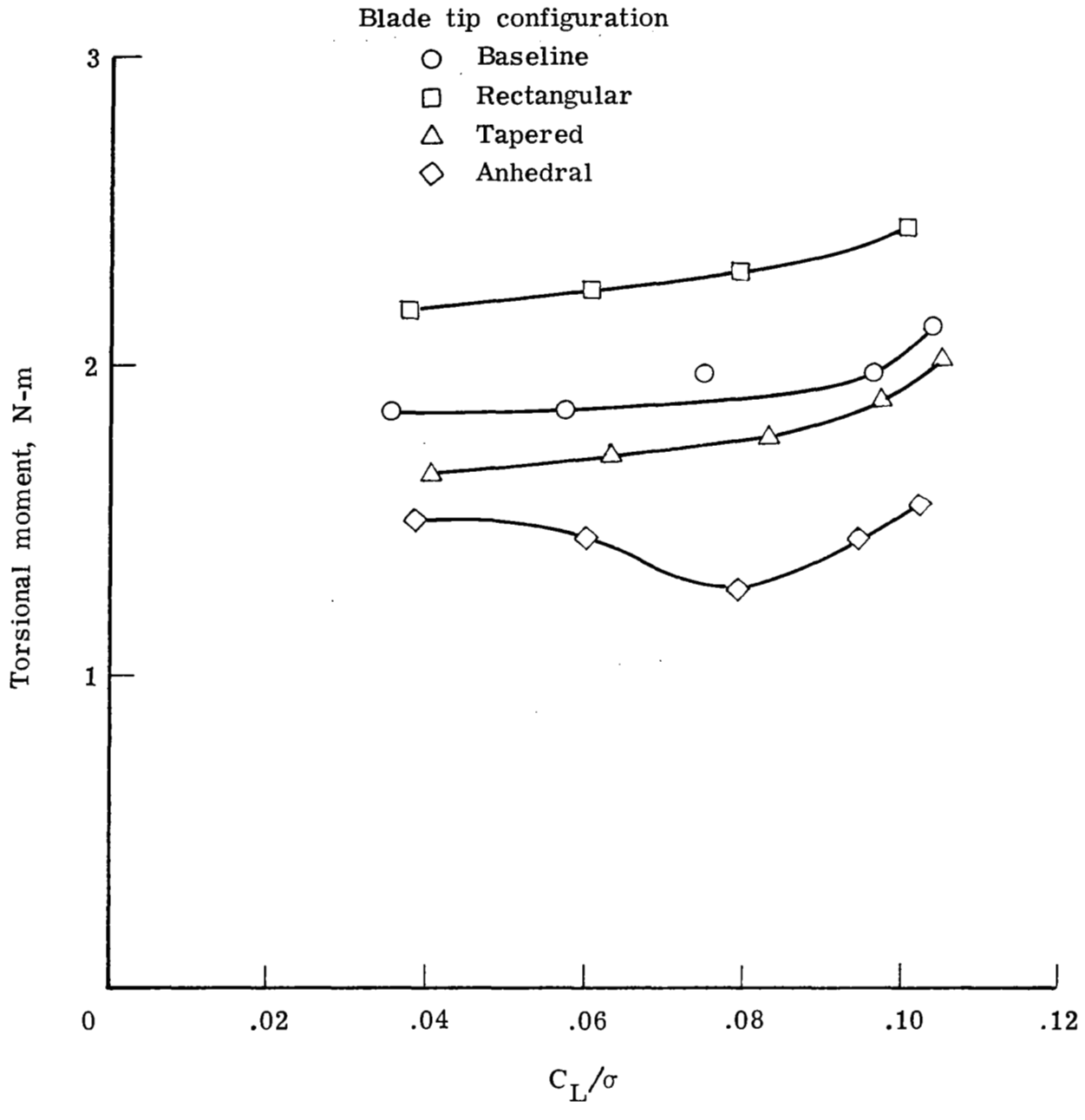


(a) Oscillatory moment.

Figure 20.- Variation of torsional moment (x = 0.23) with lift for four tip configurations. $\mu = 0.35$; $\alpha_s = -6^o$.

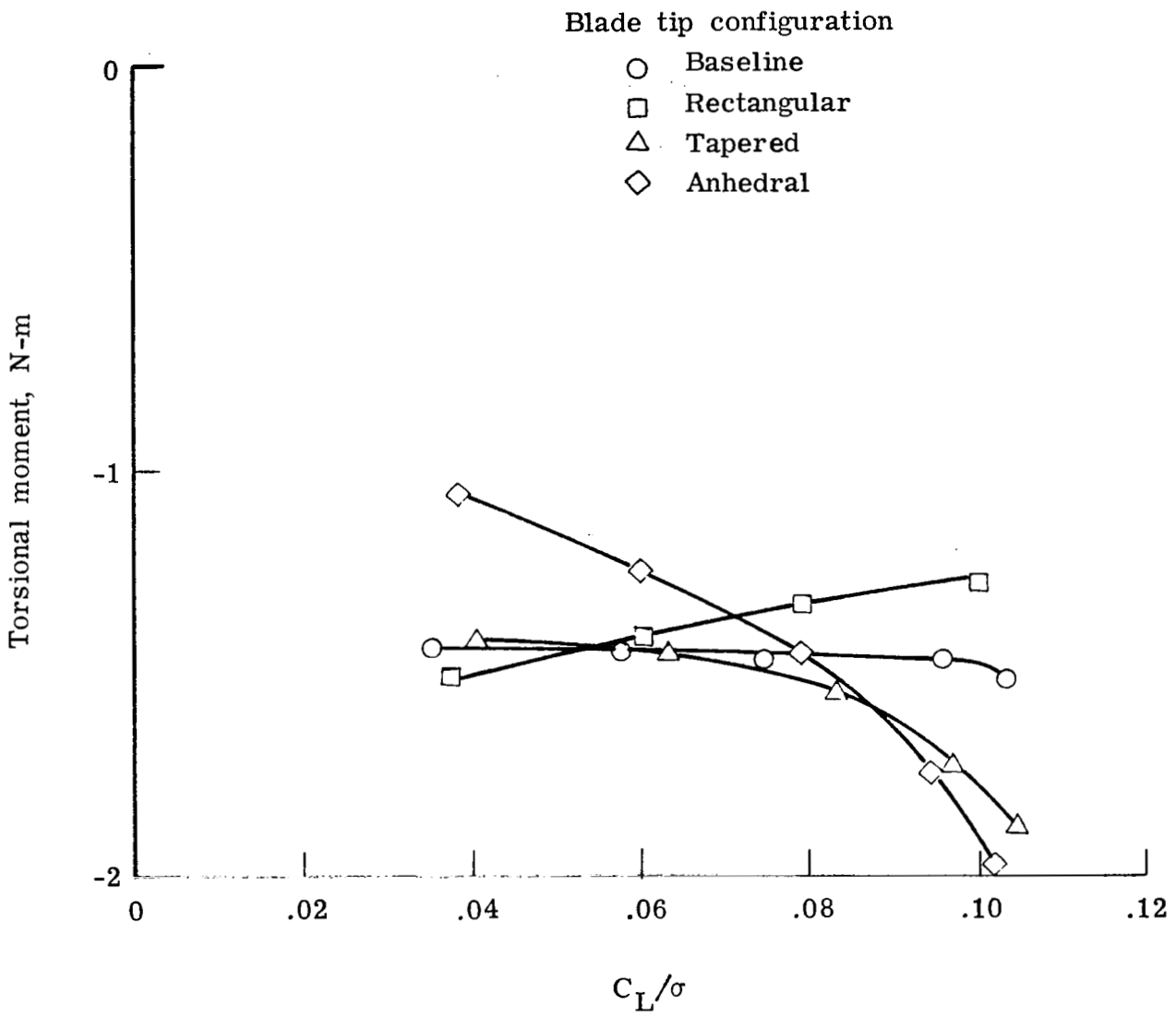


(b) Mean value of moment (positive nose-up).

Figure 20.- Concluded.

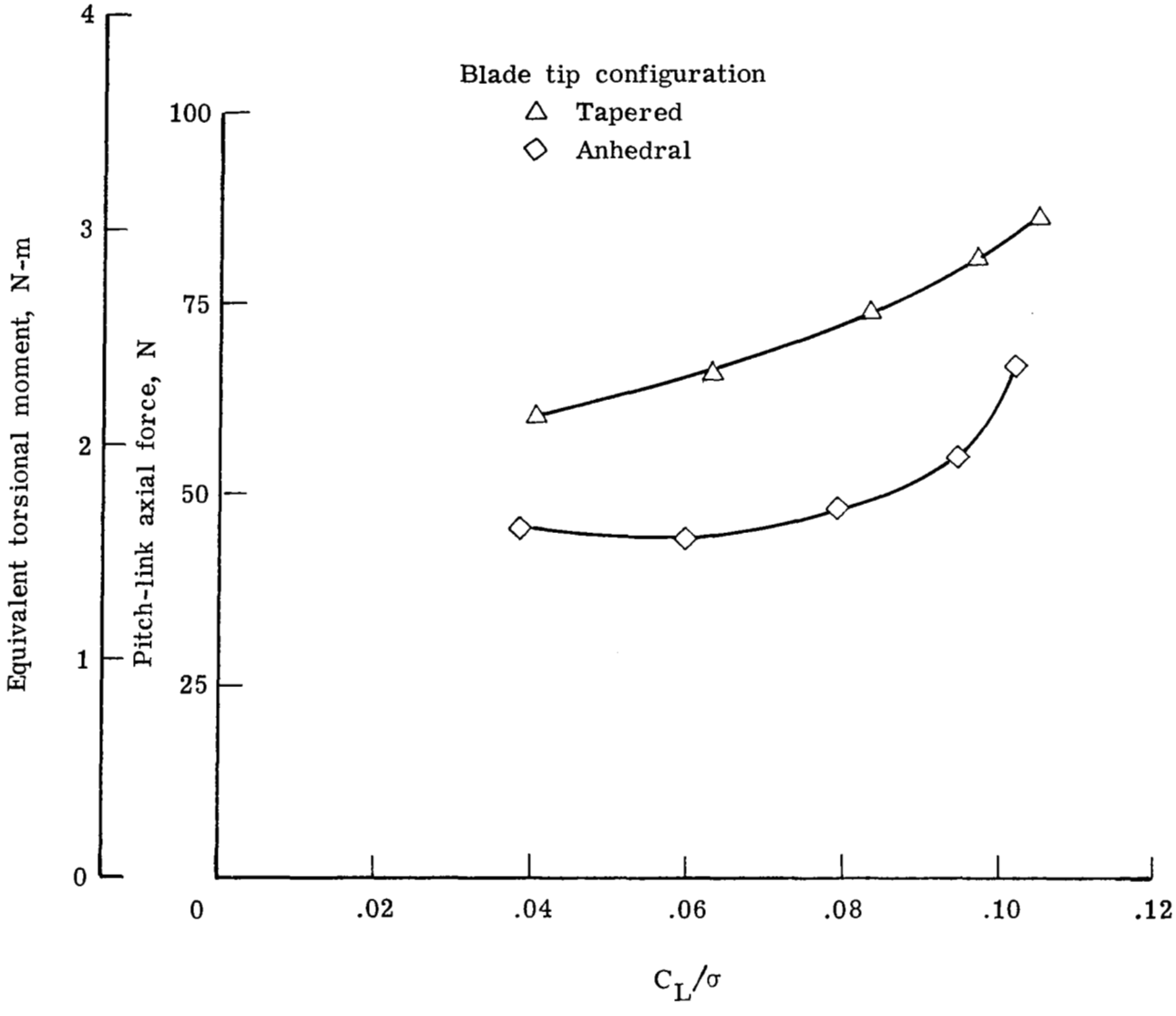


(a) Oscillatory force or moment.

Figure 21.- Variation of pitch-link force with lift for two tip configurations. $\mu = 0.35$; $\alpha_s = -6^\circ$.

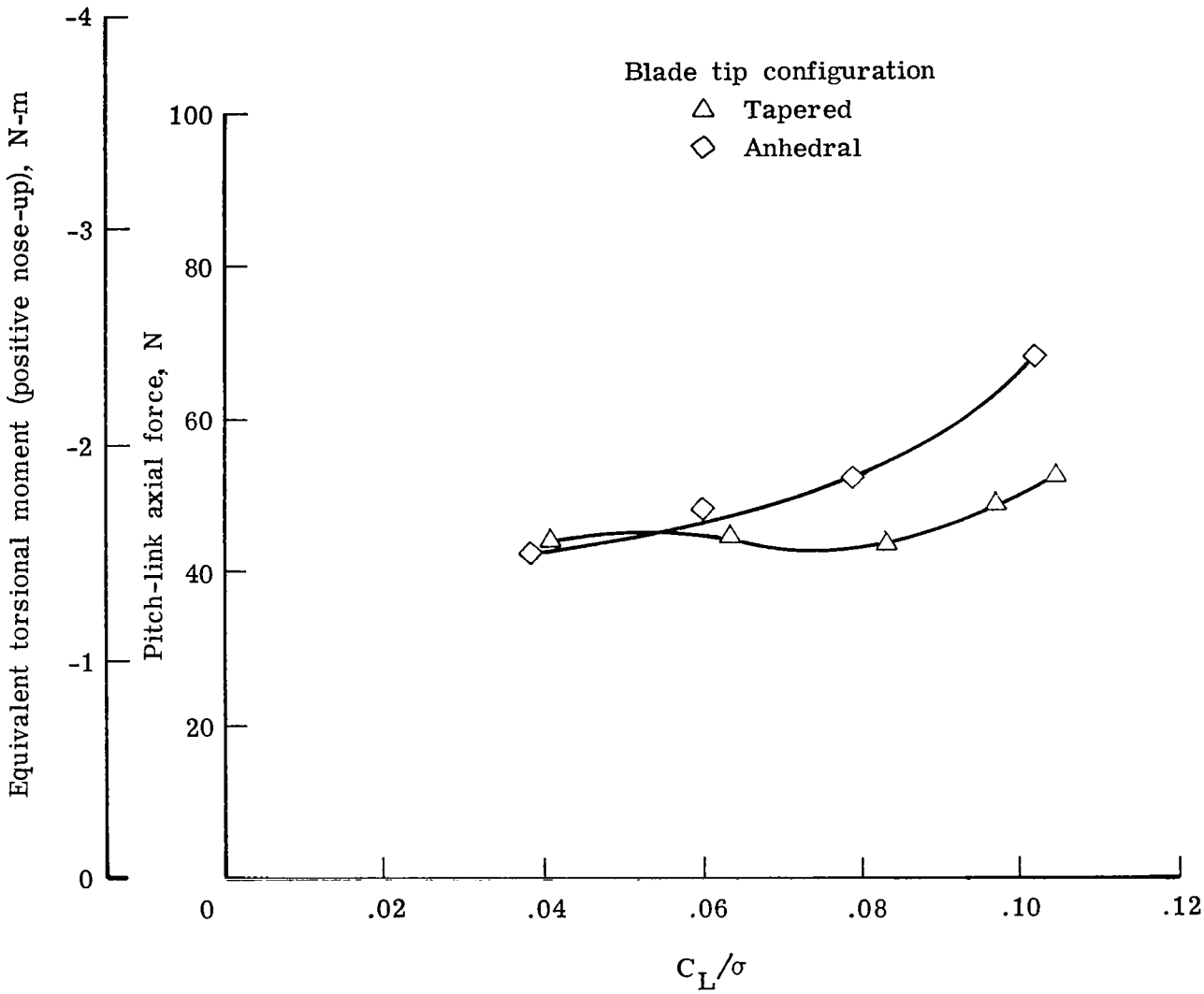


(b) Mean value of force or moment (positive in tension, nose-up).

Figure 21.- Concluded.

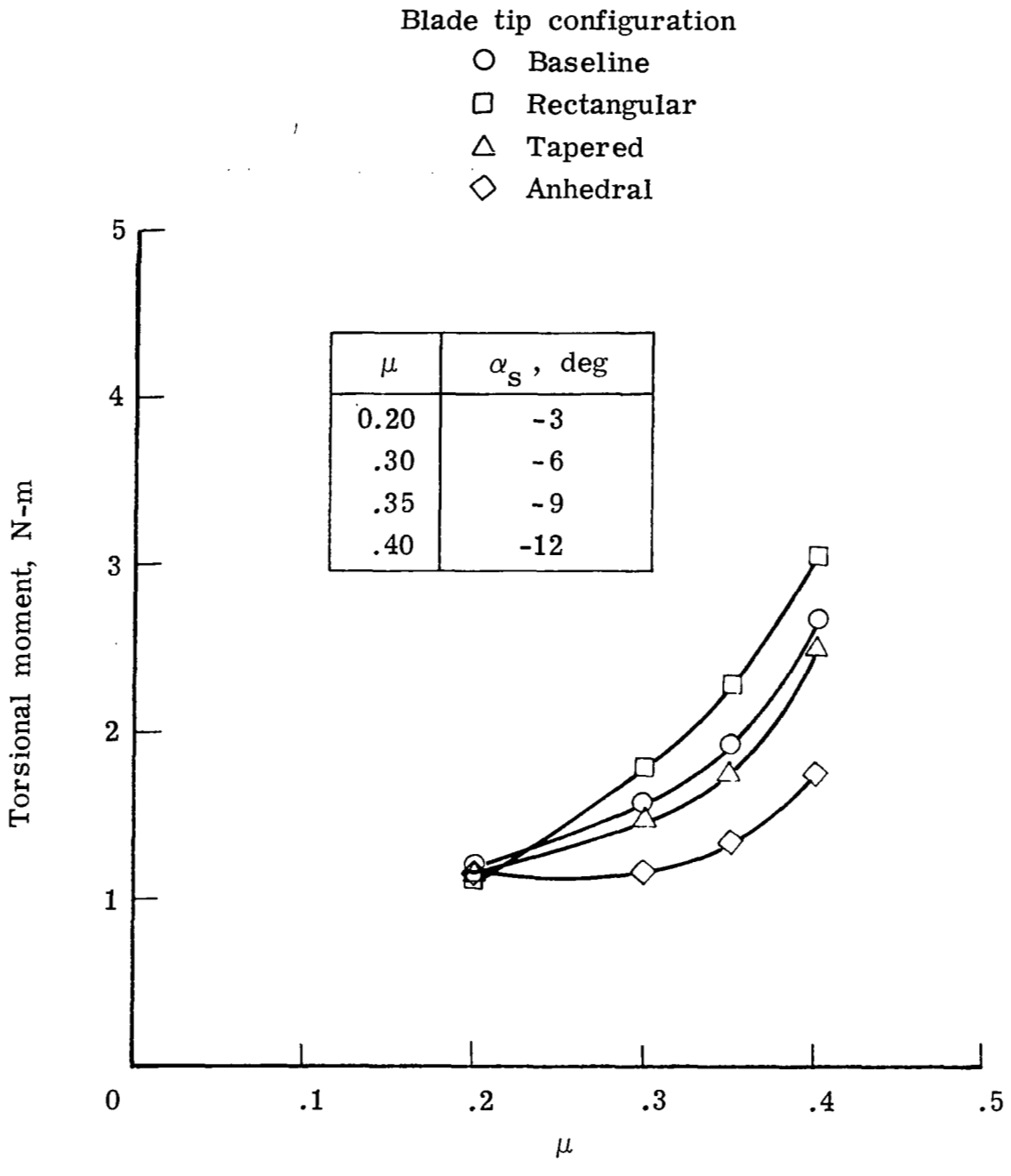


(a) Oscillatory moment.

Figure 22.- Variation of torsional moment (x = 0.23) with advance ratio for four tip configurations. $C_L/\sigma$ = 0.08.

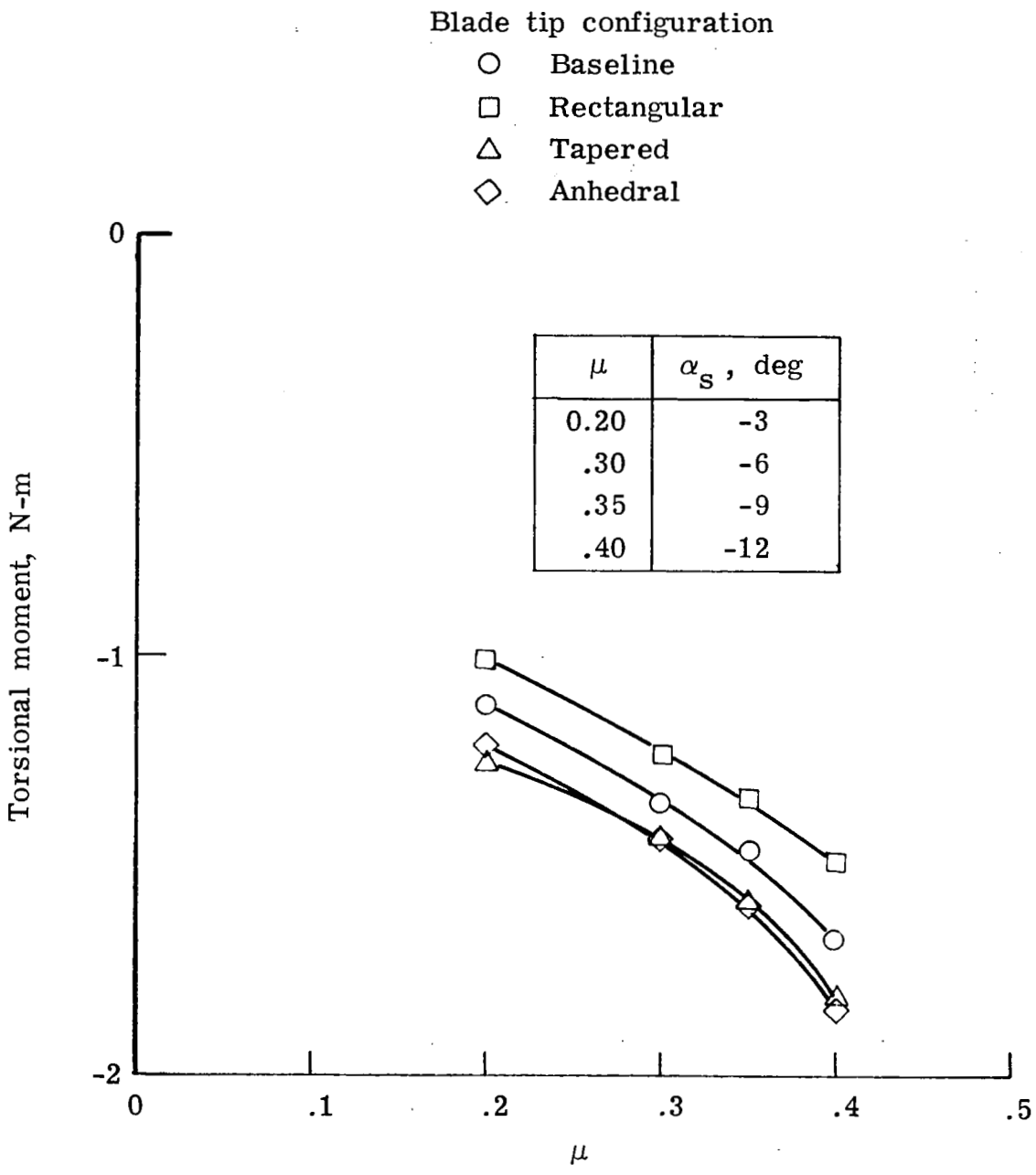


(b) Mean value of moment (positive nose-up).

Figure 22.- Concluded.

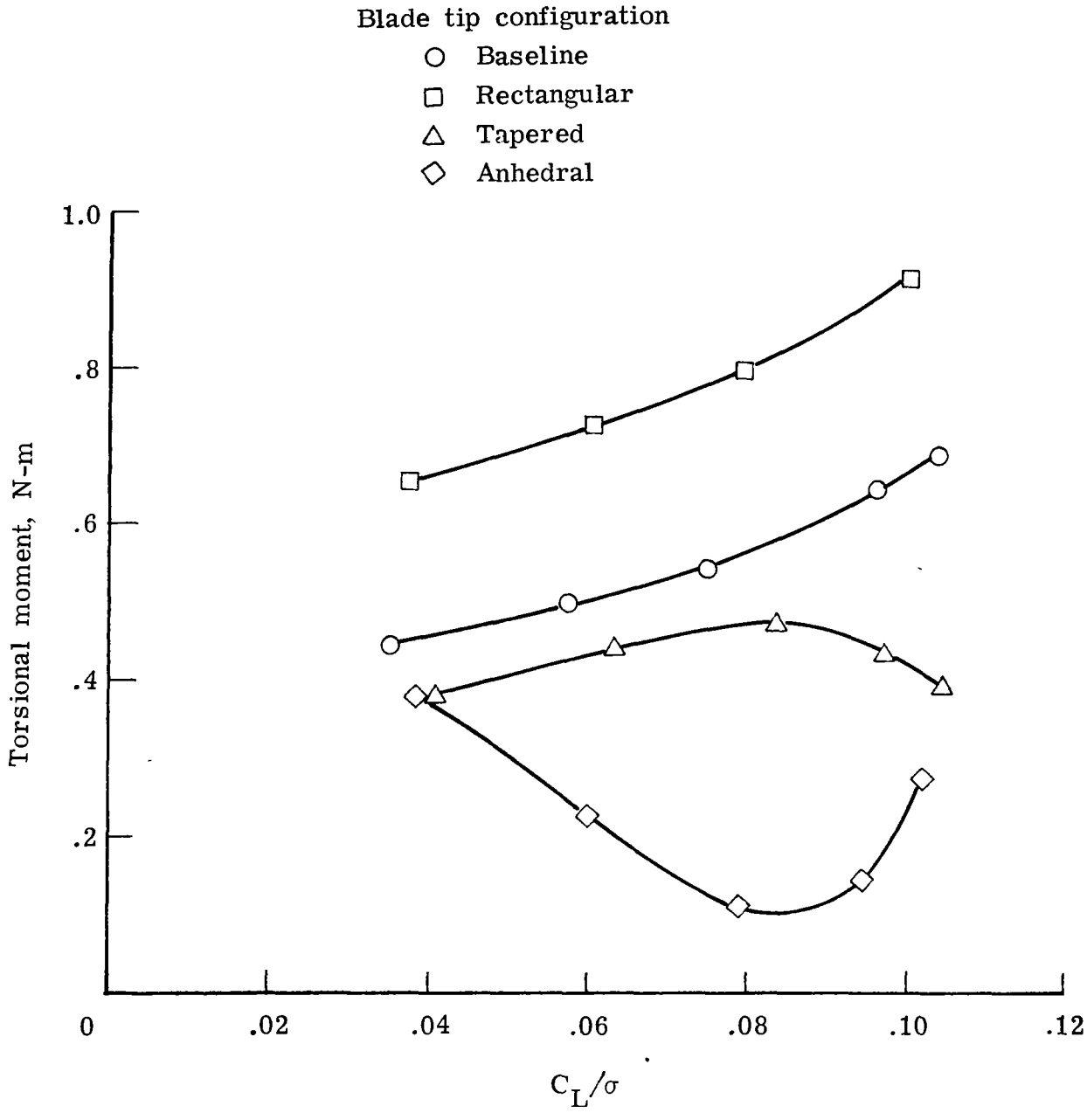


(a) First harmonic moment.

Figure 23.- Variation of torsional moment (x = 0.81) with lift for four tip configurations. $\mu = 0.35$; $\alpha_s = -6^o$.

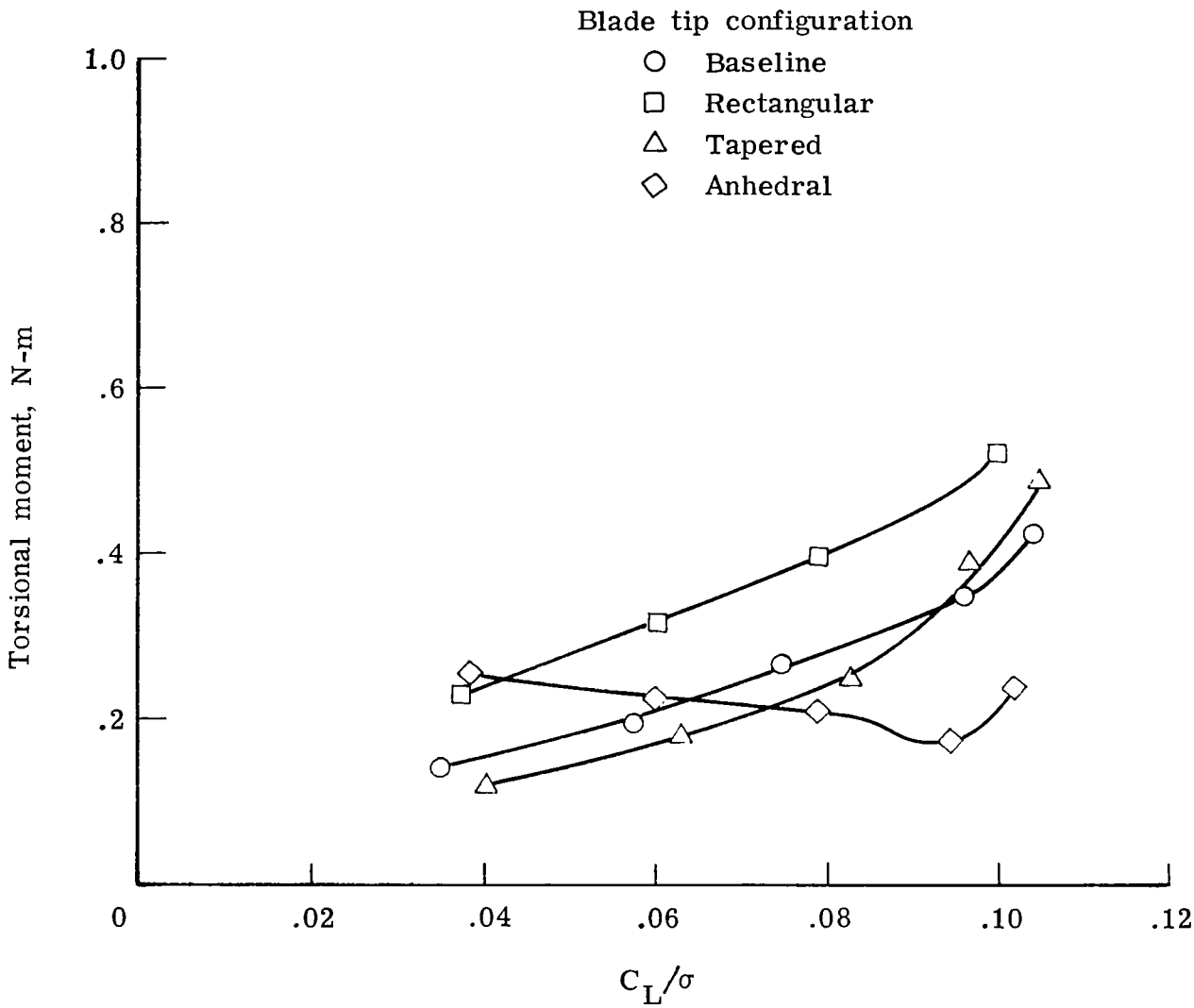


(b) Second harmonic moment.

Figure 23.- Continued.

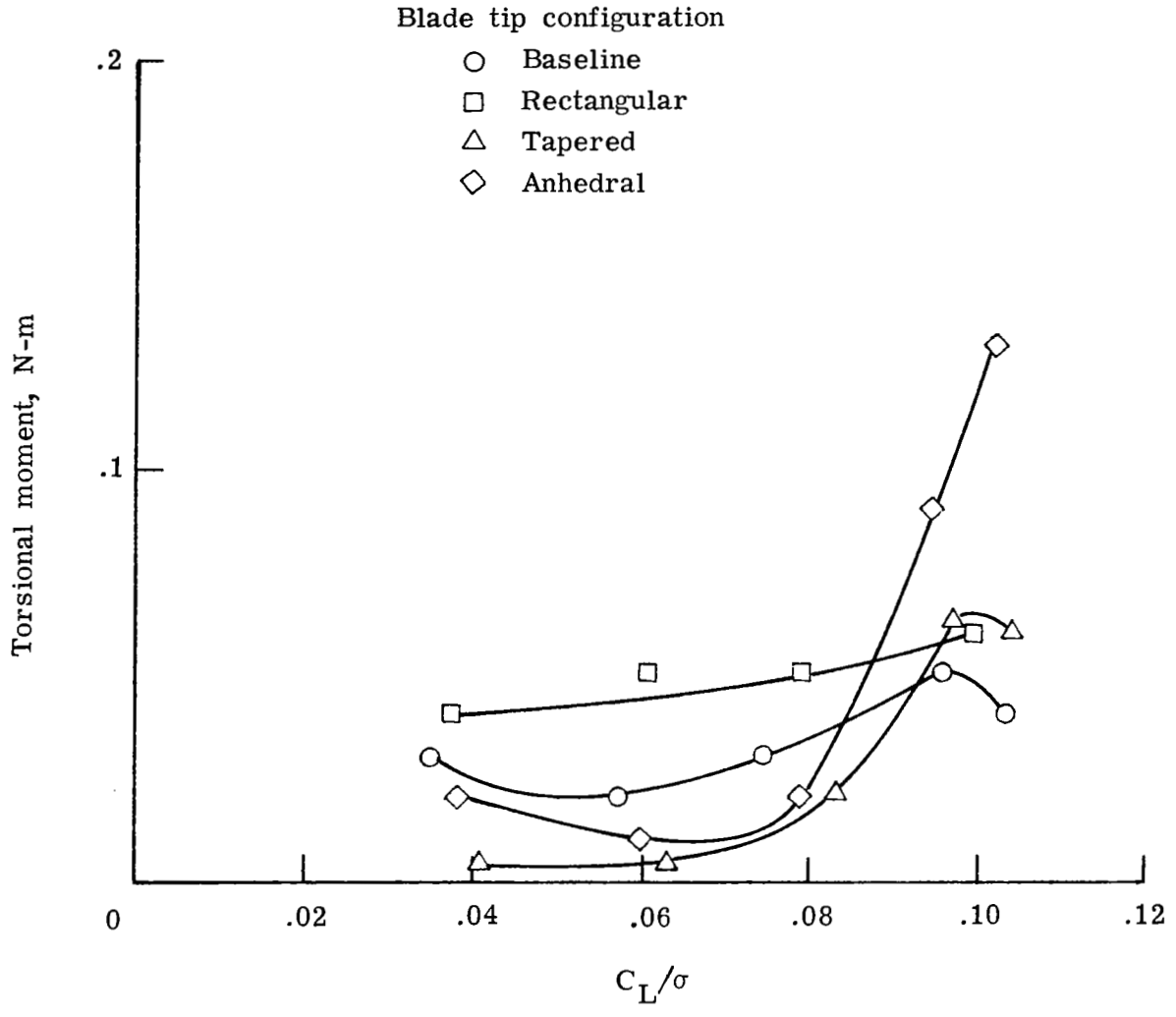


(c) Sixth harmonic moment.

Figure 23.- Continued.

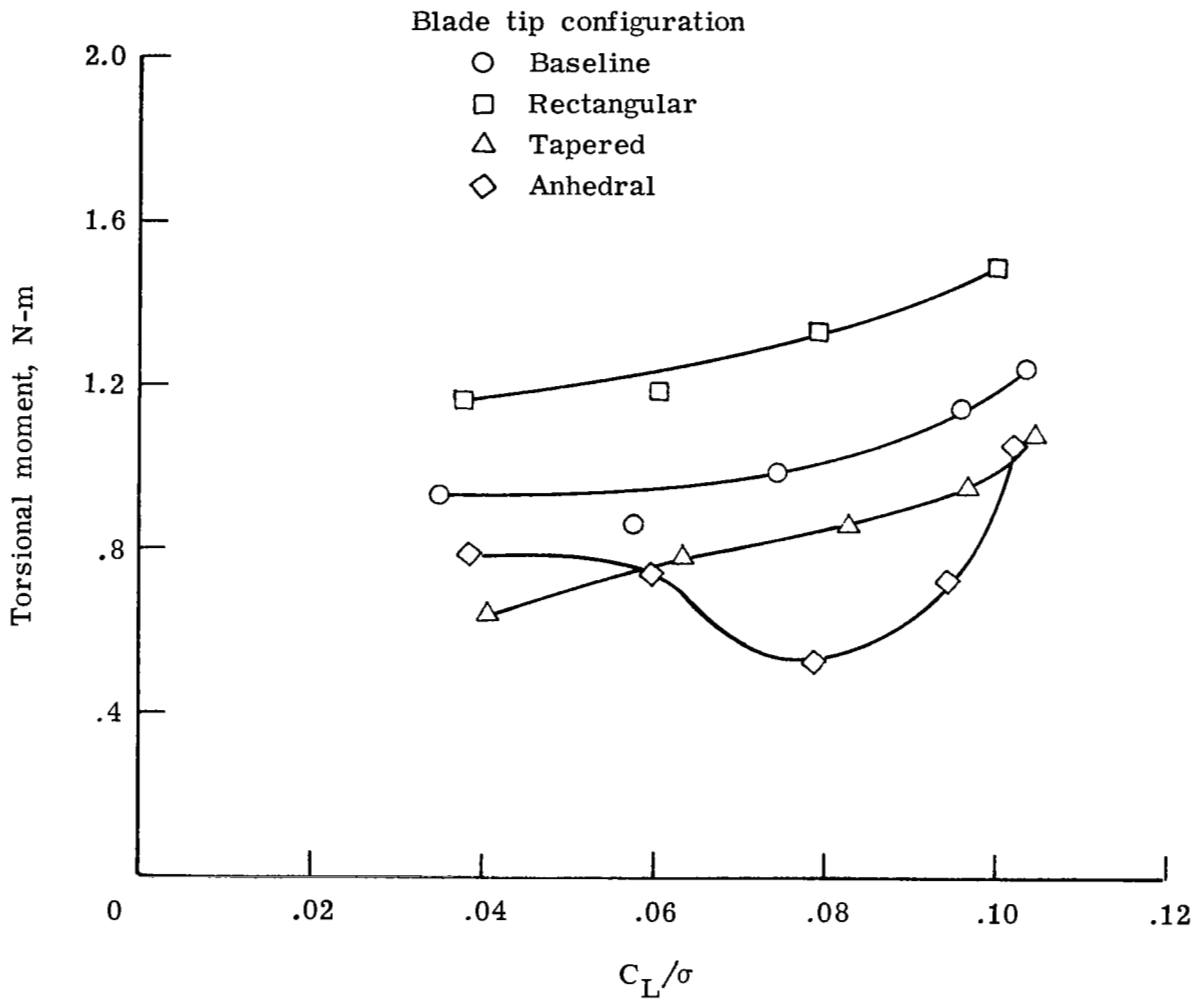


(d) Oscillatory moment.

Figure 23.- Continued.

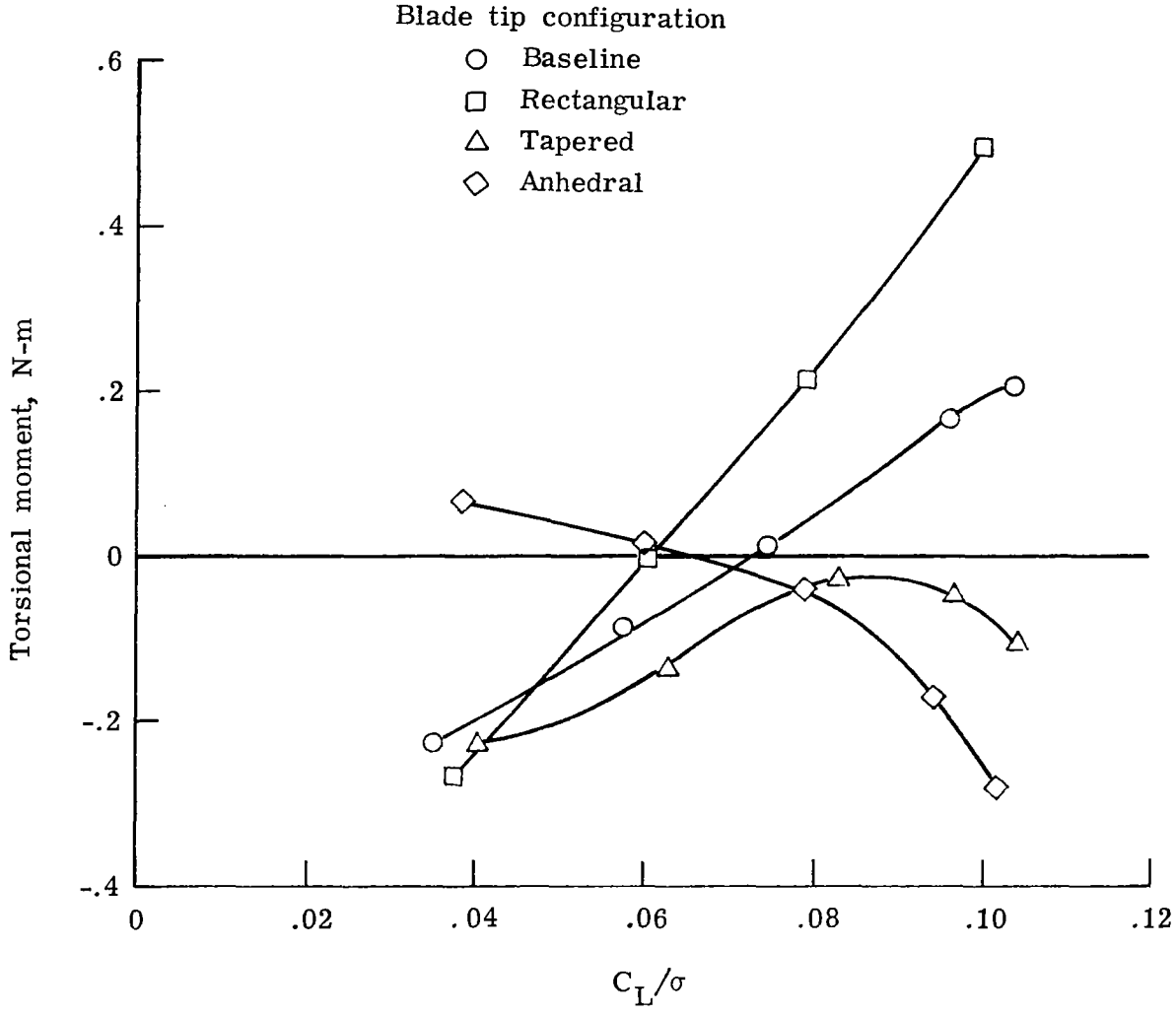


(e) Mean value of moment (positive nose-up).

Figure 23.- Concluded.

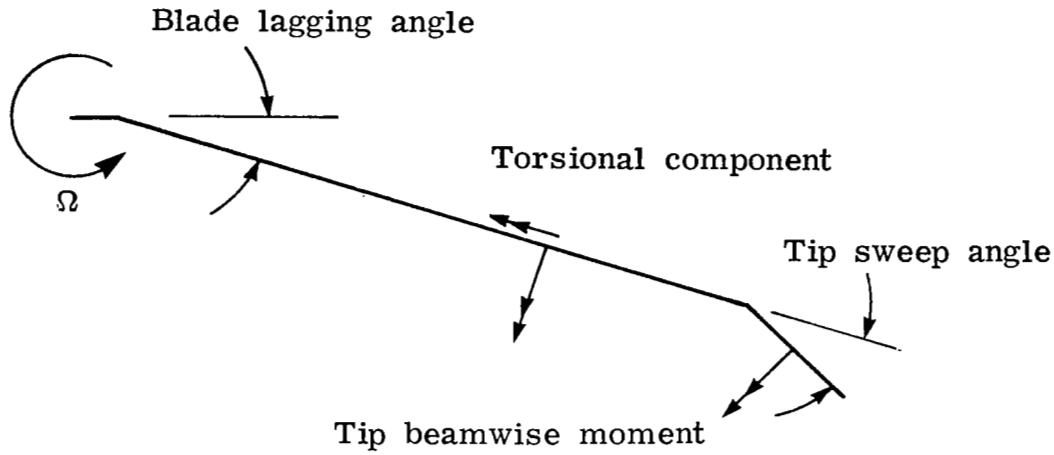


(a) Blade tip sweep.

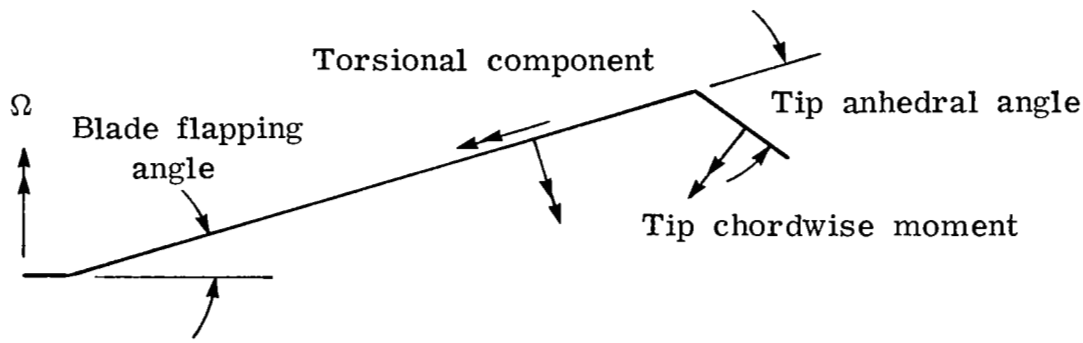


(b) Blade tip anhedral.

Figure 24.- Illustration of the torsional moment components resulting from blade tip sweep and anhedral.

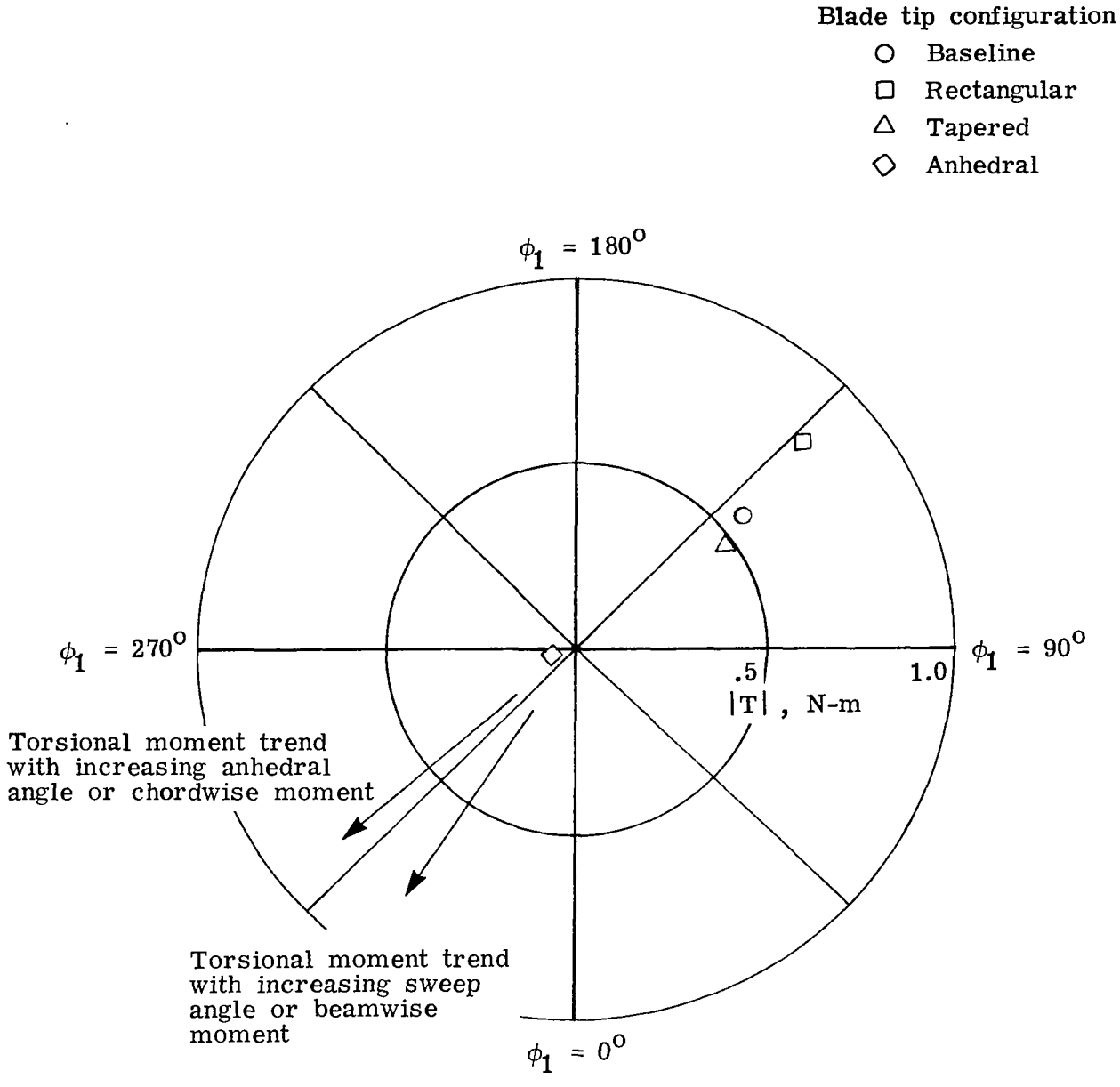


(a) First harmonic component, $T = |T| \sin(\psi + \phi_1)$.

Figure 25.- Variation of harmonic phase angles for torsional moment (x = 0.81) with blade tip configurations. $\mu = 0.35$; $C_L/\sigma = 0.08$; $\alpha_s = -9^o$.

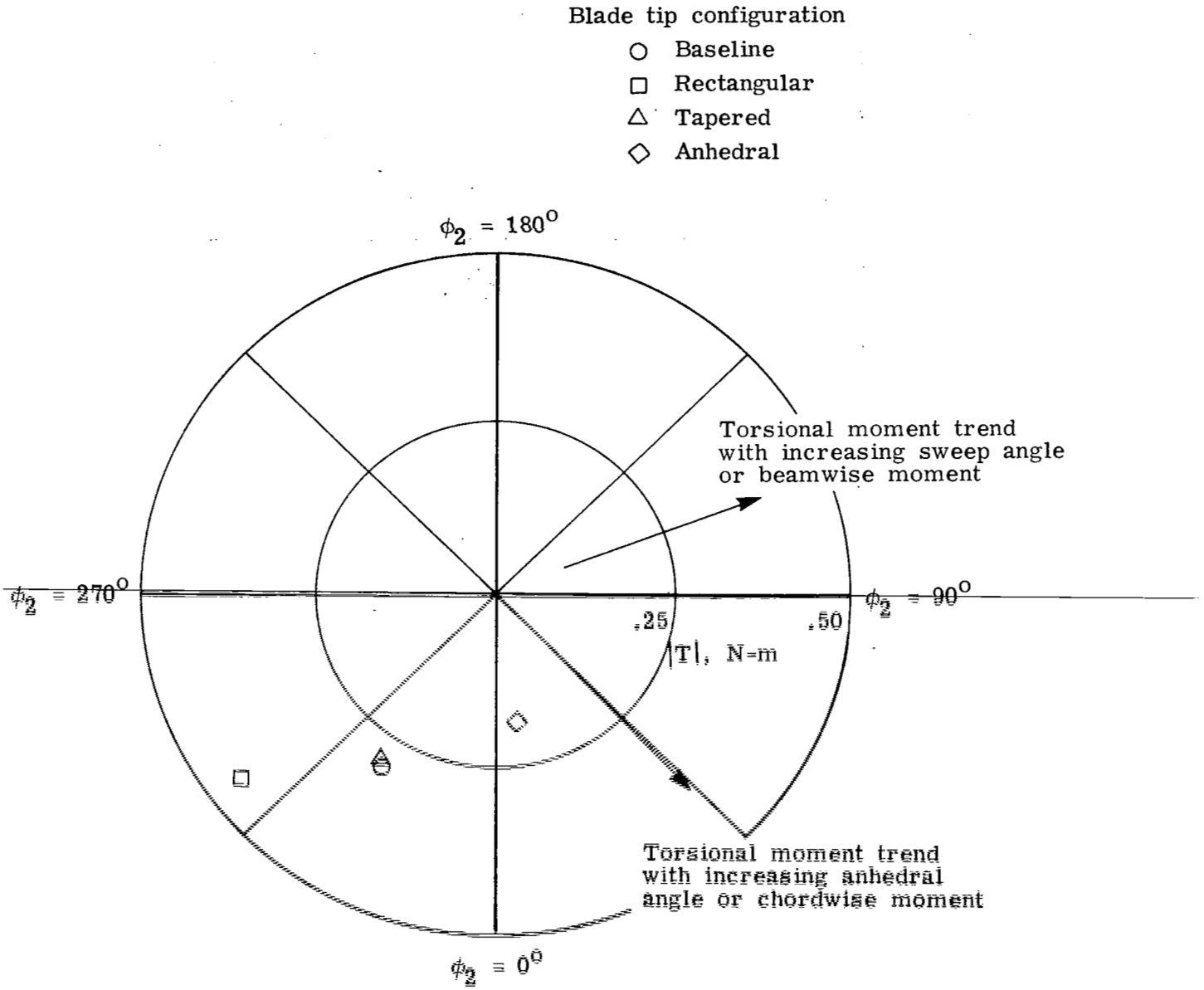


(b) Second harmonic component, $T = |T| \cos(2\psi + \phi_2)$.

Figure 25.- Concluded.

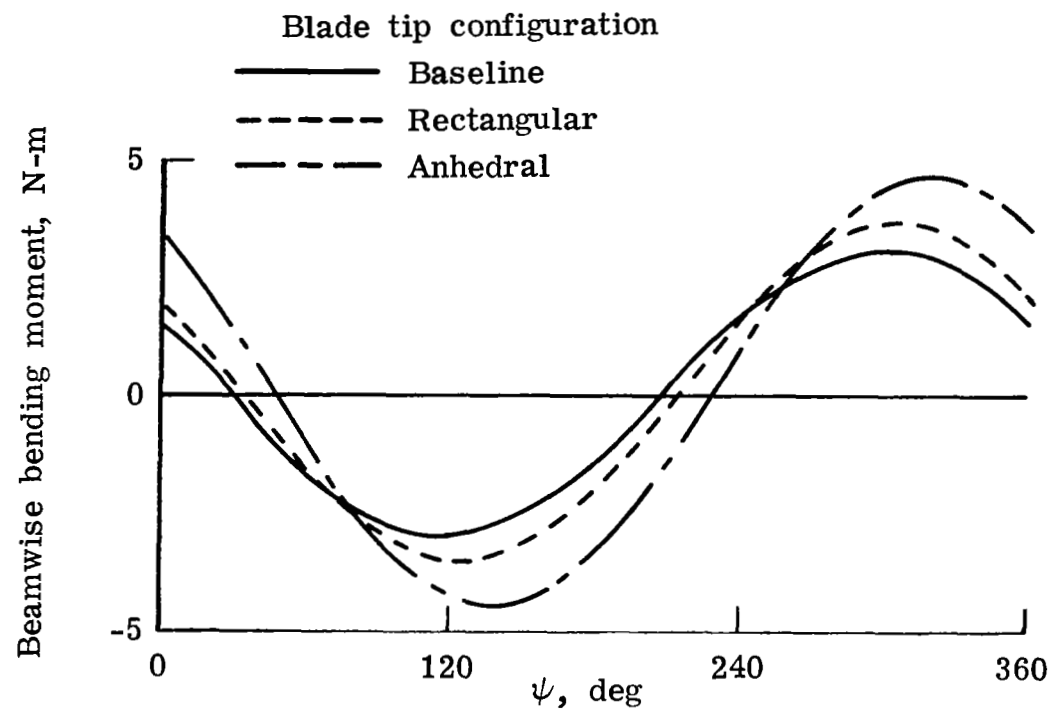


(a) Beamwise bending at x = 0.8 (positive up).

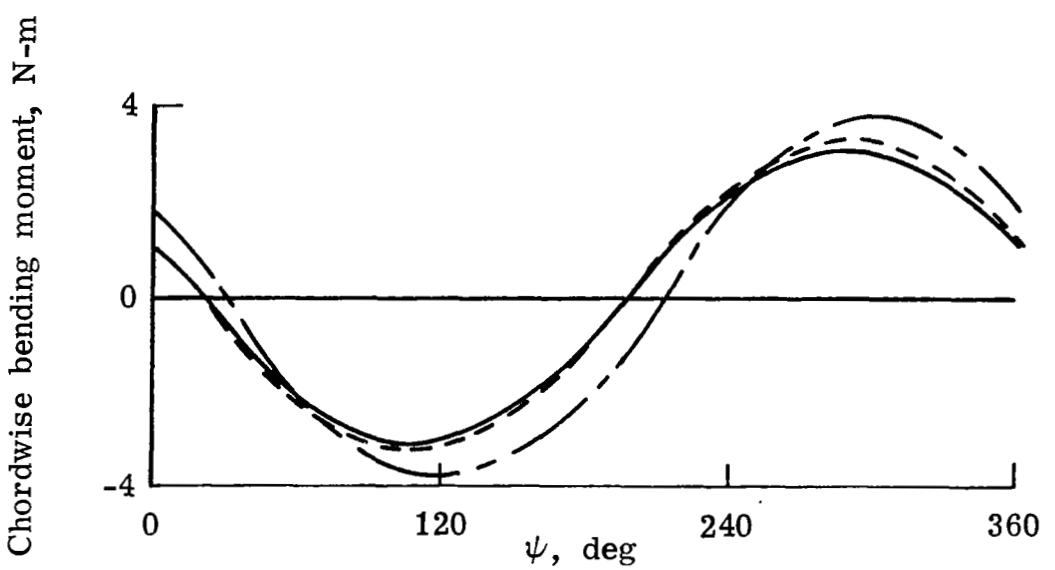


(b) Chordwise bending at x = 0.6 (positive aft).

Figure 26.- Azimuthal variation of the first harmonic bending moments for three tip configurations. $\mu = 0.35$; $C_L/\sigma = 0.08$; $\alpha_s = -9^\circ$.

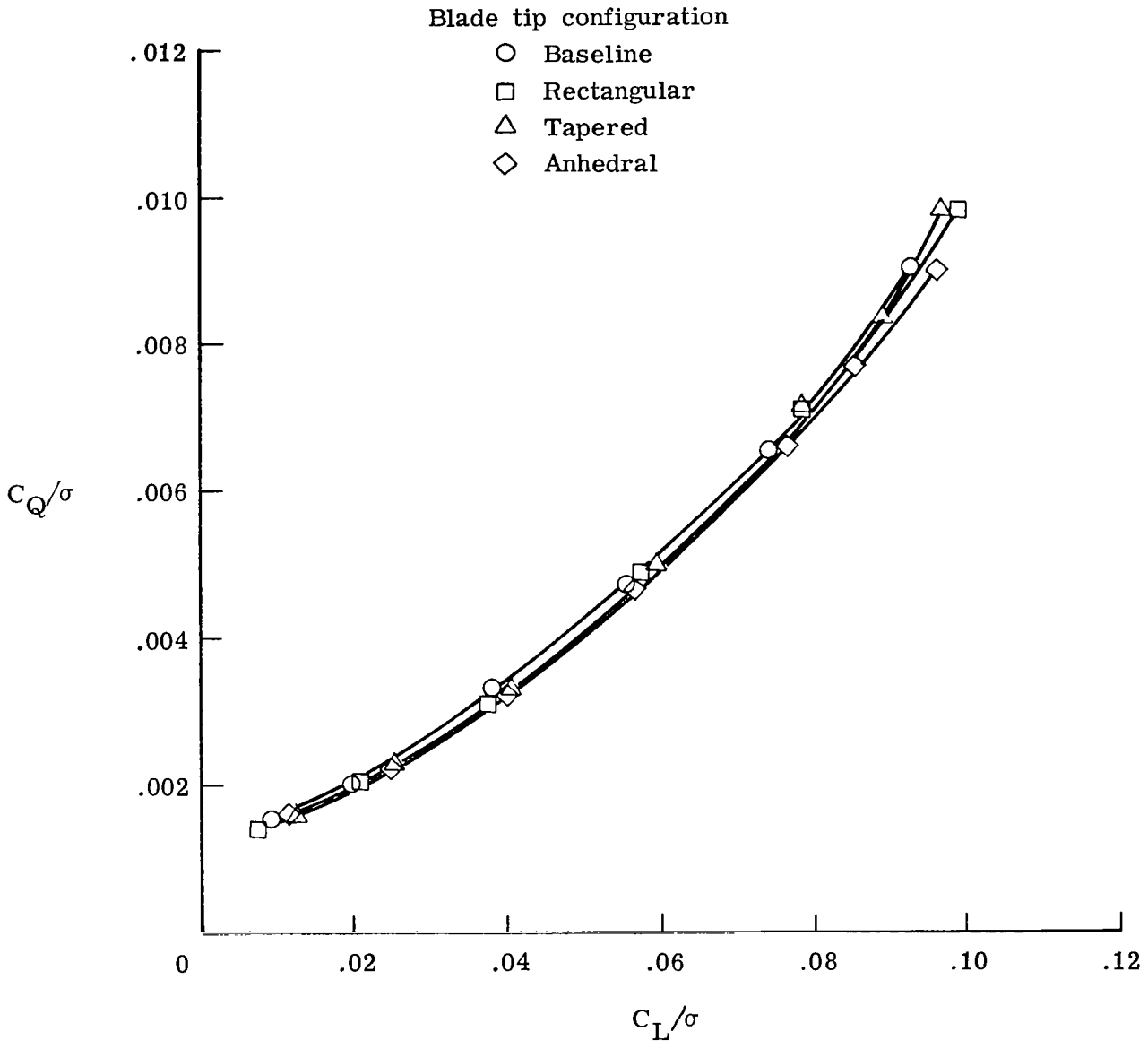


Figure 27.- Comparison of rotor performance in ground-effect hover for four blade tip configurations. $\alpha_s = 5^o$.

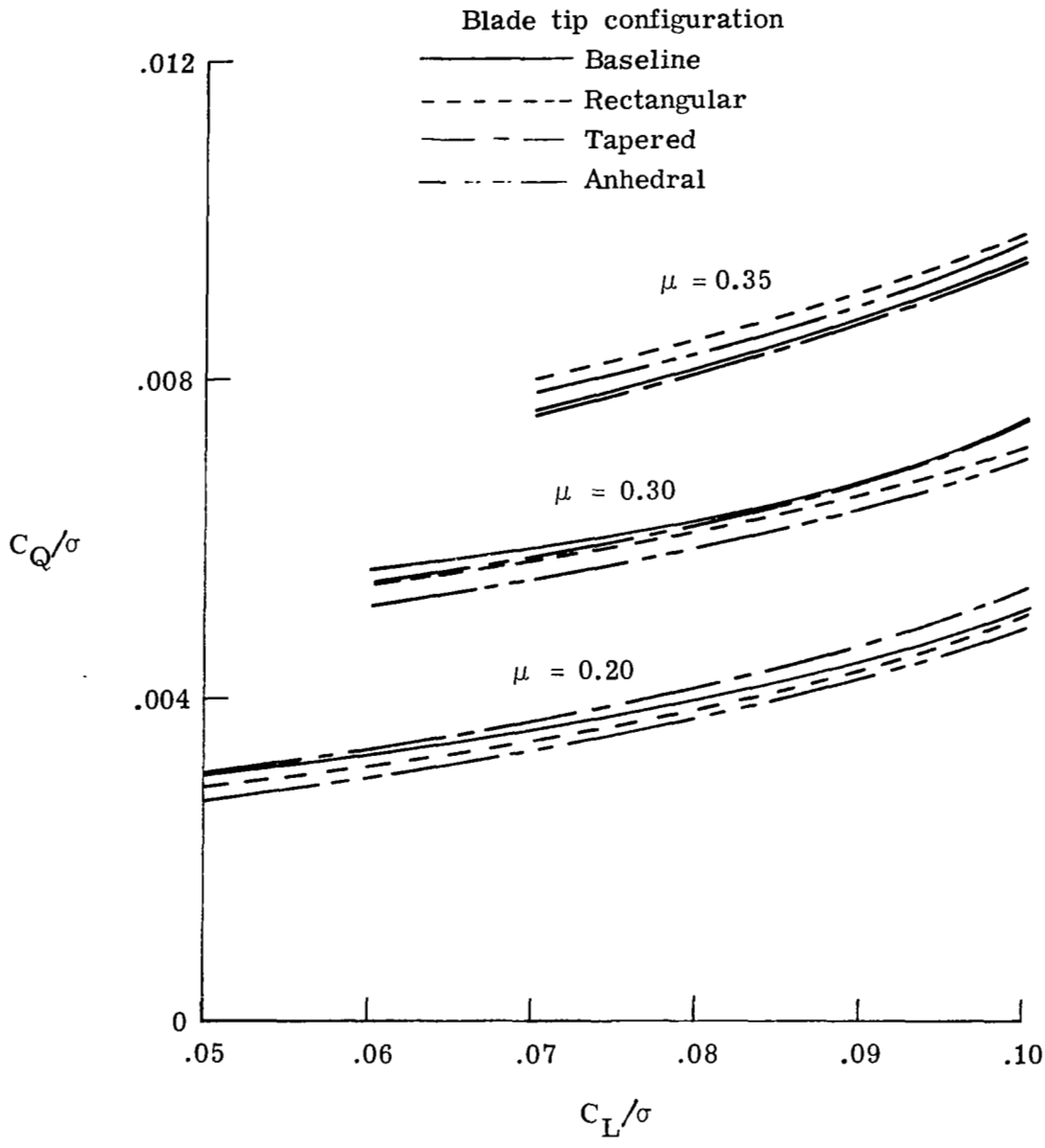


Figure 28.- Comparisons of rotor performance with advance ratio for four blade tip configurations. $A_F$ = 2.42 $m^2$; $M_t$ = 0.628.

| 1. Report No. | 2. Government Accession No. | 3. Recipient's Catalog No. |
|---|---|---|
| NASA TP-1303 AVRADCOM TR 78-53 | | |

| 4. Title and Subtitle | 5. Report Date |
|---|---|
| EXPERIMENTAL INVESTIGATION OF EFFECTS OF BLADE TIP GEOMETRY ON LOADS AND PERFORMANCE FOR AN ARTICULATED ROTOR SYSTEM | January 1979 |
| | 6. Performing Organization Code |

| 7. Author(s) | 8. Performing Organization Report No. |
|---|---|
| William H. Weller | L-12153 |
| | 10. Work Unit No. |
| | 505-10-23-03 |

| 9. Performing Organization Name and Address | 11. Contract or Grant No. |
|---|---|
| Structures Laboratory<br>AVRADCOM Research and Technology Laboratories<br>NASA Langley Research Center<br>Hampton, VA 23665 | |
| | 13. Type of Report and Period Covered |
| | Technical Paper |

| 12. Sponsoring Agency Name and Address | 14. Army Project No. |
|---|---|
| National Aeronautics and Space Administration<br>Washington, DC 20546<br>and<br>U.S. Army Aviation Research and Development Command<br>St. Louis, MO 63166 | 1L262209AH76 |

15. Supplementary Notes

William H. Weller: Structures Laboratory, AVRADCOM, Research and Technology Laboratories.

16. Abstract

Wind-tunnel tests of an aeroelastically designed helicopter rotor model were carried out to determine the effects on dynamic response and aerodynamic performance of varying the design of the outboard 8 percent of the blade lengths. Four different blade tip geometries or shapes having different amounts of planform sweep, thickness and chordwise taper, and anhedral angle were studied. Each configuration was tested at several shaft angles of attack for advance ratios of 0.20, 0.30, 0.35, and 0.40. For each combination of shaft angle and advance ratio, rotor lift was varied over a wide range to include high lift conditions.

| 17. Key Words (Suggested by Author(s)) | 18. Distribution Statement |
|---|---|
| Blade tip geometry<br>Helicopter rotor<br>Model rotor testing | Unclassified - Unlimited<br><br>Subject Category 05 |

| 19. Security Classif. (of this report) | 20. Security Classif. (of this page) | 21. No. of Pages | 22. Price* |
|---|---|---|---|
| Unclassified | Unclassified | 76 | $6.00 |

*For sale by the National Technical Information Service, Springfield, Virginia 22161

NASA-Langley, 1979